VLÁKNA a TEXTIL

FIBRES AND TEXTILES

3

Volume 25.
September
2018

STU
FCHPT

TECHNICAL UNIVERSITY OF LIBEREC
Faculty of Textile Engineering

Trenčianska univerzita Alexandra Dubčeka v Trenčíne
Fakulta priemyselných technológií v Púchove

VÚCHV

VÚTCH
CHEMITEX

Spoločnosť priemyselnej chémie
ZSVTS

CHEMOSVIT
FIBROCHEM

Indexed in:
SCOPUS
Chemical Abstracts
World Textiles

ISSN 1335-0617
print version

ISSN 2585-8890
online version

Fibres and Textiles
Vlákna a textil

Published by	*Vydáva*
Slovak University of Technology in Bratislava, Faculty of Chemical and Food Technology	Slovenská technická univerzita v Bratislave, Fakulta chemickej a potravinárskej technológie
Technical University of Liberec, Faculty of Textile Engineering	Technická univerzita v Liberci, Fakulta textilní
Alexander Dubček University of Trenčín, Faculty of Industrial Technologies	Trenčianska univerzita Alexandra Dubčeka v Trenčíne, Fakulta priemyselných technológií
Slovak Society of Industrial Chemistry, Bratislava	Slovenská spoločnosť priemyselnej chémie, Bratislava
Research Institute of Man-Made Fibres, JSC, Svit	Výskumný ústav chemických vlákien, a.s. Svit
VÚTCH – CHEMITEX, Ltd., Žilina	VÚTCH – CHEMITEX, spol. s r.o., Žilina
Chemosvit Fibrochem, JSC, Svit	Chemosvit Fibrochem, a.s., Svit

Editor in chief *(Šéfredaktor)*: Anna Ujhelyiová

Executive editor *(Výkonný redaktor)*: Marcela Hricová

http://www.vat.ft.tul.cz

Editorial office and distribution of the journal
(Redakcia a distribúcia časopisu)

Ústav prírodných a syntetických polymérov
Fakulta chemickej a potravinárskej technológie
Slovenská technická univerzita v Bratislave
Radlinského 9, 812 37 Bratislava, SK
Tel: 00 421 2 59 325 575
e-mail: marcela.hricova@stuba.sk

Order and advertisement of the journal
(Objednávka a inzercia časopisu)

Slovenská spoločnosť priemyselnej chémie,
člen Zväzu vedecko-technických spoločností
Radlinského 9, 812 37 Bratislava, SK
Tel: 00 421 2 59 325 575
e-mail: marcela.hricova@stuba.sk

Order of the journal from abroad – excepting Czech Republic
Objednávka časopisu zo zahraničia – okrem Českej Republiky

SLOVART G.T.G, s.r.o. EXPORT-IMPORT
Krupinská 4, P.O.Box 152, 852 99 Bratislava, SK
Tel: 00421 2 839 471-3, Fax: 00421 2 839 485
e-mail: info@slovart-gtg.sk

Typeset and printing *(Sadzba a tlač)*

FOART, s.r.o., Bratislava

Journal is published 4x per year Subscription 60 EUR	Časopis vychádza 4x ročne Ročné predplatné 60 EUR

Evidenčné číslo MKCR SR Bratislava EV 4006/10

Fibres and Textiles (3) 2018
Vlákna a textil (3) 2018
September 2018

Content

STUDY OF THE EFFECT OF CROSSLINKING AGENTS ON THE PHYSICAL PROPERTIES OF POLYMER FILMS BASED ON STARCH

Tatyana Asaulyuk, Yulia Saribyekova, Olga Semeshko and Sergey Myasnikov

Kherson National Technical University, Berislav Highway 24, 73008 Kherson, Ukraine
tatisevna@gmail.com

Abstract: *The effect of the chemical structure of crosslinking agents from the dicarboxylic acids class on the physical properties of polymer films based on starch is investigated in this article. As a result of complex studies it has been established that the best indexes of the polymer films stability are achieved with the use of malonic acid. An increase in the degree of crosslinking of the starch in the polymer film makes it possible to use this polymer composition to create special coatings on cotton textile materials.*

Keywords: *polymer films, starch, crosslinking agents, dicarboxylic acids, physical properties.*

1 INTRODUCTION

Today, there has been an increase in interest in textile materials with a set of special properties. The imparting special properties to textile materials are obtained by creation of polymer coatings for various purposes on the surface of fabrics.

The areas of use of materials with a polymer coating are various, because they have high mechanical strength, low gas, water, vapor permeability and resistance to aggressive media. A special place is occupied by textile materials with an antimicrobial coating containing stabilizers and biocides [1-4].

In terms of the peculiarities of creating a polymer coating, the main requirements for components of a polymer composition are high indices of their resistance to physical and chemical influences. This condition is ensured by a sufficient degree of crosslinking of the polymer components with each other to form a spatially crosslinked structure on the surface of the textile material.

Most often, precondensates of thermosetting resins are used to increase the density of polymer formation in the technology of the textile industry. As a result of the ability of thermosetting resins to release formaldehyde during the processing and use of products, these substances do not meet the requirements of Oeko-Tex Standard 100. This fact directly affects the competitiveness of products in the global and internal market.

The growing demand for high chemical stability and mechanical strength of polymer coatings, as well as limitations associated with the release of volatile organic compounds, led to the need to develop new polymer compositions for the textile industry. In this regard, studies aimed at creating environmentally friendly protective polymer systems are relevant. Promising is the use of polymer compositions based on natural polymers [5-11]. Polysaccharides, in particular starch, are widely used as natural film-forming substances. Starch is an affordable renewable environmentally friendly raw material. The disadvantage of individual starch polymer films is insufficient mechanical strength, rigidity and hydrolytic instability. Theoretically, the problem of improving the physical and mechanical properties of starch films is solved by increasing the content of the plasticizer in the composition. However, in practice, the use of a plasticizer in large quantities leads to instability in the mechanical properties of starch films. In this connection, into the polymer composition based on starch the crosslinking agents are added in addition to the plasticizer.

The crosslinking agents must provide a chemical interaction between the plasticizer and the starch via a covalent bond. Polycarboxylic acids and their derivatives are known as environmentally friendly crosslinking agents. The authors [12, 13] proposed the use of citric acid in polymer compositions based on starch for the purpose of forming spatially cross-linked three-dimensional structures. It should be noted that citric acid is a tribasic carboxylic hydroxyacid by its chemical structure. The presence of three carboxyl groups, as well as hydroxyl group, can cause less conformational mobility of citric acid during the formation of a spatially crosslinked structure with a plasticizer and starch.

In this connection, it was of interest to study the effectiveness of the use of crosslinking agents from the class of polycarboxylic acids of various chemical structures to improve the physical and mechanical properties of polymer films based on starch.

2 THE GOAL OF THE STUDY

The goal of present work was to study the effect of dicarboxylic acids with different lengths of the hydrocarbon chain on the physical properties of polymer films based on starch.

3 MATERIALS AND METHODS

3.1 Materials

Potato starch was used as a film-forming substance. Glycerine was used as a plasticizer. Succinic, malonic and oxalic acids were chosen as crosslinking agents. Citric acid was used to compare the experimental results obtained.

3.2 Methods

Polymer films are made from an aqueous solution. The crosslinking agent is added in an amount of 1% by weight of the composition. Boiling of the solution is carried out at 85-90°C for 30 min. The formed films are dried at 60°C with subsequent heat treatment at 150°C.

Hygroscopicity is determined as the mass part of moisture absorbed by the polymer film in 4 h at atmospheric moisture of 100%.

Water sorption is determined as the mass part of water absorbed by the polymer film in 24 h at 25°C.

Hydrolytic stability characterizes the degree of stability of a polymer film to the action of water and is determined by the weight method.

The degree of swelling of polymer films is determined by the change in the samples mass depending on time of stay in water.

4 RESULTS AND DISCUSSION

The effect of the selected crosslinking agents on the change in the physical properties of starch films, such as thickness, surface density and appearance, was determined at the first stage of the work. The results are shown in Table 1.

Table 1 The effect of crosslinking agents on the physical properties of starch films

Crosslinking agent	Physical properties		
	Thickness [µm]	Surface density [g/m^2]	Appearance
Without a crosslinking agent	190	190	transparent, rigid
Citric acid	130	130	turbid, elastic
Succinic acid	120	158	whitish, elastic
Malonic acid	110	175	transparent, elastic
Oxalic acid	150	163	transparent, elastic

The data obtained (Table 1) show that addition of selected carboxylic acids into the composition helps to reduce the thickness of starch films by 21-42%. The surface density of all samples decreases compared to the individual starch film. The lowest value of this index is observed when citric acid is used. It should be noted that the starch film has the greatest surface density with the smallest film thickness when malonic acid is used. All the acids studied contribute to the rise of starch films elasticity. However, the use of succinic acid causes the whitish color of starch film, which can be explained by the formation of acid crystals on the film surface during drying and heat treatment.

An important characteristic of starch polymer coatings is attitude to the action of atmospheric moisture and resistance to wet treatments. In this connection, the effect of crosslinking agents on the hygroscopicity, water sorption and hydrolytic stability was determined at the next stage of the work. The results of the experiment are shown in Figures 1, 2.

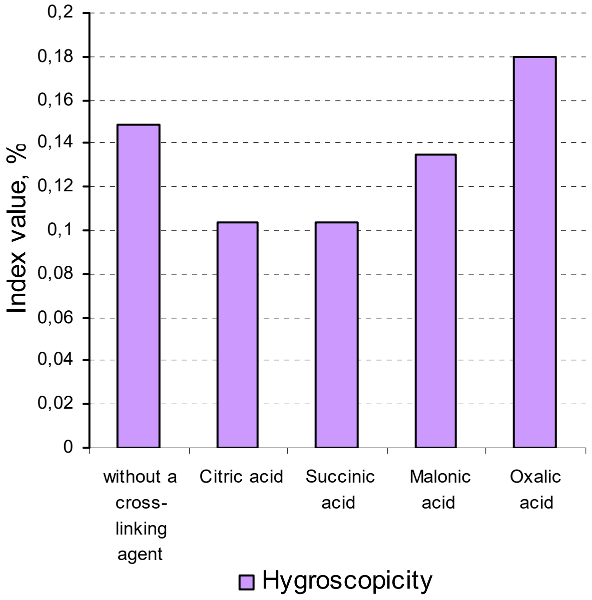

Figure 1 The effect of crosslinking agents on the hygroscopicity of starch films

Hygroscopicity is an important characteristic of starch polymer coatings, since changes in atmospheric moisture can lead to a change in moisture content in the films. This fact is reflected on the technological properties of starch films. The results of the study (Figure 1) show that at atmospheric moisture of 100% the hygroscopicity of films containing citric and succinic acids decreases by 30% compared to a starch film without a crosslinking agent. In the presence of malonic acid, this index is reduced by 9%. When oxalic acid is used, the hygroscopicity of the film is increased by 21%. Thus, as the length of the hydrocarbon chain of the polycarboxylic acids under study decreases, an increase in the hygroscopicity of the starch polymer films is observed.

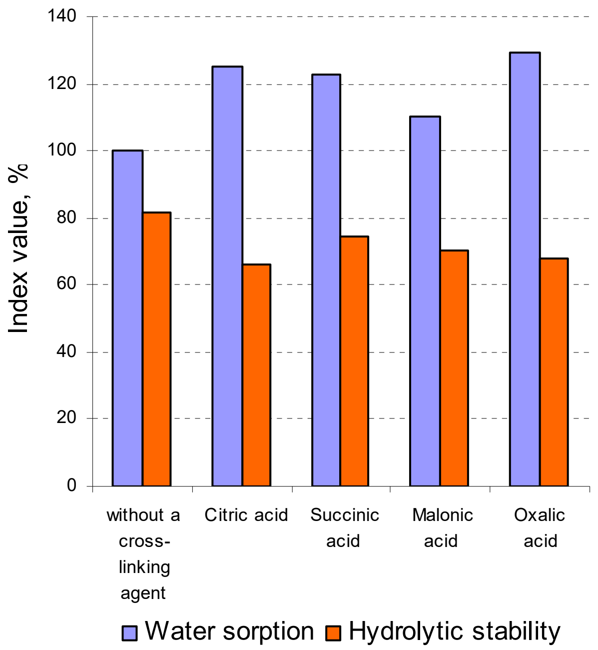

Figure 2 The effect of crosslinking agents on the attitude of starch films to wet treatments

The data presented in Figure 2 show that when all studied crosslinking agents are added into the polymer compositions, the water sorption of the samples is increased compared to the starch film without a crosslinking agent. The lowest increase of this index is observed when malonic acid is used.

Hydrolytic stability characterizes the degree of stability of the polymer film to the action of water. The results of the experiment (Figure 2) show that the addition of polycarboxylic acids in the polymer composition leads to a decrease in the stability of starch films to hydrolytic destruction by 9-19%. It should be noted that the lowest index of hydrolytic stability (66.2%) is observed when citric acid is used.

The degree of crosslinking of the starch in the polymer material can be assessed indirectly by the degree of swelling of the polymer film. In this connection, the effect of crosslinking agents on the process of swelling of starch films was investigated at the next stage of the work. The results of the experiment are shown in Figure 3.

The results obtained (Figure 3) show that the use of citric acid leads to the greatest swelling of the starch film. The sample mass increases by 65% after 72 h of treatment. The degree of swelling of a starch film without a crosslinking agent over the same period of time is 51%. A longer stay in the water of an individual starch film, as well as films containing citric and succinic acids, leads to a gradual loss of the mass of the samples. This fact can be explained by removal of non-crosslinked starch. A sample containing oxalic acid begins to lose weight after 120 h of treatment. It should be noted that the film with the content of malonic acid is characterized by the lowest degree of swelling and continues to swell after 120 h of treatment. This fact indicates a high degree of crosslinking of starch.

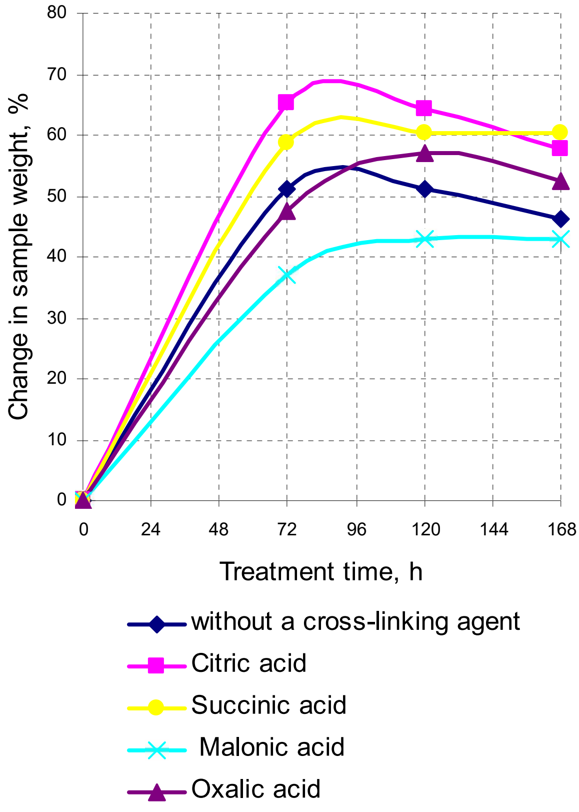

Figure 3 The effect of crosslinking agents on the degree of swelling of starch films

5 CONCLUSIONS

The effect of the chemical structure of dicarboxylic acids on the physical properties of polymer films based on starch was studied. It was determined that the use of malonic acid as a crosslinking agent makes it possible to obtain transparent elastic starch polymer films that are characterized by a lower thickness while maintaining a high surface density, as well as low hygroscopicity, water sorption and high resistance to hydrolytic destruction. This polymer composition can be used to create special coatings on cotton textile materials in order to improve the ecological character of finishing work.

6 REFERENCES

1. Golja B., Tavčer P.F.: Textile functionalisation by printing fragrant, antimicrobial and flame-retardant microcapsules, Tekstilec 59(4), 2016, pp. 278-288, DOI: 10.14502/Tekstilec2016.59.278-288
2. Onar N., Mete G.: Development of water-, oil-repellent and flame-retardant cotton fabrics by organic-inorganic hybrid materials, Journal of the Textile Institute 107(11), 2016, pp. 1463-1477, DOI: 10.1080/00405000.2015.1128208

3. Camlibel N.O., Arik B., Avinc O.: Antibacterial, UV protection, flame retardancy and coloration properties of cotton fabrics coated with polyacrylate polymer containing various iron ores, Journal of the Textile Institute 2018, DOI: 10.1080/00405000.2018.1423937
4. Kim Y.S., Min B.G.: Preparation of bio-polyurethane using castor oil and antibacterial hybrid films thereof with silver-doped hydroxyapatite, Fibers and Polymers 18(10), 2017, pp. 1841-1847, DOI: 10.1007/s12221-017-7340-3
5. Pan H., Song L., Ma L., Hu Y.: Layer-by-layer assembled thin films based on fully biobased polysaccharides: Chitosan and phosphorylated cellulose for flame-retardant cotton fabric, Cellulose 21(4), 2014, pp. 2995-3006, DOI: 10.1007/s10570-014-0276-5
6. Jimenez M., Guin T., Bellayer S., Grunlan J.C.: Microintumescent mechanism of flame-retardant water-based chitosan-ammonium polyphosphate multilayer nanocoating on cotton fabric, Journal of Applied Polymer Science 133(32),2016, DOI: 10.1002/app.43783
7. Su C.H., Kumar V., Adhikary S., Anbu P., Velusamy P., Kannaiyan P.: Preparation of cotton fabric using sodium alginate-coated nanoparticles to protect against nosocomial pathogens, Biochemical Engineering Journal 117, 2016, pp. 28-36, DOI: 10.1016/j.bej.2016.10.020
8. Scacchetti F.A.P., Pinto E., Soares G.M.B.: Thermal and antimicrobial evaluation of cotton functionalized with a chitosan-zeolite composite and microcapsules of phase-change materials, Journal of Applied Polymer Science 135(15), 2017, DOI: 10.1002/app.46135
9. Arza C.R., İlk S., Demircan D., Zhang B.: New biobased non-ionic hyperbranched polymers as environmentally friendly antibacterial additives for biopolymers, Green Chemistry 20(6), 2018, pp. 1238-1249, DOI: 10.1039/C7GC03401F
10. Muzaffar S., Ahmad I., Zuber M., Shahid M., Bhatti H.: Synthesis and characterization of aqueous chitosan-polyurethanes dispersion for textile applications with multipurpose performance profile, Fibers and Polymers 19(3), 2018, pp. 587-598, DOI: 10.1007/s12221-018-7896-6
11. Arshad N., Zia K.M, Jabeen F., Anjum M.N., Akram N., Zuber M.: Synthesis, characterization of novel chitosan based water dispersible polyurethanes and their potential deployment as antibacterial textile finish, International Journal of Biological Macromolecules 111, 2018, pp. 485-492, DOI: 10.1016/j.ijbiomac.2018.01.032
12. Shubina E.V., Nikiforov A.L., Melnikov B.N.: The new technology of anticrease finish of textile materials (Novaya tekhnologiya malosminayemoy otdelki tekstil'nykh materialov). Izvestiya Vysshikh Uchebnykh Zavedenii, Seriya Teknologiya Tekstil'noi Promyshlennosti 1(270), 2003, pp. 73-76
13. Scacchetti F.A.P., Pinto E., Soares G.M.B.: Preparation and characterization of cotton fabrics with antimicrobial properties through the application of chitosan/silver-zeolite film, Procedia Engineering 200, 2017, pp. 276-282, DOI: 10.1016/j.proeng.2017.07.039

THERMO-PHYSIOLOGICAL COMFORT OF BRUSHED WOVEN FABRICS

Amal Boughattas[1], Sofien Benltoufa[1], Musaddaq Azeem[2], Lubos Hes[2] and Faten Fayala[1]

[1]Laboratoire d'Etudes des Systèmes Thermiques et Energétiques, University of Monastir, Tunisia
[2]Faculty of Textile Engineering, Technical University of Liberec, Studentska 2, 460 15 Liberec, Czech Republic
boughattasamal@gmail.com

***Abstract:** Satisfaction of wearing of clothing is generally affected by clothing comfort properties and specifically by psychological perceptions of the wearer. A woven fabric mostly contains protruding fibers on the surface, which should be removed by burning, clipping, or brushing for appropriate processing. This paper deals with the effect of brushing on thermo-physiological comfort properties of woven fabrics. Three basic woven structures (plain, twill and sateen) were selected for this study. Thermal conductivity, thermal resistance and thermal absorptivity of these fabrics were measured by the Alambeta tester. Moreover, also water vapor permeability and air permeability were experimentally determined. The brushing treatment was applied manually by 1% and 3% of weight loss. A sample without brushing was considered as reference. Consequently, brushing affected the thickness, thermal properties, air permeability and water vapor permeability. With the increase in brushing application water vapor transmission decreased but thermal resistance increased.*

***Keywords:** brushing, woven fabrics, thermal comfort properties, water vapor permeability*

1 INTRODUCTION

From last decade, the innovative textile technology and versatile living standards has changed the fabric demands. Nowadays, clothing is not only a belonging of aesthetic reasons but also comfort parameters, so textile fibre manufacturing industry is being flourished by new special fibres which have influential thermal and physiological comfort properties [1]. Generally, comfort is defined as “the absence of displeasure or discomfort” or “a neutral state compared to the more active state of pleasure” [2]. Comfort may be defined as a pleasant state of psychological, physiological and physical harmony between a human being and environment [3].

Many researchers have focused on the analysis of thermal comfort of woven fabrics [4, 5]. The fibre and fabric composition are influencing parameters to thermal properties of clothing. For the hot season, natural fibre is preferred to wear. Human thermal comfort is closely associated to a combination of climate, clothing and physical activity [4].

Thermophysiology is basically not a textile property but a mind condition which expresses satisfaction with thermal environment. Factors having to do with heat, moisture and air transport are associated with thermal comfort. Thermo-physiological properties are closely linked to this research area. So ultimately fibre type, yarn properties, fabric structure, finishing treatments and clothing conditions are the main factors affecting thermos-physiological comfort [6, 7]. The thermal comfort is involving into fabric ability to sustain the temperature of the skin through transfer of heat and sweat produced from human body [8].

A woven fabric usually shows pronounced hairiness and fibers on its surface, which, before digitization, must be removed by burning, clipping, or brushing for a suitable image. Brushing is the procedure used on fabrics to produce a nap, a novelty textured effect and hairy surface. Fabric brushing or surface rinsing is a mechanical finishing process. It is an effective way to increase the ability of the fabric to retain heat or provide a thermal barrier. This process makes fabrics fluffy and warm, with a soft handle. Brushed fabrics are commonly used to make pants or trousers, jackets (sports), shirts, brushed denim and even for sleeping garments and bed sheets. Practically, warp and weft yarns are not distributed in straight lines and at right angles, so before capturing the image, they have to be adjusted in parallel and perpendicular directions [9]. For underwear applications, the fabric must be hydrophilic to move away moisture for the skin interface and spread the limit on the largest possible area to favor evaporation. Often to help this phenomenon, a "brushed" fabric is used causing a considerable increase in surface area thus enhancing the comfort level.

Thus, in this study, different types of woven fabrics were manually brushed and the effect of brushing on thermo-physiological comfort properties was studied.

2 MATERIALS AND METHODS

2.1 *Materials*

Woven fabric samples which dimension is 50 mm^2 with three basic weave structures (plain, twill and sateen) were woven using a flexible rapier weaving machine; GamMax (Picanol) under the same technological conditions. PC (Polyester/Cotton) yarn with ratio 50:50 was used as warp and weft yarn for all samples. Table 1 presented detailed yarns composition.

Table 1 Yarn specifications for fabrics

Woven fabric type	Composition	Ends/cm	Picks/cm
Plain	50/50 Polyester/Cotton	24	24
Twill 3/1			
Turkish sateen			

2.2 *Methods*

After pretreatments, woven fabric samples were analyzed for thermal properties as well as air and water vapor permeability. For each sample, three measurements were considered.

2.2.1 Brushing

All samples were manually brushed by using very fine brushing paper. To ensure comparability of brushing results, three samples were brushed for each woven fabric type. It was achieved the reduction of the sample weight by 1 and 3%. It was measured the weight of fabric sample before Alambeta evaluation and brushed it manually till it lost 1% weight. After experimentation of all thermal properties the samples were brushed again till the loss of 3% weight. So this mechanism was manually done on the specimens to produce the desired nap and uniform aspect ratio. This is the novelty of work which was not done before that's why no literature of work is reported on this research.

2.2.2 Principle of ALAMBETA instrument - tester and thermal properties of fabrics

This apparatus used in this study enables the measurement of the following thermal parameters: thermal conductivity, thermal absorptivity, thermal resistance and sample thickness. The Alambeta simulates the dry human skin and its principle depends in mathematical processing of time course of heat flow passing through the tested fabric due to different temperatures of bottom measuring plate (22°C) and measuring head (32°C) under the contact pressure 200 kPa. When the specimen is inserted, the measuring head drops down, touches the fabrics and the heat flow levels are processed in the computer and thermo-physical properties of the measured specimen are evaluated [10]. The measurement lasts for several minutes only. Thus, reliable measurements on wet fabrics are possible, since the sample moisture during the measurement keeps almost constant.

Table 2 Thermal properties specifications

Parameter	Symbol	Unit
Thermal conductivity (coefficient)	λ	W.m-^{1}.K-^{1}
Thermal absorptivity, Thermal activity coefficient	b	W.s$^{1/2}$.m-^{2}. K^{-1}
Thermal resistance	R	K.m^{2}.W^{-1}

Thermal conductivity coefficient λ presents the amount of heat, which passes from 1 m^2 area of material through the distance 1 m within 1 s and create the temperature difference 1 K. Thermal conductivity of textile structures generally extends from 0.033 to 0.01 W/m/K. Thermal conductivity of steady air by 20°C is 0.026 W/m/K while thermal conductivity of water is 0.6 W/m/K, which is 25 times more. That is why the water presence in textile materials is undesirable [11].

Thermal absorptivity b of fabrics was introduced by Hes [11] to characterise thermal feeling (heat flow level) during short contact of human skin with the fabric surface. Providing that the time of heat contact (τ) between the human skin and the textile is shorter then several seconds, the measured fabric can be simplified into semi-infinite homogenous mass with certain thermal capacity ρc [J/m^3] and initial temperature t_2. Unsteady temperature field between the human skin (with constant temperature t_1) and fabric with respect to boundary conditions offers a relationship, which enables to determine the heat flow q [W/m^2] course passing through the fabric:

$$q = \frac{b\left(t_1 - t_2\right)}{\left(\pi\tau\right)^{1/2}} \quad , \quad b = \left(\lambda\rho c\right)^{1/2} \qquad (1)$$

where ρc [J/m^3] is thermal capacity of the fabric and the term b presents thermal absorptivity of fabrics.

The higher is thermal absorptivity of the fabric, the cooler is its feeling.

Thermal resistance expresses the thermal insulation of fabrics and is inversely proportional to thermal conductivity. In a dry fabric or containing very small amounts of water it depends essentially on fabric thickness and, to a lesser extent, on fabric construction and fiber conductivity [12]. Thermal resistance R [m^{2}K/W] depends on fabric thickness h and thermal conductivity λ:

$$R = \frac{h}{\lambda} \qquad (2)$$

2.2.3 Relative water vapor permeability

Relative water vapor permeability was measured on a Permetest instrument by a similar procedure to that given by Standard ISO 11092 [13] *RWVP* (%) of the textile clothing samples in the isothermal steady state is measured by the given equation:

$$RWVP(\%) = \frac{Heat\ loss\ measured\ with\ sample}{Heat\ loss\ measured\ without\ sample} \times 100 \qquad (3)$$

2.2.4 Air permeability

Air permeability is described as the rate of air flow passing perpendicularly through a known area, under a prescribed air pressure differential between the two surfaces of a material. TEXTEST Air Permeability Tester (FX3300) is used to measure the air permeability according to standard ISO 9237. The air pressure differential between the two surfaces of the textile material was 100 Pa.

3 RESULTS AND DISCUSSION

3.1 Air permeability

The twill and sateen weaving structure have the highest air permeability value as compared to plain weave. These results can be explained by fabric porosity. However, brushing treatment showed non-significant change in the case of plain structure as shown in Figure 1.

In the case of the sateen and the twill fabrics the air permeability increased significantly (reaching 296.2 l/m^2/s for the weight loss of 1% after brushing compared to 175 l/m^2/s without brushing for the twill structure). In fact, the brushing effect is more important due to the floats at the fabric surface. In addition, brushed fibres are more apparent in the surface. This will make yarns more porous. The allied fibres will be more mobile and the velocity of the air through the surface will be more important. However, in the case of 3% fabric weight loss (accentuated brushing), the allied fibres will be oriented in the fabric parallel direction and not out of the surface, so fibres will obstruct the inter-yarn pores and the air permeability will slightly decrease as illustrated in the Figure 1. It can be seen from the results in Table 4 that the independent variables (weave type) have a statistically significant (s) results regarding air permeability.

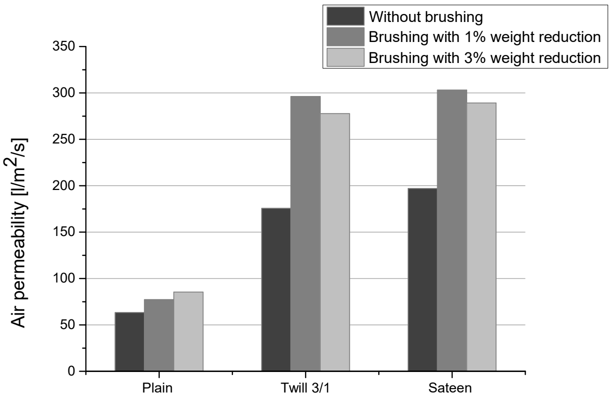

Figure 1 Air permeability of plain, twill and Turkish sateen without and after brushing

3.2 Relative water vapor permeability

The relative water vapor permeability is the percentage of water vapor transmitted through the fabric sample compared with the percentage of water vapor transmitted through an equivalent thickness of air. It can be seen from Figure 2 that, before brushing, all structures have almost the same value of relative water vapor permeability.

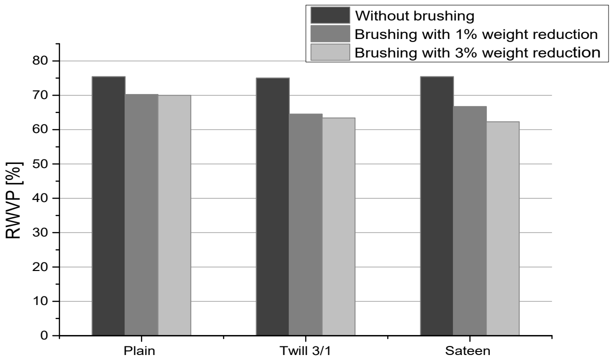

Figure 2 Relative water vapor permeability of plain, twill 3/1 and Turkish sateen without and after brushing

Table 3 Mean values of air and water vapor permeability parameters of different fabrics

Weaving structure	Brushing treatment	Thickness [mm]	Air permeability [l/m^2/s]	Relative water vapor permeability [%]
Plain	without brushing	0.45	63.3	75.4
	brushing with 1% weight reduction	0.72	77.2	70.2
	brushing with 3% weight reduction	0.84	85.4	70
Twill 3/1	without brushing	0.63	175	75
	brushing with 1% weight reduction	1.07	296.2	64.5
	brushing with 3% weight reduction	1.08	277.7	63.4
Turkish sateen	without brushing	0.56	197	75.4
	brushing with 1% weight reduction	1.08	303	66.7
	brushing with 3% weight reduction	1.16	289.2	62.3

After brushing, plain weaving structure has higher relative water vapor values than twill and sateen fabrics. It could be explained by the fact that plain weaving structure is compact (with high warp density) so brushing showed no effect. ANOVA results presented in Table 4 show statistical significance of weave type contingent upon the relative water vapor permeability of the fabric.

Table 4 ANOVA results for woven fabrics

Weave type	Brushing treatment	Air permeability [l/m^2/s]	RWVP [%]
Plain	without brushing	s	s
	brushing with 1% weight reduction	s	s
	brushing with 3% weight reduction	s	s
Twill 3/1	without brushing	s	s
	brushing with 1% weight reduction	s	s
	brushing with 3% weight reduction	s	s
Turkish sateen	without brushing	s	s
	brushing with 1% weight reduction	s	s
	brushing with 3% weight reduction	s	s

ns= non-significant; s= significant

3.3 *Thermal conductivity*

Thermal conductivity is an intensive and specific property of materials that indicates its ability to conduct heat. According to Figure 3 and without brushing, sateen structure has the highest thermal conductivity. Significance of the parameters is given in Table 6.

3.4 *Thermal resistance*

According to Figure 4, for each structure, the brushing treatment enhanced the insulation of fabrics as the thickness increased. After brushing, the sateen and twill structure exhibited the highest thermal resistance and this could be explained by the fact that these structures were loose and easily to brush compared to plain weave structure. In Table 6, ANOVA results of fabric for thermal resistance are presented.

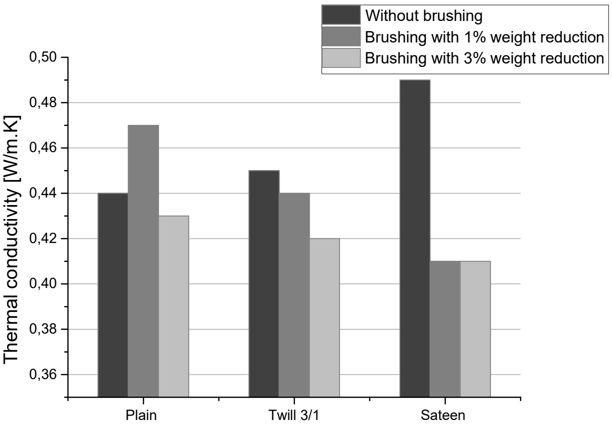

Figure 3 Thermal conductivity of pain, twill 3/1 and Turkish sateen without and after brushing

Figure 4 Thermal resistance of plain, twill 3/1 and Turkish sateen without and after brushing

Table 5 Mean values of thermal properties of different fabrics

Weave structure	Brushing treatment	Thermal conductivity [W/m.K]	Thermal resistance [K.m^2/W]	Thermal absorptivity [Ws$^{1/2}$/(m^2.K)]
Plain	without brushing	0.044	0.010	148
	brushing with 1% weight reduction	0.047	0.016	90
	brushing with 3% weight reduction	0.043	0.019	70.1
Twill 3/1	without brushing	0.045	0.014	128
	brushing with 1% weight reduction	0.044	0.024	65.2
	brushing with 3% weight reduction	0.042	0.025	64.4
Turkish sateen	without brushing	0.049	0.011	154
	brushing with 1% weight reduction	0.041	0.025	66.6
	brushing with 3% weight reduction	0.041	0.027	62.4

Table 6 ANOVA results of fabric for thermal properties

Weave type	Brushing treatment	Thermal conductivity [W/m.K]	Thermal resistance [K.m^2/W]	Thermal absorptivity [Ws$^{1/2}$/(m^2.K)]
Plain	without brushing	s	s	s
	brushing with 1% weight reduction	s	s	s
	brushing with 3% weight reduction	s	s	s
Twill 3/1	without brushing	s	s	s
	brushing with 1% weight reduction	s	s	s
	brushing with 3% weight reduction	s	s	s
Turkish sateen	without brushing	s	s	s
	brushing with 1% weight reduction	s	s	s
	brushing with 3% weight reduction	s	s	s

ns= non-significant; s= significant

3.5 Thermal Absorptivity

After brushing, thermal absorptivity decreases and we obtain warmer fabrics. The plain weaving structure has the highest thermal absorptivity and, at the same time, the coolest feeling at the moment of contact of the fabric with human skin. Likewise, the thermal conductivity, resistivity and absorptivity have also the statistically significant effect by the weave type.

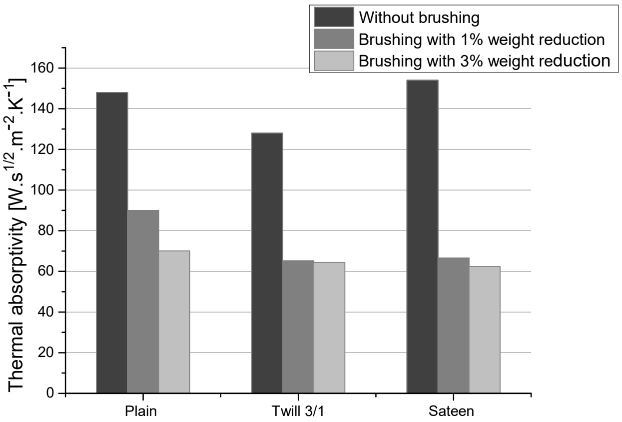

Figure 2 Thermal absorptivity of plain, twill 3/1 and Turkish sateen without and after brushing

4 CONCLUSIONS

It is concluded from the above results that the weaving structure and the brushing treatment are directly related to each other. Twill and sateen weave structure showed the highest air permeability value as compared to plain weave because of its compact weave design. Thermal properties of thrice samples were analysed differently because of brushing effect. Thermal conductivity of sateen fabric without brushing presented higher value than treated samples but the brushing treatment values were lower than the plain and twill samples. Similar values were perceived in case of thermal absorptivity. Thermal resistance values were found significantly different from the thermal conductivity and thermal absorptivity. Plain weave unveiled the less resistance with respect to twill and sateen.

5 REFERENCES

1. Arzu Marmarali A., Kadoglu H., Oglakcioglu N., Celik P., Blaga M., Ursache M., Loghin C.: Thermal comfort properties of some new yarns generation knitted fabrics. In: Proceedings of AUTEX 2009, World Textile Conference, Izmir, 2009
2. Milenković L.J., Škundrić P., Okolović RS., Nikolić T.: Comfort properties of defense protective clothings, Facta Universitatis 1(4), 1999, pp. 101-106
3. Kothari V.K.: Thermo-physiological comfort characteristics and blended yarn woven fabrics, Indian Journal of Fibre and Textile Research 31(1), 2006, pp. 177-186, doi: 10.1080/00405000801977183
4. Tzanov T., Betcheva R., Hardalov I.: Thermophysiological comfort of silicone softeners-treated woven textile materials, International Journal of Clothing Science and Technology 11(4), 1999, pp. 189-197, doi: 10.1108/09556229910281911
5. Das A., Ishtiaque SM.: Comfort characteristics of fabrics containing twist-less and hollow fibrous assemblies in weft, The Journal of Textile and Apparel, Technology and Management 3(4), 2004, pp. 1-7
6. Ozdemir H.: Thermal comfort properties of clothing fabrics woven with polyester/cotton blend yarns, AUTEX Research Journal 17(2), 2017, pp. 135-141, doi: 10.1515/aut-2016-0012
7. Murárová A., Rusnák A., Murárová Z.: Thermophysiological properties of integrated textile layers designed for an extremely low temperature environment, Vlákna a Textil (Fibres and Textiles) 12(4), 2005, pp. 150-155
8. Lizák P., Mojumdar S.C.: Thermal properties of textile fabrics, Journal of Thermal Analysis and Calorimetry 112(2), 2013, pp. 1095-1100, doi: 10.1007/s10973-013-3013-7
9. Huang C.C., Liu S.C., Yu W.H.: Fabric analysis by image processing, Part I: Identification of weave patterns, Textile Research Journal 70(6), 2000, pp. 481-485, doi: 10.1177/004051750007000603
10. Hes L.: Thermal properties of nonwovens, In: Proceedings of Congress Index vol. 87, Geneva, 1987
11. Hes L.: Heat, moisture and air transfer properties of selected woven fabrics in wet state, Journal of Fiber Bioengineering and Informatics 2(3), 2009, pp. 141-149, doi: 10.3993/jfbi12200901

12. Haghi A.K.: Moisture permeation of clothing, Journal of Thermal Analysis and Calorimetry 76(3), 2004, pp. 1035-1055, doi: 10.1023/B:JTAN.0000032288.16502.d2
13. Hes L., Dolezal I.: A new portable computer controlled skin model for fast determination of water vapor and thermal resistance of fabrics, In: Proceedings of Asian Textile Conference (ATC 7), New Delhi, 2003

DEGRADATION PROPERTIES STUDY OF LDPE AND PLASTICIZED STARCH COMPOSITE BLOWN FILM

V. Bulakh, N. Sova, B. Savchenko and O. Sleptsov

Kyiv National University of Technologies and Design, N.-Danchenko srt. 2, 01011 Kyiv, Ukraine
v.b.23@ukr.net; djanc@ukr.net; 1079@ukr.net; zikmne@ya.ru

Abstract: *The problem of producing polymer materials with accelerated degradation under ambient conditions is particularly relevant today. One of the solutions is forming synthetic – organic polymer composites and the study of properties and peculiarities of they degradation. The study is dedicated to blown films based on low density polyethylene (PE) and thermoplastic starch (TPS) compound, were thermoplastic starch was in situ formed during compounding process. Thermoplastic composite was produced on industrial scale equipment buy using standard filler incorporation techniques - trough filler masterbatch which was mixed with target polymer on film blowing equipment. Modern modification techniques were used during masterbatch production – incorporation of graft copolymer and viscosity reduction agent as well transition metal catalysis. Corn starch was first plasticized with glycerol and then used in powder form for compounding on twin screw extruder with polyethylene and additives. Thermal and pressure treatment during compounding converts plasticized starch to thermoplastic starch homogenously incorporated in polyethylene matrix. Properties changes during degradation of various starch polyethylene composites were studied. The influence of incorporation techniques and various modifying additives on the properties of PE/TPS blown films, such as polyethylene and maleic anhydride grafted polyethylene wax were studied. It was established that the introduction of modifiers leads to a decrease in the viscosity of the composites, and to an increase of the strength and technological properties, and facilitated processing. The rheological properties of modified PE/TPS composites allow the processing using the conventional industrial equipment and technological modes. The reason for the high technological and operational properties of the investigated materials is the increased compatibility of the components of composites due to the influence of modifying additives. An estimation of the properties change of the resulting blown films during degradation in different model environments was carried out. It was established that the use of metal catalysis like ferric stearate significantly increases the intensity of degradation of PE/TPS blown films as a result of initiating the degradation of the PE matrix under the effect of environmental factors. Blown films containing catalysis lose relative tensile strain at yield by 80% after 60 days of stay in the soil which is an important proof of degradation. The results obtained will allow producing polymer films with accelerated environmental degradation and compatibility.*

Key words: *thermoplastic starch, blown film, plasticized starch, ferric stearate, accelerated degradation.*

1 INTRODUCTION

A large number of consumer goods made from polymers need to be recycled after use [1]. However, most polymers degrade in the environment for a long period time, which focus grate attention to the production of biodegradable materials [2, 3]. The household products made of polymer materials should quickly degrade after their usage under the ambient environmental conditions [4]. One of the ways to produce such materials involves the introduction of special additives into synthetic polymers accelerating the degradation of polymer macromolecules. For these purposes, polysaccharides, generally starches, as well as oxo-additives [5] are widely used. Another option is the use of bio derived or based polymers as PLA, PCL, PBAT, but for the Ukrainian economy at the present stage it is still expensive.

Presently, the methods of reactive extrusion of polymers are being intensively introduced in the industry [6], thus, the technology of chemical modification of polyethylene (PE) like bonding of the functional macromolecules in the viscous state with polar vinyl monomers (maleic anhydride, itaconic acid, etc.). Modified this way, PE contains active groups in macromolecules and has an enhanced compatibility with polar polysaccharide filler that causes intensified interphase interactions [7].

The research should be considered relevant as it is aimed at finding and developing new ways to accelerate the expansion of synthetic polymers, in particular of polyethylene.

2 ANALYSIS OF LITERATURE DATA AND PROBLEM STATEMENT

The main large group of polymeric materials is composites with synthetic thermoplastics and natural polymers. The insertion of starch in PE is known as a technology for improving the degradation of products based on PE. However, it should be noted that despite a great deal of work, low compatibility of bioactive additives with PE is a serious problem.

The scientists [10] investigated the explicit dependence of rheological, physical and mechanical properties, time of biodegradation of a polymer on the content of starch. The obtained results indicate that the increase of the starch percentage in the composites is accompanied by reduction of the melt flow index, tensile strength and strain of the composite.

According to the authors [11], the greatest disadvantages of the technology of combining PE and starch are the low mechanical characteristics of the resulting composites, the degradation of starch at processing temperatures, boiling of starch, poor appearance, and sensitivity to moisture. In addition, the films obtained are not transparent that limits the scope of use of such composites, especially as packaging materials, as described in detail further [12].

Since adding of powdered pure starch into PE has a number of shortcomings as highlighted by the authors [13], the blending plasticized starch with PE is a modern approach to the production of polymeric materials with a prolonged service life on the basis of synthetic polymers, the purpose of which is to overcome these shortcomings. The term "plasticized starch" refers to a blend of starch with glycerol as a plasticizer and glycerol monostearate (GMS) as lubrication agent [14].

In the study it is stated that the transformation of plasticized starch particles in thermoplastic starch (TPS) occurs during the processing of PE blend on the extrusion equipment under the effect of pressure and temperature. In this case, the starch particles (globules) are distributed in the polymer matrix and isolated from each other by the polymer layer. The processes of transforming the crystalline phase into amorphous proceed in isolation at the level of starch globules [15].

The authors [16] consider in detail the technology of obtaining TPS by thermo-mechanical degradation of pectin component of starch in the process of extrusion processing. TPS obtained from native starch in its pure form does not possess a complex of properties necessary for processing of the packaging materials. TPS is characterized by low tensile strain, moisture sensitivity and very high melt viscosity.

In the study [17] it was established that addition of compatibiliser like PE-itaconic acid graft copolymer into PE/plasticized starch blend, a more homogeneous structure of composite films is formed that is characterized by the absence of striking interphase boundaries causing an increase in the technological characteristics of film materials (tensile strain at yield, elasticity and biodegradation).

The possibility of using compatibilisers in the PE/plasticized starch system is confirmed by the improvement of rheological, physical, mechanical and performance indicators.

It should be noted that most research in this topic is focused on laboratory scale samples produced on laboratory equipment. The main experimental objective of current study is to introduce plasticized starch technology in industrial scale production process with application of industrial filler incorporation methods.

Thus, experiments in this direction are promising and relevant.

3 PURPOSE AND OBJECTIVES

The aim of the work is to study the properties and degradation of blown films based on PE and TPS formed in industrial film production process followed by compounding and film blowing. To achieve this goal, the following tasks had to be solved:

- to study the influence of various modifiers on the properties of blown films PE/TPS;
- to study the degradation of PE/TPS blown films in various model environments.

4 MATERIALS AND METHODS

The following raw materials were used:

LDPE of type 15803-020 (MFI 2.0-2.4 g/10 min); corn starch (DSTU 4286: 2004); plasticizer - glycerol pharmacological grade, lubricant - glycerol monostearate (GMS).

Modifiers: polyethylene wax (PW-200), maleic anhydride (MA) grafted polyethylene (MA-g-PE) produced by the solid-phase synthesis method according to the technique described in [18]. As additive for accelerating the degradation of PE ferric hydroxy-stearate II (Fe stearate) synthesized by reaction in water solution was used as component of starch composition and PE matrix.

The MFI of PE was measured in accordance with ISO 1133 at the temperature 190±0.5°C and the weight of 2.16 kg. MFI of TPS was measured at a load of 21.6 kg. The preheat period of material is 5 min. The density of the composites was determined by the hydrostatic weighing method according to GOST 11035.2-93. Moisture absorption was determined as change in the mass of the specimen for 24 hours at 23°C for ISO 62 (ASTM D570).

Tensile strength was determined according to ASTM D638. Statistical processing of experimental data was carried out using standard methods. [19]. To evaluate the degradation, the film samples were boiled in water and alkali solution, aged in the soil over a period of time. The changes in mass and mechanical properties were measured.

The microstructure of the samples was studied using optical MIN-8 (×200) and electronic GEOL GSM-35 microscopes. Structural changes were estimated by the IR spectroscopy method on the TENZOR-25 FTIR instrument in the absorption frequency range of 500-4000 cm^{-1}. The optical properties of the films were measured by a photoelectric colorimeter KFK-2-UHL4.2. The index of integral light transmission at the films thickness of 0.2-0.3 mm was calculated.

Preparation of powdered plasticized starch was carried out in the two-shafted open mixer at room temperature, mixing time 30 min, at 150 rpm. The standard contents of the plasticizer and lubricant for thermoplastic starch were used [16]. Glycerol and GMS were mixed using a magnetic stirrer at T=90°C until complete dissolution of GMS in glycerol. The blend of glycerine and GMS was added to starch after drying at T=80°C for 2 hours for final moisture content of 12% in the ratio of starch: 80:20.

Standard industrial approach of the introduction of plasticized starch into a polymer matrix was used. There are two common methods for incorporation such filler in to processing stream – buy production of ready to use compound or a masterbatch (concentrate) as part of composition. The compound can be processed in to article without any additional steps and offers best known mixing quality. The masterbatch method involves compound diluting with resin before processing and is commonly used in industry.

When preparing blends, the method of masterbatch was used since it is the simplest and widely used on industrial scale. The concentrate of plasticized starch with PE was obtained by preliminary mixing the resulting plasticized starch with PE powder in a high-speed Henschel mixer. The resulting powder mixture was processed on a laboratory twin-screw extruder D=22 mm, L/D=40 at the average processing temperature of 170°C.

Granular TPS and TPS film were obtained by the method [20] at temperature of 130°C on a single-screw extruder.

TPS masterbatches were mixed with LDPE grade 15803-020 in the ratio of 50:50 during the production of blown films. The diameter of the blowing die was 40 mm. Blow ratio was 2.5. The diameter of the extruder screw is 25 mm, the ratio L/D=28. Average processing temperature is 180°C. Target film samples thickness was 50±3 micron.

5 PROPERTIES OF TPS COMPOSITE BLOWN FILM

As a result of numerous experiments, more than 30 different concentrate recipes were tested. For further studies recipes with satisfactory rheological and technological properties were listed for evaluation. For comparative studies, a few numbers of representative compositions were selected for masterbatch production with planned TPS content of 50%, which is listed in Table 1.

The pure PE film produced in a same condition with the samples and TPS film produced by flat die extrusion was used for comparison.

The following masterbatches was produced:

№1 – (St/PE) powdered pure starch with polyethylene;

№2 - (TPS/PE) - powdered plasticized starch with polyethylene;

№3 - (TPS/PE/PE-g-MA) powdered plasticized starch with polyethylene and PE-g-MA compatibiliser;

№4 - (TPS/PE/PW) powdered plasticized starch with polyethylene and PE wax as wetting and dispersion additive;

№5 - (TPS/PE/FeSt) powdered plasticized starch with polyethylene in which the prodegradant ferric stearate was pre mixed with polyethylene component;

№6 – (TPS/FeSt/PE) powdered plasticized starch with polyethylene in which the prodegradant ferric stearate was pre mixed with starch composition.

Masterbatches were produced by strand granulation with water cooling, so after production step they were dried in air circulating oven and stored in water vapor barrier bags. After production general rheological and technological properties of the masterbatches were measured (Table 2).

Table 1 Composition of masterbatches and samples

№	Component	PE	TPS	Masterbatch composition					
				№1	№2	№3	№4	№5	№6
		Weight [%]							
1	PE 15803	100	–	50	50	50	50	49.8	50
2	PE-g-MA	–	–	–	–	5	–	–	–
3	Starch composition	–	100	–	50	45	40	50	50
	Starch	–	*80*	*50*	*40*	*36*	*32*	*40*	*39.6*
	Glycerine	–	*19*	–	*9.5*	*8.55*	*7.6*	*9.5*	*9.5*
	GMS	–	*1*	–	*0.5*	*0.45*	*0.4*	*0.5*	*0.5*
	Fe stearate	–	–	–	–	–	–	–	*0.4*
4	PE wax	–	–	–	–	–	10	–	–
5	Fe stearate	–	–	–	–	–	–	0.2	–

Table 2 General properties of granular masterbatches and samples

Properties	PE	TPS	№1	№2	№3	№4	№5	№6
MFI [g/10min]	2.6	0.15*	1.0	1.3	4.2	7.5	1.3	1.2
Density [kg/m^3]	925	1419	921	929	930	931	928	929
Bulk density [kg/m^3]	570	680	620	628	630	650	630	629
Water vapor absorption [%]	0.02	2.61	0.91	0.21	0.12	0.08	0.20	0.21

*MFI at 21.6 kg

Table 3 Film samples composition obtained from concentrates

	Component	**PE**	**TPS**	**Film sample**					
				№1	**№2**	**№3**	**№4**	**№5**	**№6**
		Weight [%]							
1	PE 15803	100	–	75	75	75	75	74,8	75
2	PE-g-MA	–	–	–	–	2.5	–	–	–
3	Starch composition	–	100	–	25	22.5	20	25	25
	Starch		*80*	*25*	*20*	*18*	*16*	*20*	*19.8*
	Glycerine		*19*	*–*	*4.75*	*4.28*	*3.80*	*4.75*	*4.75*
	GMS		*1.0*	*–*	*0.25*	*0.22*	*0.20*	*0.25*	*0.25*
	Fe stearate		*–*	*–*	*–*	*–*	*–*	*–*	*0.20*
4	PE wax	–	–	–	–	–	10.	–	–
5	Fe stearate	–	–	–	–	–	–	0.20	–

Table 4 The main properties of films obtained from concentrates

Properties	**Samples**		**Composite film samples**					
	PE	***TPS***	***№1***	***№2***	***№3***	***№4***	***№5***	***№6***
MFI [g/10min]	2.20	0.15*	1.1	1.6	5.4	6.5	1.6	1.7
Moisture absorption [%]	0.01	10.0	2.60	1.50	1.00	0.80	1.40	1.45
Density [kg/m^3]	925	1419	918	928	925	930	927	929
Tensile strength [MPa]	16.0	9.4	3.6	6.8	10.2	5.8	6.9	6.8
Elongation at break [%]	600	34	28	151	167	82	162	135

*MFI at 21.6 kg

Water vapor absorption of granular masterbatches and samples were measured at room temperature, 80% RH after 72 hour of open air storage. The results indicate the importance of vapor barrier packaging for such compounds.

MFI data show reduction comparative to native resin, highest reduction in composition of pure starch and less with plasticized starch. Visual appearance of composition #1 is milky white; all other composition is semi-transparent which can be potentially colored in desired way more freely.

Masterbatches were mixed with PE resin and processed in blown film, properties of film samples are listed in Table 3.

MFI, deformation-strength parameters as well as the degradation kinetics of obtained films in soil and stimulated medium were investigated (Table 4).

The film №1 has low quality surface appearance (matte surface) despite composition was produced on twin screw extruder. Other composition has much better surface gloss especially composition containing PE wax and compatibiliser which is valuable for film end use application in packaging area. The film №2 has a smooth outer surface, homogeneous in composition and characterized by slight turbidity. The film №3 is externally smooth with a glossy surface, homogeneous in composition and more transparent compared to the film №2 that may indicate a better compatibility of components of the blend. Improvement of mixing of components with the introduction of a compatibiliser MA-g-PE can be explained by the chemical interaction between the starch and PE molecules under the influence of high temperatures and shear during formation.

As for the film №4, PE wax reduces the viscosity of the system by wetting the particles of starch that provides more homogeneous distribution of components in the polymer volume. The appearance and properties of films №5 and №6 are similar to film №2 and ferric stearate is well dispersed in a polyethylene environment.

When PE-g-MA and PE wax are introduced in the films №3 and №4, MFI increases compared to the film №2 which leads to a better processing of blends. These films are sufficiently resistant to water; the degree of water absorption does not exceed 1.0%. This is of fundamental importance, since if the film is water resistant, thus when the film material enters the conditions of intense moisture, the physical and mechanical properties may deteriorate. Low degree of water absorption leads to the expansion of areas of the application of the films, moisture absorption of film from TPS is almost 10%.

It was established that the strength of the film №3 samples compared with the initial PE (see Table 4) decreases slightly and the strength of the films №2 and№4-6 is lower than the index of the initial PE and TPS. In case of the film №4 with a compatibiliser PE wax, there is a decrease in the tensile strength and relative elongation compared to other films because wax reduces intermolecular interaction in the system. It should be noted that the relatively high strength ratios in films with MA-g-PE compatibiliser confirms the improvement of the compatibility of the blend components.

In accordance with the established tasks, the kinetics of moisture absorption of the films in a humid environment was investigated. The obtained results are presented in the form of corresponding graphs of mass change of samples depending on their duration time in a humid environment (Figure 1).

Being under conditions of moisture, in all the samples, the growth of moisture absorption associated with the swelling of starch in the surface layers of the film is initially observed, after then the moister level was stabilized. The maximum equilibrium moisture absorption of films №3 and №4 is 1.5 times lower than of the films №2, №5 and №6, since the compatibiliser improves the compatibility of the blend components and reduces the access of moisture to the starch component.

In accordance with the research objective, the ability of the films degrade was studied. For this purpose, the behavior of property change in various mediums was studied. There was monitored the weight change of the samples, which were subjected to boiling in water and 0.1 N NaOH solution for 24 hours. The weight of the samples was determined in weight %. The results obtained are presented in the Figures 2 and 3.

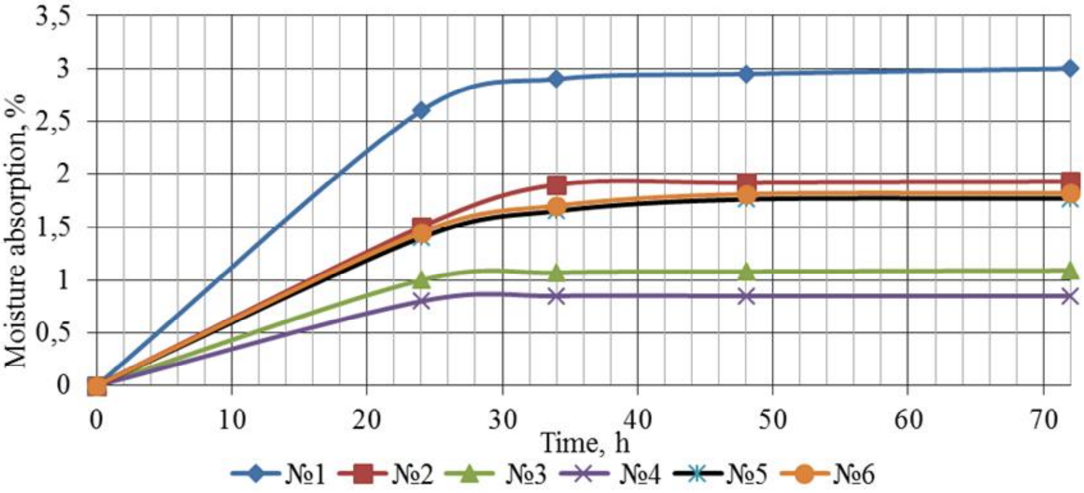

Figure 1 Dependence of moisture absorption of film samples №1-6 on duration time humid medium

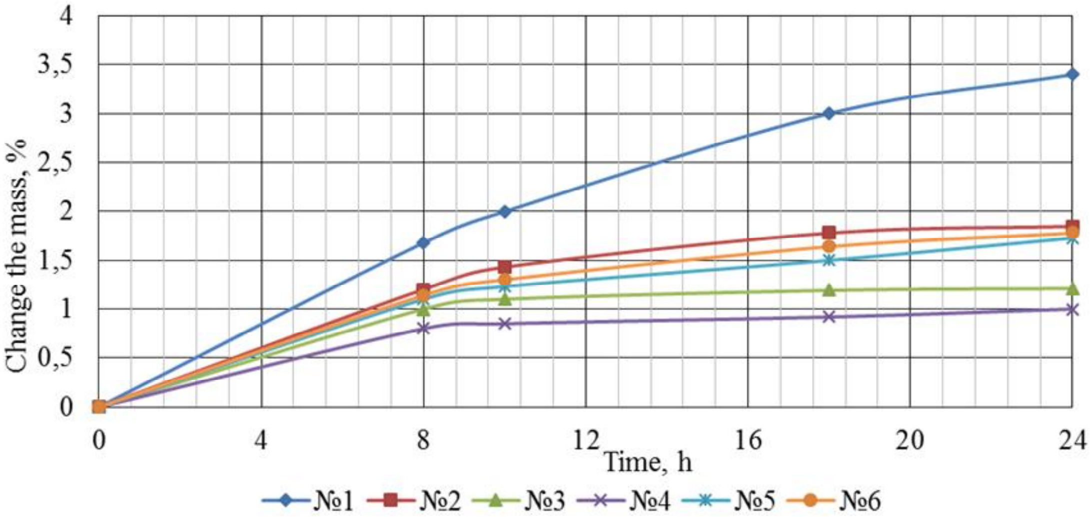

Figure 2 Mass changes of films samples №1-6 during boiling in water

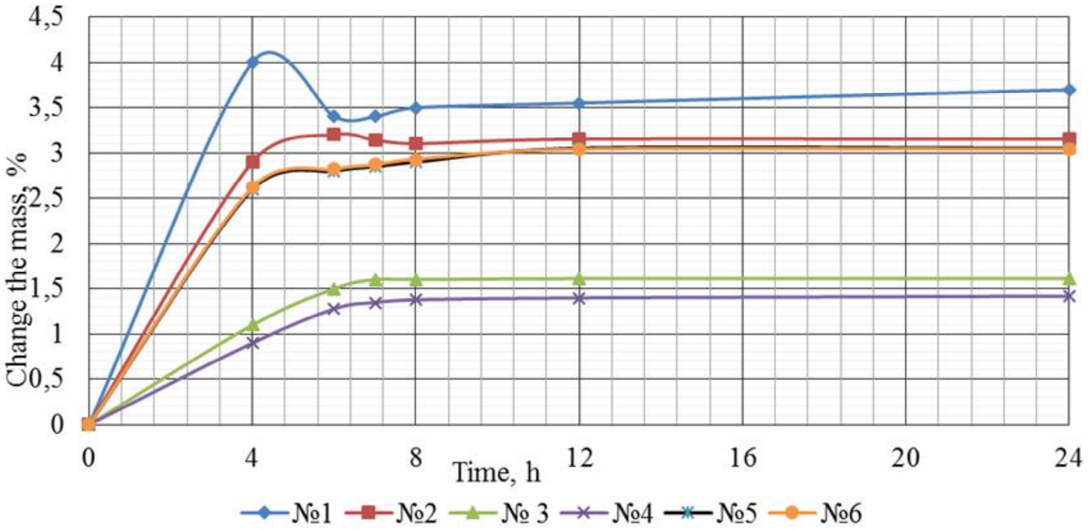

Figure 3 Mass changes of films samples during boiling in a 0.1 N solution of NaOH

When boiling in water all samples of films, there is a process of mass growth due to the swelling of the starch component. The comparative analysis of the films behavior during boiling in an alkaline medium (Figure 3) showed the following: the mass change of film samples №3 and №4 is almost two times less than for the films №2, №5 and №6, indicating that the starch is washed off intensively from films surface that do not contain a compatibiliser.

For film №1 there is a spike of a mass change after 4 hours of boiling as the possible result of a significant swelling of starch in alkaline solution. Further reduction of mass is related to the washing of starch from film №1.

The mechanical properties of the films after boiling in the stimulated medium were also determined.

The tensile strain at yield (δ) and tensile strain at break (ε) before and after boiling of films in water and 0.1 N NaOH solution are shown in Table 5.

The microstructure of samples of the film №3 was also studied before and after boiling hydrolysis using an optical microscope MIN-8 (×200).

In the Figure 4 one can see a clear boundary between the phases of the PE matrix - the starch grain in the initial film (a), indicating a relatively low compatibility between the matrix and the starch.

Table 5 Mechanical characteristics of films before and after 24 h boiling in different medium

Film	Initial values		After boiling in water		After boiling in 0.1N NaOH solution	
	δ	ε	δ	ε	δ	ε
PE	16.0	600	16.0	600	15.8	597
№1	3.6	28	3.0	18	2.2	18
№2	6.8	151	6.4	125	4.2	98
№3	10.2	107	9.9	94	7.9	90
№4	8.8	82	7.6	72	5.8	31
№5	6.9	162	3.6	61	2.8	76
№6	6.8	135	3.9	72	3.3	81

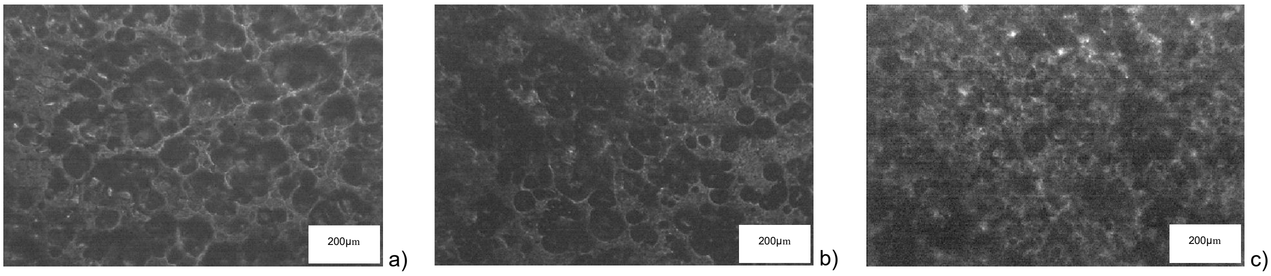

Figure 4 Microstructure of the film №3, a) before hydrolysis; b) after hydrolysis in water; c) after hydrolysis in 0.1 N solution of NaOH

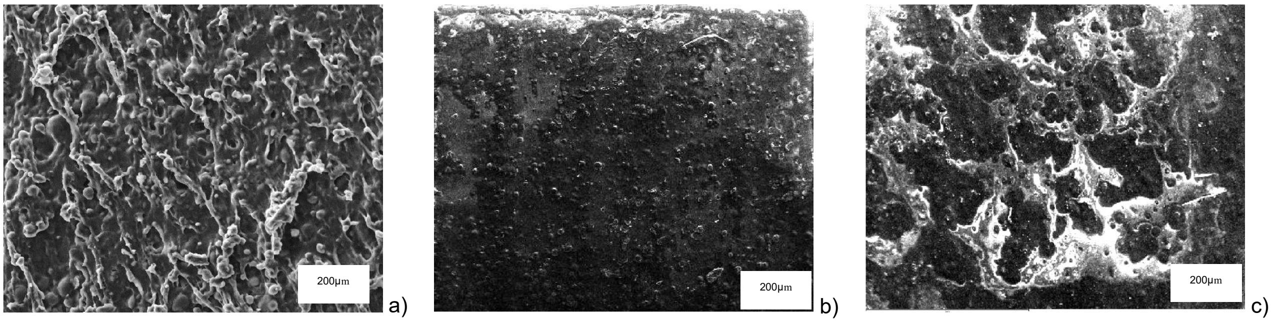

Figure 5 SEM images of films with different composition: a) TPS film; b) film №3; c) film №3 after boiling in 0.1 N solution of NaOH

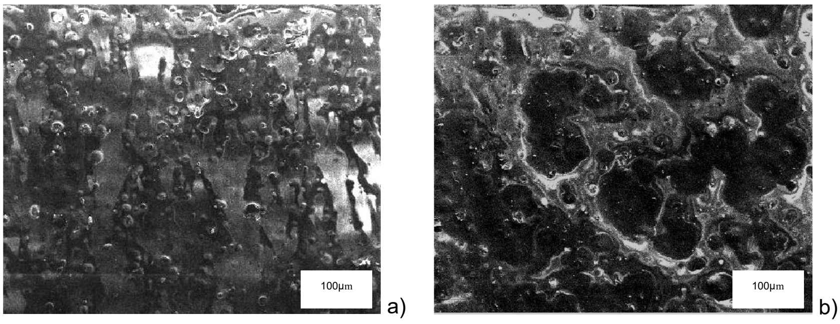

Figure 6 SEM images of film №3, an increase by 100 µm: a) film №3; b) film №3 after boiling in 0.1 N solution of NaOH

Boiling in distilled water (b) causes minor changes on the surface of the film due to partial starch washing off. After boiling in a 0.1 N solution of NaOH (c), the boundaries of the phase separation become more blurry, indicating a process of more intense washing of starch from the surface layers of the film. The starch in the inner layers remains encapsulated in the PE. In Figures 5 and 6 are SEM images of the films with different composition.

Figure 6 shows the SEM images for film №3 before and after boiling in 0.1 N solution of NaOH.

As for the film sample №3, the effect of the alkalis is characterized by a smoother surface, without cavities, and after boiling, there is sight of porous structure, indicating the formation of erosion and washing of starch from the surface layers.

From the figures it is seen that the structure of the polymer material is heterogeneous: the starch grains are permeated with the "threads" of the polymer binder and in the surroundings of each grain (or agglomerate of grains) there is a shell formed by a film based on synthetic PE. In addition, there is a fairly large number of pores in the material structure that makes the material potentially accessible to the effect of moisture and microorganisms.

Infrared spectra of the films are presented in Figure 7. For the study, film №3 and film №3 after boiling in 0.1 N solution of NaOH and PE and TPS films were selected for comparison. On spectra (samples 1-3), in the frequency range 1302-1076 cm^{-1}, there are characteristic peaks of starch absorption [13]. The introduction of plasticized starch into PE leads to a peak shift at a frequency of 888 cm^{-1} to the frequency range of 861-853 cm^{-1}. The intense absorption peak in the range 3400-3100 cm^{-1} corresponds to the -OH groups [21].

The mark of PE degradation is absorption peak at a wavelength of 1760 cm^{-1} on the IR spectrum. After boiling of the film №3 in 0.1 N solution of NaOH, no significant changes were noted. Therefore, it is expedient to introduce in the composition of TPS/PE films degradation catalysis ferric stearate II, which initiates the decomposition of PE matrix under the influence of light, oxygen and temperature (Figure 8). In Figure 8, there is an intense absorption and at a wavelength of 1760 cm^{-1} (curve 3), indicating PE component degradation.

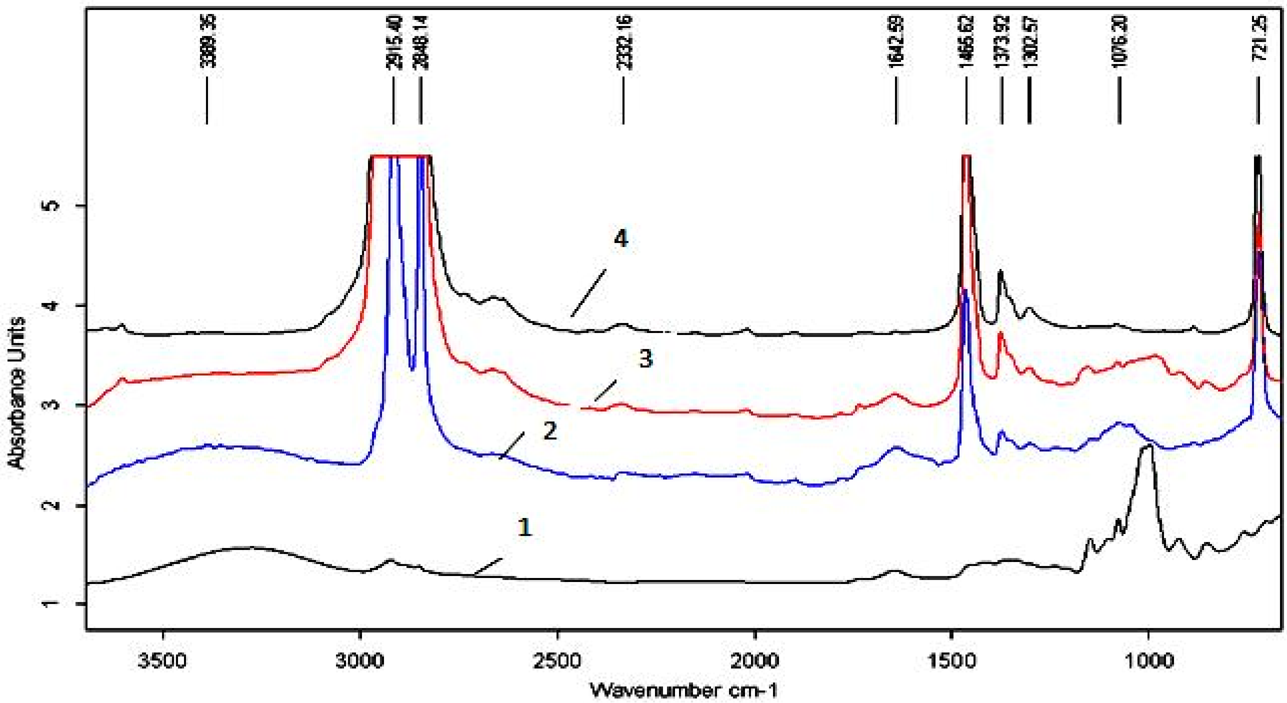

Figure 7 Infrared spectra of films: 1) TPS film; 2) film №3 after boiling in 0.1 N solution of NaOH; 3) film №3; 4) PE film

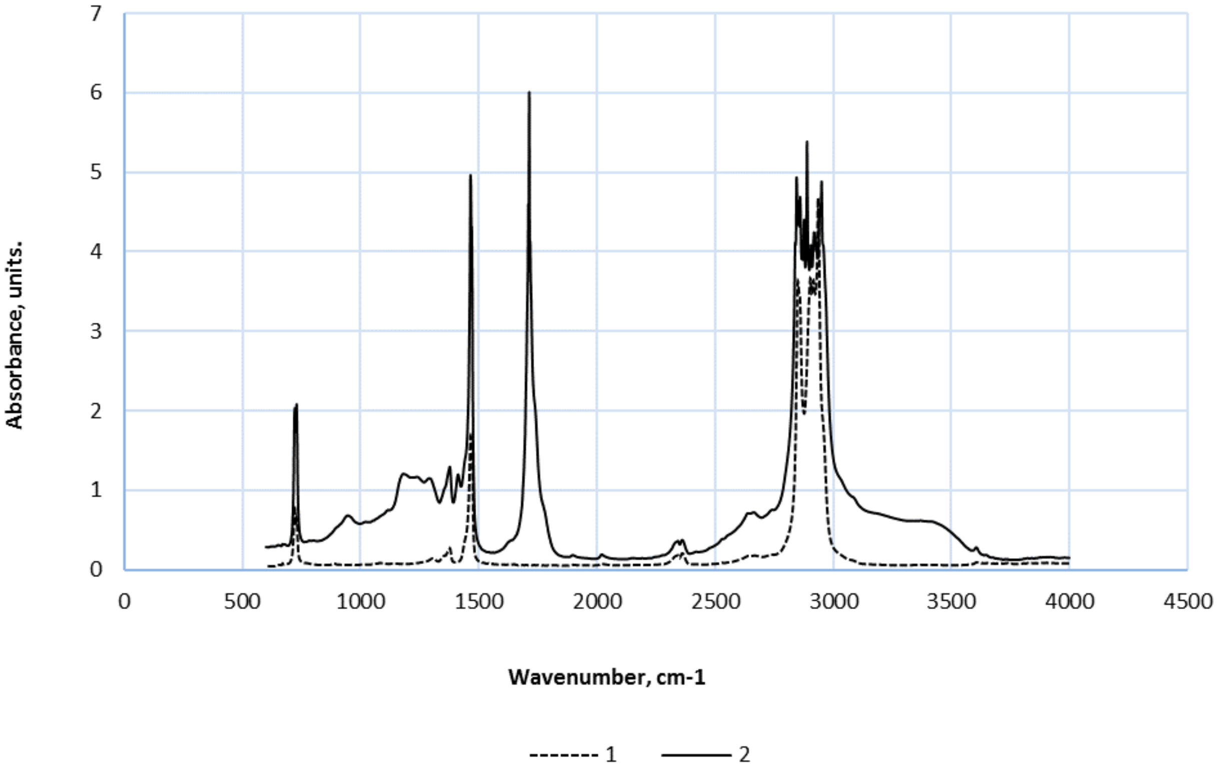

Figure 8 IR film spectra: 1) PE film; 2) film №5

Loss of the films mass after incubation in the soil (cultivated soil, pH=6.5, temperature 20-25°C, humidity 60%) is presented in Table 6.

Table 6 Change in the mass of film samples after incubation in soil

Films	**Change the mass [%]**		
	20 days later	***40 days later***	***60 days later***
№1	+3.6	-1.2	-4.6
№2	+3.7	-1.4	-4.9
№3	+1.9	+0.5	-1.7
№4	+1.6	+0.3	-1.0
№5	+3.8	-1.5	-6.7
№6	+3.6	-1.6	-7.0

After 20 days of incubation of films in the soil, the mass increases as a result of swelling of the starch component. After 40 days of exposure, they have signs of biodegradation of starch component 10-15% of the film area. After 60 days of incubation, a decrease in the mass of the films is noted as a result of the biodegradation of starch.

The low ability of the investigated films to biodegrade in the soil may be due to the following. It is known that the biodegradation of films in soil is mainly on the surface enriched with starch. With low content of starch (up to 20%), its particles remain encapsulated in the polymer and therefore are hard to reach for the microorganisms. The process of biodegradation is slowing down. The second reason that reduces the ability of films to biodegrade is an increase of the barrier properties due to the presence in a system of a compatibiliser or a wax. It should be noted that the initial PE was not biodegradable throughout the study period.

Analysis of the results of studies of the mechanical properties of films after incubation in soil showed that after 60 days in the soil for films №5 and №6, the relative tensile strain at break is significantly reduced by 80-88%. This is due to the acceleration of the PE matrix degradation by the degradation catalysis and the diffusion of moisture into the inner layers of the film that is a characteristic feature of the polymer film degradation (Table 7).

Table 7 Mechanical characteristics of films after incubation in soil

Film	**initial**		**20 days**		**40 days**		**60 days**	
	δ	***ε***	***δ***	***ε***	***δ***	***ε***	***δ***	***ε***
PE	16.0	600	16.0	600	16.0	600	16.0	580
№1	3.6	28	3.3	16	2.9	16	2.4	13
№2	6.8	151	6.2	148	5.2	121	4.7	108
№3	10.2	107	9.5	93	9.3	60	8.5	51
№4	5.8	82	5.5	78	5.3	61	4.9	49
№5	6.9	162	5.6	89	4.4	42	3.1	20
№6	6.8	135	6.0	84	5.0	48	3.4	28

Optical surface images of films at different stages of incubation in the soil (before incubation, after 20 days and 40 days) are presented in Figure 9 (a, b, c - respectively).

The samples of films №3 (upper row) and №4 (bottom row) were studied. It is evident that two-phase structure is characteristic for both types of films. However, the morphology of the samples varies. In the film №3 mainly observed individual grains, starch particles which are fairly evenly distributed in the volume of the PE matrix. The structure of such film is homogeneous that, apparently, determines its higher mechanical performance.

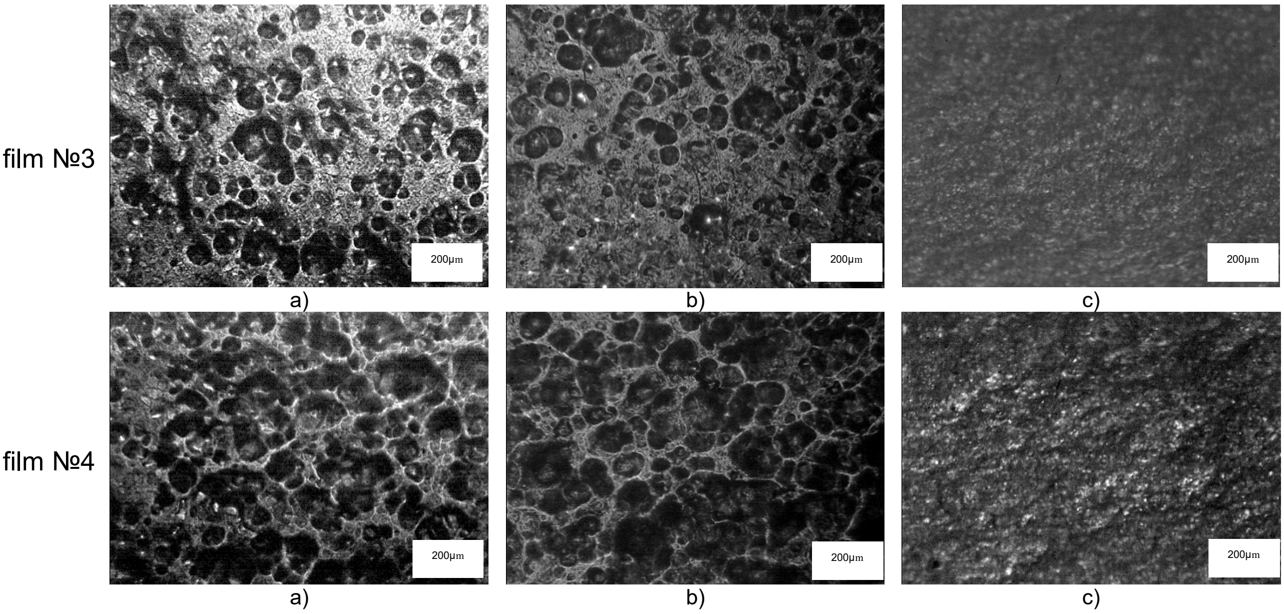

a) b) c)

a) b) c)

Figure 9 Surface images of films (×200) with different incubation duration; a) the original sample; b) after 20 days; c) after 40 days

For the film №4 a structure with significant defects is observed. This is due, first of all, to the aggregation of starch particles as they have varying lengths, and there is an uneven distribution of these aggregates in the PE matrix. Such structural features may indicate a low compatibility of the PE matrix with the starch particles.

After 20 days of incubation in the soil in the structure of the film №3 there is a decrease in the number of starch particles, that is, their biodegradation begins in the surface layers of the film. As for film №4, the process of biodegradation is slower; there is only a partial degradation of starch aggregates and appearance of individual grains of a bio component.

After 40 days of stay of both types of films in the soil, their structure undergoes some changes. The boundaries between the phases are blurred or virtually absent. It can be assumed that the process of biodegradation of starch in the surface layers of the film is almost complete. Removing starch from the outer layers of the films leads to a reduction in pores and defects associated with starch particles that extend to the surface of the samples. The stiffness of the films decreases, a smoother surface appears. Further, the destruction process will occur due to starch particles that are already located in the inner layers of the film. This process is much slower, since the access of microorganisms inside the film is much smaller than that to the surface layers.

Optical properties of films were studied. The index of integral light transmission at the thickness of films combined layer 0.1 mm (Table 8) was calculated.

Table 8 Optical properties of films

Films	Coefficient of integral light transmission [%]
PE	88
TPS	64
№1	52
№2	67
№3	83
№4	79
№5	68
№6	69

It was found that the samples containing MA-g-PE and PE wax are more transparent than the original ones which is a technologically favorable factor, but on the other hand, they are less prone to degradation in the environment.

6 DISCUSSION ABOUT THE RESEARCH FINDINGS

Starting from general idea of researching the modern methods of production of degradable PE films, an attempt to introduce degradable filler, like native starch into PE matrix, was made. The obtained film (the film №1) was characterized by an uneven distribution of the filler in the matrix, low mechanical properties and transparency.

The next step was to obtain films based on a mixture of PE with plasticized starch (film №2). In this case, there was a noticeable improvement in the structure of the film, smooth surface, partial transparency, but mechanical properties were still quite low.

Therefore, the next stage is the introduction of modifiers which due to their compatibilising effect of various nature, allow to improve the mechanical properties of the films obtained (the films №3 and №4). In addition, MA-g-PE acts as chemical compatibiliser, due to the interaction of reactive functional groups with hydroxyl groups of starch that positively affects the strength of the resulting film. PE wax acts as a physical compatibiliser i.e. lubricant and viscosity regulator of the PE-plasticized starch system improving production effectiveness while processing, although the tensile strain at yield and tensile strain at break in this case are somewhat lower compared to film №3.

All the results of experiments allowed to obtain films with acceptable for end application mechanical properties, good production effectiveness, but not significant accelerated degradation, since the degradation and washing of starch was observed mainly in the surface layers of films. Therefore, it was decided to introduce another modifier into the developed system - degradation catalysis for the PE matrix ferric stearate II (the films №5 and №6) which greatly accelerates the process of joining oxygen to PE macromolecules, and enhance oxidative degradation. The result of its action is the intensification of the degradation processes of the PE matrix under the influence of light or temperature [15]. Thus, as a result of a series of experiments, it was possible to obtain a blown film that is capable of accelerated degradation under the ambient conditions and can be used to make a wide range of packaging materials.

7 CONCLUSIONS

1. The influence of various modifiers on the properties of PE/TPS blown films was studied. It was established that the use of compatibilisers allows to improve the technological properties of the films, transparency through the improvement of the compatibility of the components. There is an increase in the mechanical properties of the film №3 containing MA-g-PE modifier in 1.5 times and a decrease in moisture absorption by 30% compared to the unmodified film №2 (a blend of polyethylene with plasticized starch) due to the encapsulation of starch in the inner layers of the film. The film №4 containing PE wax as modifier has a lower moisture absorption of 47% and a higher index of integral light transmission (79%) compared to the film №2 (67%).

2. The peculiarities of the degradation of PE/TPS blown films in different stimulated mediums were studied. It was found that the ability to accelerated degradation in the environment for the films №3 and №4 is observed predominantly in the surface layers. For the film №3 after being in the soil, there is a decrease in tensile strain at yield by 17% and of tensile strain at break by 52%. For the film №4, respectively, 16% and 40%. The films №5 (a blend of polyethylene with plasticized starch and ferric stearate introduced into polyethylene) and №6 (a blend of polyethylene with plasticized starch and ferric stearate introduced into starch) after incubation in the soil for 60 days, 50 to 55% lose tensile strain at yield and 80-88% - tensile strain at break. Such significant losses of mechanical properties of films are due to the presence in them of a ferric stearate II, which initiates the degradation of the polyethylene component and promotes the degradation of starch in the inner layers of the film.

8 REFERENCES

1. Pogrebnyak I.L.; Sova N.V.; Savchenko B.M.; Pakharenko V.A.; Moisyuk V.S.: A wood-filled composite based on recycled polyethylene terephthalate. Production and properties, International Polymer Science and Technology 42(1), 2015, pp. 41-43
2. Medina-Jaramillo C., Ochoa-Yepes O., Bernal C., Famá L.: Active and smart biodegradable packaging based on starch and natural extracts, Carbohydrate Polymers 176(15), 2017, pp. 187-194, https://doi.org/10.1016/j.carbpol.2017.08.079
3. Sudhakar Y., Selvakumar M.: Lithium perchlorate doped plasticized chitosan and starch blend as biodegradable polymer electrolyte for super-capacitors, Electrochimica Acta 78(1), 2012, pp. 398-405, https://doi.org/10.1016/j.electacta.2012.06.032
4. Cazón P., Velazquez G., Ramírez J., Vázquez M.: Polysaccharide-based films and coatings for food packaging: A review, Food Hydrocolloids 68, 2017, pp. 136-148, https://doi.org/10.1016/j.foodhyd.2016.09.009
5. Rybkina S.P., Pakharenko V.V, Bulakh V.Yu., Pakharenko V.A.: Biodegradable packaging materials based on polysaccharides (starch), International Polymer Science and Technology 40(6), 2013, pp. 43-48, https://doi.org/10.1177/0307174X1304000609
6. Beloshenko V., Voznyak Y., Voznyak A., Savchenko B.: New approach to production of fiber reinforced polymer hybrid composites, Composites Part B: Engineering 112(1), 2017, pp. 22-30, https://doi.org/10.1016/j.compositesb.2016.12.030
7. Bulakh V., et al.: Polyethylene compositions with starchy and other fillers. Double effect in decomposition, Chemical Industry of Ukraine 5, 2012, pp. 34-40, (in Ukraine)
8. Nguyen D.M., Do T.V.V., Grillet A.-C., Ha Thuc H., Ha Thuc C.N.: Biodegradability of polymer film based on low density polyethylene and cassava starch, International Biodeterioration & Biodegradation 115, 2016, pp. 257-265, https://doi.org/10.1016/j.ibiod.2016.09.004
9. Ortega-Toro R., Contreras J., Talens P., Chiralt A.: Physical and structural properties and thermal behaviour of starch-poly(ε-caprolactone) blend films for food packaging, Food Packaging and Shelf Life 5, 2015, pp. 10-20, https://doi.org/10.1016/j.fpsl.2015.04.001
10. Nguyen Vu H.P., Lumdubwong N.: Starch behaviors and mechanical properties of starch blend films with different plasticizers, Carbohydrate Polymers 154(10), 2016, pp. 112-120, https://doi.org/10.1016/j.carbpol.2016.08.034
11. Mortazavi S., Ghasemi I., Oromiehie A.: Effect of phase inversion on the physical and mechanical properties of low density polyethylene/thermoplastic starch, Polymer Testing 32(3), 2013, pp. 482-491, https://doi.org/10.1016/j.polymertesting.2013.01.004
12. Siracusa V., Rocculi P., Romani S., Dalla Rosa M.: Biodegradable polymers for food packaging: a review. Trends in Food Science & Technology 19(12), 2008, pp. 634-643, https://doi.org/10.1016/j.tifs.2008.07.003
13. Mendes J.F., Paschoalin R.T, Carmona V.B., Sena Neto A.R., Marques A.C.P., Marconcini J.M., et al.: Biodegradable polymer blends based on corn starch and thermoplastic chitosan processed by extrusion, Carbohydrate Polymers 137(10), 2016, pp. 452-458, https://doi.org/10.1016/j.carbpol.2015.10.093
14. Khanoonkon N., Yoksan R., Ogale A.: Effect of stearic acid-grafted starch compatibilizer on properties of linear low density polyethylene/thermoplastic starch blown film, Carbohydrate Polymers 137(10), 2016, pp. 165-173, https://doi.org/10.1016/j.carbpol.2015.10.038
15. Gilfillan W.N, Moghaddam L., Bartley J., Doherty W.: Thermal extrusion of starch film with alcohol, Journal of Food Engineering 170, 2016, pp. 92-99, https://doi.org/10.1016/j.jfoodeng.2015.09.023
16. Bulakh V., et al.: Thermoplastic starch. Obtaining, properties, recycling, Chemical Industry of Ukraine 3, 2011, pp. 28-30, (in Ukraine)
17. Sailaja R., Seetharamu S.: Itaconic acid – grafted – LDPE as compatibilizer for LDPE – plasticized Tapioca starch blends, Reactive and Functional Polymers 68(4), 2008, pp. 831-841, https://doi.org/10.1016/j.reactfunctpolym.2007.12.003
18. Sleptsov O., Sova N., Savchenko B.: Grafted polyolefins. Obtaining, properties and applications, Chemical Industry of Ukraine 3-4, 2016, pp.62-64, (in Ukraine)
19. Sova N., Savchenko B., Plavan V., Beloshenko V.: Methods of creating environmentally safe polymer packaging in Ukraine, Packing 4, 2017, pp. 31-34, (in Ukraine)
20. Bulakh V., Sova N., Savchenko B.: Features of recycling of thermoplastic starch, Chemical Industry of Ukraine 5-6, 2016, pp. 56-58, (in Ukraine)
21. González-Cruz L. Montañez-Soto J.L., Conde-Barajas E., et al.: Spectroscopic, calorimetric and structural analyses of the effects of hydrothermal treatment of rice beans and the extraction solvent on starch characteristics, International Journal of Biological Macromolecules 107, Part A, 2018, pp. 965-972, https://doi.org/10.1016/j.ijbiomac.2017.09.074

THE USE OF THE MODIFIED STARCH IN BIOLOGICALLY ACTIVE SYSTEM

Olena Ishchenko[1], Olga Sumska[2], Viktoriia Plavan[1], Irina Liashok[1] and Illya Resnytskyi[1]

[1]Kyiv National University of Technologies & Design, 2, Nemirovich-Danchenko str. Kyiv, 01011, Ukraine
[2]Kherson National Technical University, Beryslavskoe highway, 24 Kherson, Ukraine
e.ishchenko5@gmail.com; sumskaetdt@gmail.com

***Abstract:** A biologically active system based on modified starch and quaternary ammonium salt has been studied. The influence of QAS on the rheological properties of CMS solutions has been investigated. Antimicrobial activity of textile materials treated with warehouse on the basis of CMS was studied. The formation of chemical bonds between functional groups of carboxymethylated starch and cationic bactericidal preparation is established by IR spectroscopy.*

***Keywords:** biologically active systems, modified starch, fungicidal activity, bactericidal properties.*

1 INTRODUCTION

The concept of "biological activity" covers a wide range of the phenomena. From the point of view of chemical exposure, biologically active agents (BAA) are understood as substances that can act on the biological systems (including the human body), regulating their vital functions [1]. The use of polymeric systems allows to impart BAA absolutely new properties and to increase their efficiency considerably. Besides, high-molecular connections can have biological activity at the expense of the macromolecular nature. At the present time, the development and research of new biologically active systems (BAS) obtained on the basis of polymers and intended for the use in the medicine [2], plant growing and livestock production, biotechnology [3], the food and cosmetic industry [4] are intensively carried out in many laboratories of the world.

One of current trends of the world state in the field of the use of polymers in the BAS is a production and a consumption of textile materials with antimicrobial properties [5].

Despite the improvement quality of life, hygienic education, observance of rules of personal hygiene, the incidence caused by microorganisms remains high without visible tendency to decrease, especially at close contact between people. The quality of life and work of a large number of people in the conditions which aren't providing the appropriate level of hygiene (transport, shift work, expeditions, field conditions of the military personnel, rescue efforts) or connected with increased requirements to microbiological safety (medical institutions, pharmaceutical and food productions) can be improved considerably by the use of biocidal protection of textile materials [1, 5, 6].

One of ways of receiving such materials is the formation of the BAS. Earlier fabrics were given antimicrobial properties due to processing by their antiseptic agents however such protection was temporary, as through several washings the agent was completely washed away. Now, thanks to the formation of the BAS, there was an opportunity to create textiles with antibacterial properties, steady against numerous washings. There is a set of the ways of creation the BAS influencing microorganisms on different mechanisms.

Their biocidal activity can be connected with initial structure of polymer, is caused by its chemical modification or introduction to structure of polymer of organic or inorganic antimicrobial agents [7], for example, silver ions [8]. Now the large number of BAA is known [9]. Nevertheless, in many cases a possibility of application of the known BAA use insufficiently, quite often with the efficiency far from maximum. It is possible to carry the quaternary ammonium salts (QAS) to such BAA.

It should be noted that the use for formation of the BAS is QAS rather perspective. Quaternary ammonium salts are capable to be attached to walls of cages of bacteria and to destroy them from within. The effect of bacterial action is gained thanks to a positive charge which is born by their molecules, at the expense of it they are attracted to an external surface of the bacterial membrane loaded negatively [4]. Though the effect of substitution of quaternary ammonium salts of other positively charged ions isn't so high, it appears enough for destabilization of a microbe [8].

As it is established by researches [10], these defects can be eliminated or their role can be considerably lowered when using BAA in the form of chemical compounds with certain carriers or modifiers as most of which often use various polymers.

Authors [10] propose a method based on thiol-epoxy click chemistry to achieve durable antibacterial properties on cotton fabrics. The cotton fabric was first modified with 3-mercaptopropyltriethoxysilane (KH-580) to introduce thiol groups. Then, cotton fabric was treated with a quaternary ammonium salt by thiol-epoxy click chemistry. The results demonstrated that such treatment provides durable antibacterial properties for cotton fabric due to the chemical bonding formed between the quaternary ammonium salt and the substrate.

Proceeding from this, the purpose of the work was developing of BAS applying of carboxymethylated starch and quaternary ammonium salt as biologically active agents.

2 MATERIALS AND METHODS

As the textile carrier have been used cotton coarse calico an art. 264 and a gauze art. 033.

As a polymeric matrix for biocidal medicine was used carboxymethylated starch (Na-CMS) (TU U 6-04872 671.061-96).

BAA is a quaternary ammonium salt $[R(CH_3)_2NCH_2C_6H_5]^+Cl^-$ (CAS №: 21954-74-5).

Classical single-bath processing methods were used to give the antimicrobial activity to cotton fabrics. In the same finishing bath both film former and antibacterial substances were dissolved. Cotton fabrics were applied to that solution for 1 minute, then they were pressed to achieve 100% humidity and dried step by step.

To evaluate the rheological properties of the composition a rotating viscosimeter "Rheotest-2" was used at shifts in the range γ = 3 - 1312 s^{-1}. BAS sorption was determined by mass method.

The efficiency of antimicrobial finishing was estimated by means of a test method on the dense environment to an action of pathogenic bacteria: Escherichia coli, Bacillus subtilis and Staphylococcus aureus (received from a collection of Institute of microbiology and virology of Ukraine). Processing of results was carried out for bacteria in 2-6 days and for mushrooms in 5-7 days. It was considered bactericidal and bacteriostatic effect of substances which contain in fabric.

For our research we use IR-Fure's device spectrometer THERMO Nicolet mark AVATAR 370 FT IR (range of wavelengths 400-4000 cm^{-1}), crystal ZnSe, compressed sample from KBr.

Main objective of the work was formation of the BAS which would eliminate such lack of textiles with antimicrobial processing as low resistance of bactericidal effect to repeated washings.

Such chemical compound actually is a new biologically active polymer (I), a different chemical structure from initial polymer carrier, in the case studied by us is the scheme of formation of a new BAA.

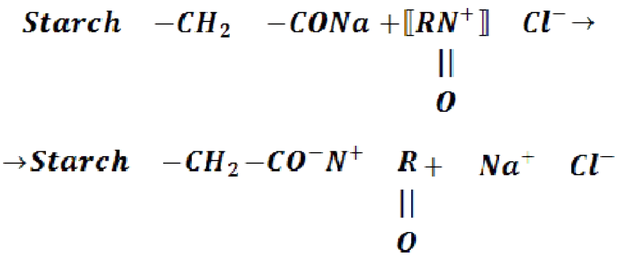

$$Starch\ -CH_2\ -\underset{\underset{O}{||}}{C}ONa + [\![RN^+]\!]\ Cl^- \rightarrow$$

$$\rightarrow Starch\ -CH_2-\underset{\underset{O}{||}}{C}O^-N^+\ R + \ Na^+\ \ Cl^-$$

At the same time, it is possible to assume that ionic bond of QAS with the polymeric carrier (Na-CMS) can be steady during functioning of biologically active polymer (such polymers often call systems with the immobilized, that is "immobilized" BAA).

3 RESULTS AND DISCUSSION

A prerequisite for the formula of a composition for tissue processing is the availability of data on the nature of the dependence of the system viscosity on the concentration of the polymer. In this work, rheological research was carried out and the dependence of the initial viscosity (η_0) Na-CMS on the concentration of dry matter (C) was calculated according to the equation (1):

$$\eta_0 = K.C^{\alpha} \qquad (1)$$

where $K = 19.5.10^{-4}$ and $\alpha = 3.35$.

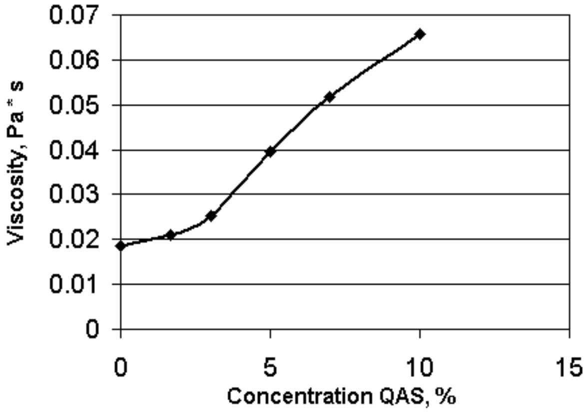

Figure 1 Influence of QAS supplements on the rheological properties of Na-CMS solutions at γ = 243 s^{-1}

The change in effective viscosity across the studied range of shift velocities has been calculated. The dependence of the effective viscosity (η_e) of the polymer composition on the shift rate (γ, s^{-1}) and the initial viscosity (η_0) can be expressed by equation (2) (correlation coefficient R = 0.918 for a concentration of 3%)

$$\eta_e = \eta_0 / [1 + 1.79(\eta_0 \cdot \gamma)^{0.47}] \qquad (2)$$

During the study of Na-CMS-QAS flow curves, it was found that the addition of QAS leads to a decrease in the area of the hysteresis loop, which is presented in Figure 2).

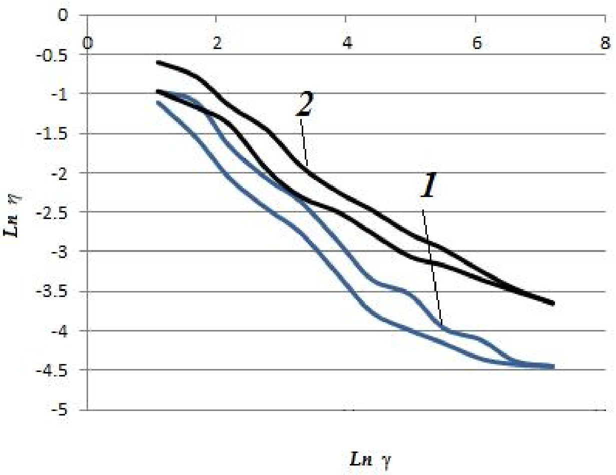

Figure 2 Rheological properties of solutions 1. Na-CMS 30 g/l; 2. Na-CMS 30 g/l, QAS 7 g/l;

The magnitude of the degree of thixotropic restoration of viscosity was calculated by the formula:

$$S = \frac{\Sigma \eta_{1i}}{\Sigma \eta_{0i}} \cdot 100\% \qquad (3)$$

where S - degree of thixotropic restoration of the viscosity of solutions;

η_{1i} - is the viscosity at the i-th shift velocity, measured in the gradient mode of the decreasing rate of speed;

η_{0i} - is the viscosity at the i-th shift velocity, measured in the gradient mode of the increasing velocity;

i - speed of the shift;

n - the number of fixed values of the gradient of the rate of displacement.

The values of S for solutions of starch, Na-CMS and Na-CMC concentrations of 1-3% are presented in Table 1.

Table 1 The magnitude of the degree of thixotropic restoration of viscosity

Polysaccharide	S [%]		
	Concentration of polysaccharide		
	1%	2%	3%
Starch	87.9	83.2	74.6
Na-CMS	92.5	91.8	90.2
Na-CMS + QAS	93.8	92.6	92.3

The rheological properties of 1-3% solutions of Na-CMS and Na-CMS+QAS in the range of shift velocities from 3 to 1312 s^{-1}, the viscosity of the solutions is subject to the step-by-law and is described by the Ostwald-de-Vila equation. It has been established that the modified starch-based compositions form 1-3% of solutions, which are characterized by a sufficiently high degree of thixotropic restoration of viscosity (90.2 - 93.8%).

The kinetic dependence of an experimental additional weight of the BAS on the textile carrier depending on time of contact of phases has been defined: the influence of quaternary ammonium salt on sorption of starch and the modified starch cotton fabric. Results are presented in Figure 2.

Analyzing the sorption curves, it was established that the degree of sorption of the composition using Na-CMS and QAS is higher in mass terms by 0.0025 g/g fibers, compared with Na-CMS, and 0.0010 g/g fiber, if starch is used as a polymer carrier.

Thus, when giving an antimicrobial finish by dressing with a composition containing BAS, a sorption of the compound takes place from the coupling agent (Starch – CH_2 – CO – QAS).

The efficiency of the BAS, realized technically by the padding method has been defined. Results are represented in Table 2.

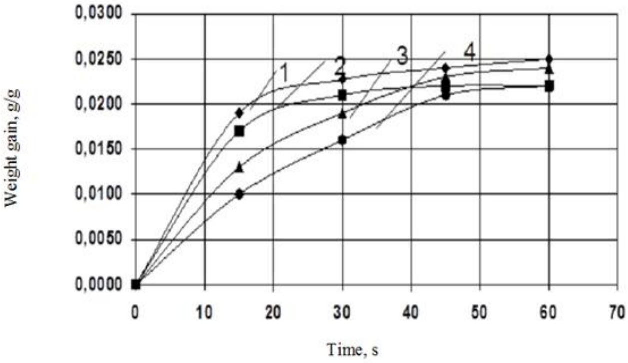

Figure 3 Kinetic dependence of an experimental additional weight of the BAS on the textile carrier depending on time of contact of phases:
1. Na-CMS 30 g/l, QAS 7 g/l; 2. Na-CMS 30 g/l; 3. starch 30 g/l, QAS 7 g/l; 4. starch 30 g/l

Testifying data of the Table 2 reveals the selective influence of the BAS on the basis of Na-CMS and QAS on gram-positive (Bacillus subtilis, Staphylococcus aureus) and gram-negative (Escherichia coli) bacteria. None of the samples gave sterile zones (bactericidal action) on the lawns of Escherichia coli. For this type of bacteria, the samples acted bacteriostatically (delayed growth of the culture).

Analyzing the received results, it is possible to draw a conclusion that despite a large number of scientific works in the field of formation of the BAS, the mechanism of their action isn't quite clear.

But probably, in the presence of a small amount of moisture there is a slow hydrolysis and continuous transition of the bactericidal reagent connected with functional groups of the polymer applied on fabric. With direct contact of the chipping-off reagent with microbes there is a suppression of their activity.

Transmittance spectrums of Na-CMS and Na-CMS + QAS are presented in Figures 4 and 5.

Characteristic bands clearly seen on spectra, indicating the existence of links -C-H (frequency of oscillations is close to 2890 cm^{-1}, the band is relatively small intensity), groups –OH (frequency of oscillations is close to 3290-3550 cm^{-1}, wide bands of sufficiently high intensity, which indicate the presence of intermolecular hydrogen bonding and is characteristic of chelate compounds), carbonyl groups (frequency of oscillation is close to 1600 cm^{-1}, the band is relatively small intensity) and carbon – carbon bonds in the corresponding compounds. Fluctuations in a simple etheric connection are not characteristic, but on an area with a frequency closed to 1000 cm^{-1} an intensive band appears due to the participation in the oscillation of the polar bond -C-O.

Table 2 Antibacterial and fungicide activity of the BAS on the basis of Na-CMS and QAS

Preparation	Concertation [g\l]	Way of processing a fabric	Escherichia coli		Bacillus subtilis		Staphylococcus aureus		Fusarium oxysporum
			BC	BS	BC	BS	BC	BS	BC
-	-	-	0	0	0	0	0	0	0
	7	impregnation, drying	0	5	1	0	3	0	1
QAS	7	impregnation, drying, washing	0	4	1	0	3	0	1
Na-CMS	30	dressing	0	3	0	0	1	0	1
Na-CMS	30	dressing, washing	0	1	0	0	0	0	0
Na-CMS QAS	30 7	dressing	0	10	3	0	1	0	1
Na-CMS QAS	30 7	dressing, washing	0	5	2	0	1	0	1
Starch	30	dressing	0	0	0	0	0	0	0
Starch QAS	30 7	dressing, washing	0	4	0	0	3	0	1

Note: BC is a bactericidal activity; BS is a bacteriostatic activity; "0" – the activity is absent; "-" – didn't defined.

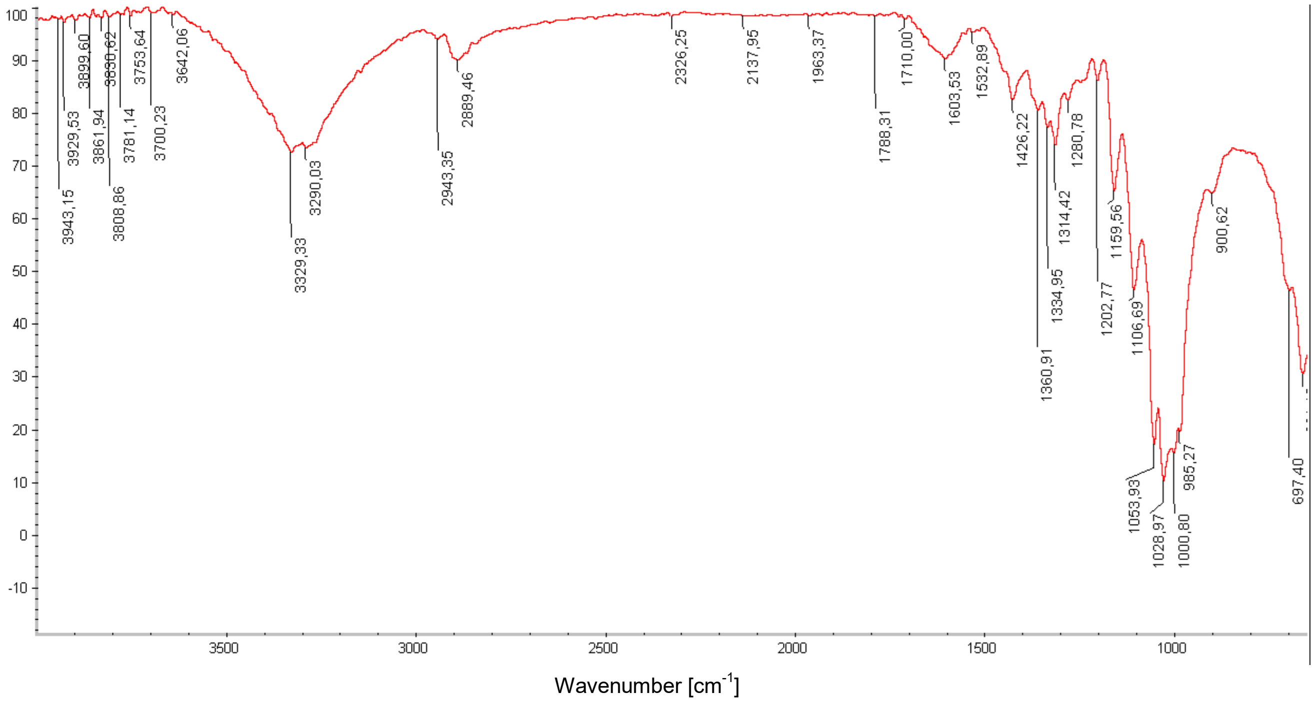

Figure 4 Transmittance spectrum of Na-CMS

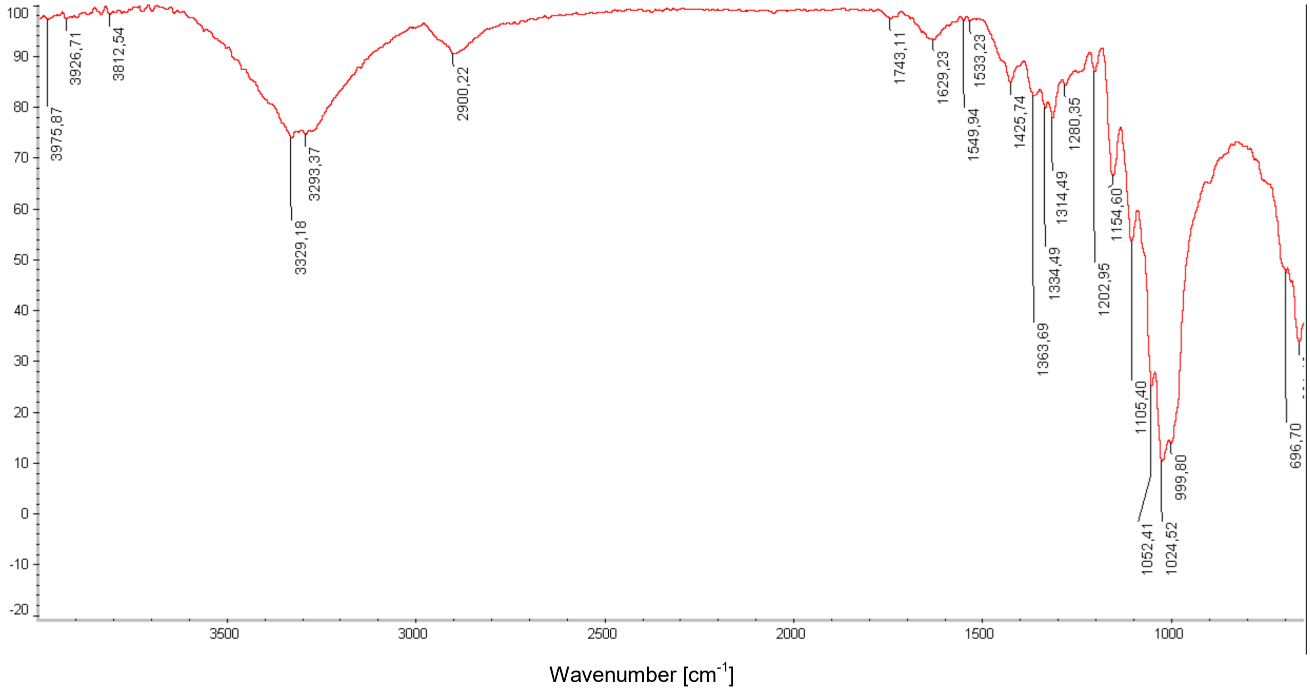

Figure 5 Transmittance spectrum of Na-CMS + QAS

However, when studying the spectrum formed during the investigation of textile material, processed with finishing solutions, it has been established that the spectrum do not have bands that are characteristic of the QAS (the connection typical for quaternary amines, the absorption band at the frequency of oscillations is close to 1440-1400 cm^{-1}). Consequently, studying the graphic material it can be concluded that new chemical bonds with the fabric are not formed. So, it can be assumed that the antimicrobial substances are contained on the textile material in a layer of the polymeric film-forming agent.

4 CONCLUSION

As a result of the research, the compound of the composition was established to provide antimicrobial properties to cotton fabrics based on carboxymethyl starch (30 g/l) and tetrachloride ammonium salt (7 g/l). It has been established that the addition of an antimicrobial agent improves the viscoelastic properties of solutions. The use of modified starch improves the sorption properties of the textile material. As far as possible, the QAS is 3 mm, as a result of the use of a polymeric modifier CMS. Another picture is observed when forming the BAS based on Na-CMS and QAS, in this case the sterile zone around the samples is much more - 10 mm.

This paper shows that the BAS on the basis of Na-CMS and QAS is rather effective. In this case it is possible to allow an explanation of the obtained data formation of new chemical compound which actually is a new biologically active polymer, a different chemical structure from initial polymer carrier and initial BAA.

5 REFERENCES

1. Mikolajczuk T., Wolowska-Czapnik D.: Highly porous polyacrylonitrile fibers with antibacterial and antifungal properties, Fibers and Textiles in Eastern Europe 38(3), 2002, pp. 18-22
2. Ulery B.D., Nair L.S., Laurencin C.T.: Biomedical applications of biodegradable polymers, Journal of Polymer Science Part B: Polymer Physics 49(12), 2011, pp. 832-864, doi:10.1002/Polb.22259
3. Ottenbrite R.M.: The Impact of Chemistry on Biotechnology, Chapter 9: Polymers in Biotechnology, M. Phillips, S.P. Shoemaker, R.D. Middlekauff, R.M. Ottenbrite (Eds.), 1988, pp 122–124, doi: 10.1021/bk-1988-0362.ch009
4. Hegstad K., Langsrud S., Lunestad B.T., Scheie A.A., Sunde M., Yazdankhah S.P.: Does the wide use of quaternary ammonium compounds enhance the selection and spread of antimicrobial resistance and thus threaten our health? Microbial Drug Resistance 16(2), 2010, pp. 91-104, doi: 10.1089/mdr.2009.0120.
5. Gilbert P., Moore L.E.: Cationic antiseptics: diversity of action under a common epithet, J. Appl. Microbiol. 99 (4), 2005, pp. 703-715
6. Kourai H., Yabuhara T., Shirai A., Maeda T., Nagamune H.: Synthesis and. antimicrobial activities of a series of new bis-quaternary ammonium compounds, Eur. J. Med. Chem. 41(4), 2006, p. 437-444

7. Ige O.O., Umoru L.E., Aribo S.: Natural products: A minefield of biomaterials, ISRN Materials Science 2012, Article ID 983062, 2012, 20 p., http://dx.doi.org/10.5402/2012/983062
8. Suprun N.P., Brichka S.Ya., Litvinova O.I.: Development and investigation of nonwoven wound dressings with antimicrobial properties on the basis of natural fibers, Vlakna a textil (Fibres and Textiles) 24(2) 2017, pp. 3-11
9. Marini M., Bondi M., Iseppi R., Toselli M., Pilati F.: Preparation and antibacterial activity of hybrid materials containing quaternary ammonium salts via sol-gel process, Eur. Polym. J.. 43(8), 2007, pp. 3621-3628
10. Gulrajania M.L., Gupta D.: Emerging techniques for functional finishing of textiles, Indian Journal of Fibre & Textile Research 36, 2011, pp. 388-397
11. Dan Yu, Lijin Xu, Yi Hu, Yani Li, Wei Wang: Durable antibacterial finishing of cotton fabric based on thiol–epoxy click chemistry RSC Advances 7, 2017, pp. 18838–18843

GLOSS AND HARDNESS EVALUATION OF WATER-BASED UV CURABLE POLYURETHANE ACRYLATE FILM USED IN TEXTILE PRINTING

Berdan Kalav, Gülçin Baysal and Burçak Karagüzel Kayaoğlu

Istanbul Technical University, Faculty of Textile Technologies and Design, Department of Textile Engineering, Gumussuyu, Beyoglu, Istanbul, Turkey
kalavbe@itu.edu.tr, bkayaoglu@itu.edu.tr

Abstract: *In the current study, it is aimed to evaluate the hardness and gloss properties of water-based UV curable polyurethane (PU) acrylate films by using two types of photoinitiators at different ratios. For this purpose, UV curable water-based unpigmented and pigmented formulations were prepared. Formulations were applied on glass plates and UV cured under gallium and mercury (Ga/Hg) lamps at three different power levels, i.e., 60, 90 and 120 W/cm. After UV curing process, gloss and hardness values of polymeric films were measured. The highest film hardness values implying the highest curing level was obtained with the formulation A1, including only Omnirad® 819 DW (former Irgacure® 819 DW) which is effective in deep curing, and formulation A3 including Omnirad® 819 DW and Omnirad® 500 (former Irgacure® 500) effective in surface and deep curing at 2:1 ratio, respectively. Among these two formulations, the highest gloss value was obtained with the formulation A3. GaHg lamp combination provided the highest gloss values while highest film hardness values were obtained with GaHg and GaGaHg lamp combinations. Compared to clear films, pigmented films rendered higher gloss values which was more prominent in single lamp (Ga, Hg) cured films. Results showed that photoinitiators (Omnirad® 819 DW and Omnirad® 500) provided better hardness and gloss values at 1:1, 1:2 and 2:1 ratios. Gloss values increased due to the increase in film hardness. The increase in the total applied energy resulted in an increase in the film hardness values of all clear and pigmented formulations. In terms of film hardness and gloss values, films prepared with Omnirad® 819 DW and Omnirad® 500 at 1:1 ratio and cured under GaHg lamp combination provided better results.*

Keywords: *Water-based, polyurethane acrylate, photoinitiator, UV curing, gloss, hardness.*

1 INTRODUCTION

UV curing technology is a fast, an easy to apply and an environmentally friendly method compared to conventional thermal curing, which can be applied in pigment printing [1, 2]. In this technology, different UV lamps may be used together due to the different spectrum of the lamps. The mercury (Hg) lamp is found sufficient for unpigmented formulations with spectral output at wavelengths <300 and 365 nm. In the case of pigmented formulations, however, the intensity of the UV sources is required to be increased to 400-450 nm range. This range can be obtained by adding gallium (Ga) to the lamp, which then called Ga lamp [3].

The UV curing mechanism is explained by the photopolymerization reaction of the binder. The photoinitiators absorb the energy of photons generated by irradiation and initiate the polymerization reaction by forming reactive groups during UV curing [2, 4]. These reactive groups lead to the cross linking of the binder which then results in film formation on the surface of the textile material. For the polymerization process of acrylic and styrene systems, different types of photoinitiators, possessing good chemical, optical and mechanical properties, have been developed. It has been reported that UV curable formulations should consist of at least 0.3% photoinitiator and at least 10% binder [1]. However, different photoinitiator types and concentrations were investigated in some researches. In a study of Jancovicova et al., polymeric films including 2,2-dimethyl-2-hydroxyacetophenone (Darocure 1173) as photoinitiator were cured under medium pressured mercury lamp. The FTIR analyses were conducted to examine the polymerization degree of cured films. Results indicated that, photoinitiator concentration, applied energy at curing and film thickness have significant effect on curing mechanism of polymeric films [4].

Macarie et al. reported the color values and mechanical properties of the UV curable acrylic coatings which were prepared with photoinitiators p-methoxybenzoyldiphenylphosphine oxide (MBDPPO) and 2,2-dimethoxy-2 phenylacetophenone (Irgacure 651). The photoinitiators were used at 5:1 ratio versus monomer (Bisphenol-A epoxydiacrylate) amount. Results showed that pendulum hardness values and appearance properties such as color and gloss of cured films were determined by the amount and content of pigment. Furthermore, appearance of the cured films was also affected by the particle size distribution of the pigment in the coating formulation. Pigments included in the formulations decreased the photoinitiator efficiency and thus the polymerization degree by absorbing UV light during curing [5].

Moreover, UV radiation doses may be changed to control film hardness and gloss for the evaluation of the polymerization level of the film [6, 7].

Pigment printing is widely applied due to its simplicity and cost effectiveness. Moreover, since the pigments have no affinity for the fibers, they are fixed on to the fibers with binders. However, in most of the pigment printing, the printing pastes include crosslinking agents, which are activated thermally. Hence, the fixation occurs at higher temperatures and requires longer fixation duration compared to UV curing systems [8].

In the current study, we aimed to evaluate the gloss and hardness values of UV cured clear and pigmented polyurethane acrylate films by the use of two different photoinitiators (*Omnirad® 819 DW* and *Omnirad® 500*) at different ratios.

2 EXPERIMENTAL

2.1 Materials

In the preparation of water-based UV curable clear and pigmented formulations, a flexible, water-based, aliphatic PU acrylate binder (Laromer® UA 9059) was used. Bisacyl phosphine (*Omnirad® 819 DW*) effective for deep curing and α-hydroxyketone (*Omnirad® 500*) effective for surface curing [9] were used as the photoinitiators. Wetting agent (Exosel 54, Acar Kimya, Turkey), defoamer (Foamaster® 8034, BASF), anionic acrylic copolymer thickener (Orgaclear P 460, Organik Kimya, Turkey), deionized water and ammonia solution (NH_4OH) were also used in the formulation. To obtain pigmented film a red pigment (Irgazin® Red K 3840, BASF) was used in the formulation.

2.2 Method

Water-based UV curable formulations were prepared using different photoinitiator ratios (0:3) of *Omnirad® 500* and *Omnirad® 819 DW*. Films of 120 µm thicknesses were obtained with a film applicator (Byk Gardner) on glass plates. The pH and the viscosity of the pigmented and clear formulations were adjusted to 8.0-9.0 (with WTW Inolab pH 7110 pH meter) and 20.000- 25.000 cP (at 20 rpm, with spindle 6 with a Brookfield DV-E viscometer), respectively. The clear formulation recipe is given in Table 1. The photoinitiator ratios used in formulations A1-A7 are given in Table 2. Formulations A1 and A3 were also prepared with 3% pigment with respect to binder amount. To determine the photoinitiator effect on gloss and hardness properties of pigmented films, the formulations were prepared according to the Table 3.

Films were cured in UV curing equipment (Raycon®, Turkey) with an adjustable belt speed (2-50 m/min), and equipped with *Ga* (380 V) and *Hg* (220 V) lamps. UV curing was performed at three *power levels* (60, 90 and 120 W/cm) at a belt speed of 10 m/min under different UV lamp combinations (*Hg, Ga, GaHg, GaGaHg*). Due to the default properties of the UV lamps, which are mounted on the UV curing equipment, the power levels can be adjusted between 60 W/cm - 120 W/cm individually. Hence, the energy output of the UV lamps depends on the adjusted power. However, depending on the belt speed, the total applied energy amount can vary. Thus, the total applied energy was measured with a UV-Integrator Type D radiometer.

The chemical changes in the cured films were characterized by FTIR spectroscopy (PerkinElmer FTIR C99089). The gloss measurements of polymeric films were made according to ASTM D523, “Standard Test Method for Specular Gloss” standard using a Rhopoint, Novo-Gloss^{TM} glossmeter at 60° geometry. After UV curing the König hardness of polymeric films were evaluated with a Byk Pendulum Hardness Tester.

Table 1 Clear formulation

Materials	Quantity [g]
Deionized water	26
Binder (Laromer® UA 9059)	66
Photoiniators	3.6
Thickener (Orgaclear® P 460)	2.63
Wetting agent	0.49
Defoamer	0.1
Ammonia	0.33
Total	100

Table 2 Photoinitiator ratios used in the clear pastes

Formulations	Omnirad® 500	Omnirad® 819 DW
A1	-	3
A2	0.5	2.5
A3	1	2
A4	1.5	1.5
A5	2.0	1.0
A6	2.5	0.5
A7	3.0	-

Table 3 Photoinitiator ratios used in the pigmented pastes

Formulations	Omnirad® 500	Omnirad® 819 DW
X1	1	1
X2	1	2
X3	1	3
X4	1	4
X5	1	5
Y2	2	1
Y3	3	1
Y4	4	1
Y5	5	1

3 RESULTS AND DISCUSSION

3.1 Hardness measurements

The highest clear film hardness was obtained with the formulation A1, including only *Omnirad® 819 DW* which is effective in deep curing, and formulation A3 including *Omnirad® 819 DW* and *Omnirad® 500* effective in deep and surface curing at a ratio of 2:1 (Figure 1).

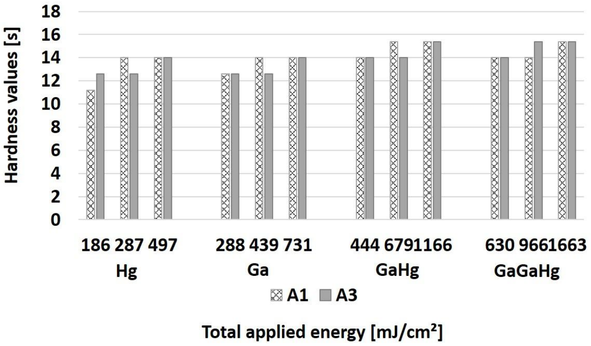

Figure 1 The effect of applied energy on hardness properties in clear formulations A1 and A3

In general, the film hardness values decreased with the decrease in the amount of *Omnirad® 819 DW* photoinitiator (effective in deep curing) in the formulation. The increase in the total applied energy resulted in an increase in the film hardness values of all clear formulations. Both *GaHg* and *GaGaHg* lamp combinations yielded higher film hardness values. Among the films cured under *GaHg* lamp combination at 120 W/cm power level, the difference between the highest hardness values (A1) and the lowest hardness value (A6) is 42.8%. Photographic images of clear films are given in Figure 2.


A1-GaHg 120 A3-GaHg 120

Figure 2 Photographic images of clear films prepared with A1 and A3 formulation cured under *GaHg* lamp combination at power level of 120 W/cm

The effect of applied energy on hardness values in pigmented formulations A1 and A3 is shown in Figure 3. Hardness results showed that pigmented films have low hardness values when compared with those of clear films (Figure 1). The highest hardness values were obtained in pigmented films which are obtained after curing under both *GaHg* and *GaGaHg* lamp combinations. The polymerization degree of the films prepared with pigmented formulations decreases in comparison with that of clear formulations. Since, pigments absorb more UV light and hinder the formation of the free radicals, which provides the polymerization reaction of the binder, the polymerization degree decreases in pigmented films [10]. Photographic images of pigmented films are given in Figure 4.

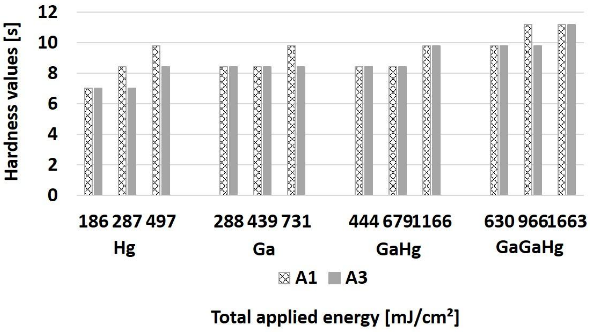

Figure 3 The effect of applied energy on hardness properties in pigmented formulations A1 and A3

To determine the effect of photoinitiator type on hardness properties of pigmented films prepared according to Table 3 were subjected to pendulum hardness test. Results showed that the highest hardness values were obtained in films prepared with X1 formulation including the same *Omnirad® 819 DW* and *Omnirad® 500* ratios.

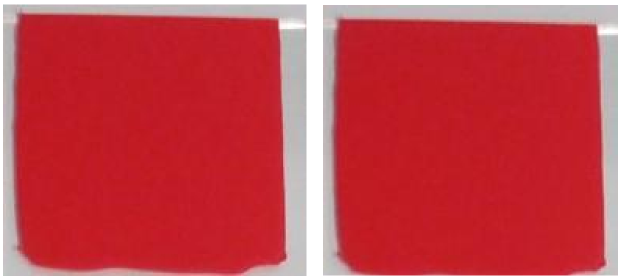
A1- GaHg 120 A3-GaHg 120

Figure 4 Photographic images of pigmented films prepared with A1 and A3 formulation cured under *GaHg* lamp combination at power level of 120 W/cm

The film hardness values decreased with the increase in the amount of *Omnirad® 819 DW* photoinitiator (effective in deep curing) in the formulation. The lowest hardness value was obtained with the formulation X5 including *Omnirad® 500* and *Omnirad® 819* at a ratio of 1:5 (Figure 5). This situation was also observed when the ratio of *Omnirad® 819* kept constant and *Omnirad® 500* was increased gradually. Hence, the film hardness values decreased with the increase only in the amount of *Omnirad® 500 DW* photoinitiator (effective in surface curing) in the formulation.

The lowest hardness value was obtained with the formulation Y4 including *Omnirad® 500* and *Omnirad® 819* at a ratio of 5:1 (Figure 6) The hardness values of the formulations X5 and Y4 were obtained the same value, which is 9.8 s under same lamp combination and total applied energy.

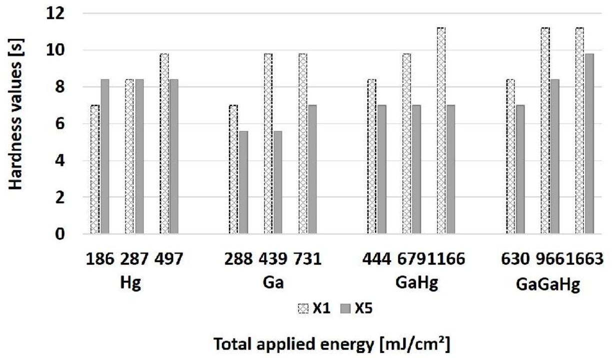

Figure 5 The effect of applied energy on hardness properties in pigmented formulations X1 and X5

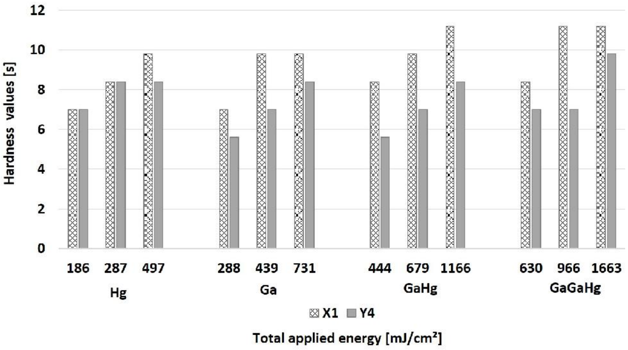

Figure 6 The effect of applied energy on hardness properties in pigmented formulations X1 and Y4

Results showed that photoinitiators should be used at the ratio of (1:1) due to the synergetic effect, instead of increasing the ratio of each photoinitiator alone. The more effective film hardness values were obtained in films prepared with X1 formulation cured under both *GaHg* and *GaGaHg* lamp combinations.

3.2 Gloss measurements

The highest gloss values were obtained in films prepared with A3 formulation cured under *GaHg* lamp combination (Figure 7). It can be suggested that there is a synergetic effect towards improvement of gloss when two photoinitiators are combined in the same formulation. In accordance, when the amount of photoinitiator *Omnirad® 500* increases, the gloss values improved until a certain value. After this value, gloss values tend to decrease.

The effect of the total energy applied in the curing process on the gloss values for both clear and pigmented films is shown in Figure 8 for A3 formulation. For clear films, the higher gloss values were obtained for *GaHg* lamp combination but in pigmented films, the higher gloss values were obtained in films cured under *Ga* lamp. However, hardness results showed that curing with a single *Ga* lamp provided low film hardness, indicating a low degree of curing. It is concluded that in order to obtain sufficient film hardness and gloss values, *GaHg* lamp combination should be preferred in curing.

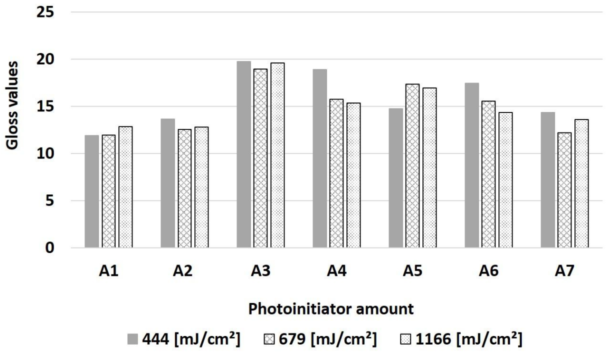

Figure 7 The effect of photoinitiator amount on gloss values of clear films cured under *GaHg* lamp combination

Gloss values of the pigmented films which were prepared according to the photoinitiator ratios given in Table 3, decreased with the increase of the *Omnirad® 819 DW* photoinitiator. The increase in the total applied energy for each lamp combination resulted in an increase in the gloss values of all pigmented formulations. The highest gloss values were obtained in films prepared with X2 formulation including *Omnirad® 819 DW* and *Omnirad® 500* at a ratio of 2:1.

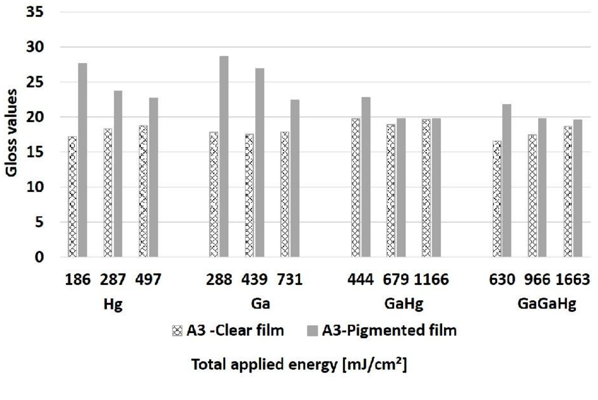

Figure 8 The effect of applied energy on gloss values of clear and pigmented films cured under different lamp combinations

The lowest gloss values were obtained with X5 formulation including *Omnirad® 819 DW* and *Omnirad® 500* at a ratio of 5:1 (Table 3). Gloss values of X2 and X5 formulations are given in Figure 9.

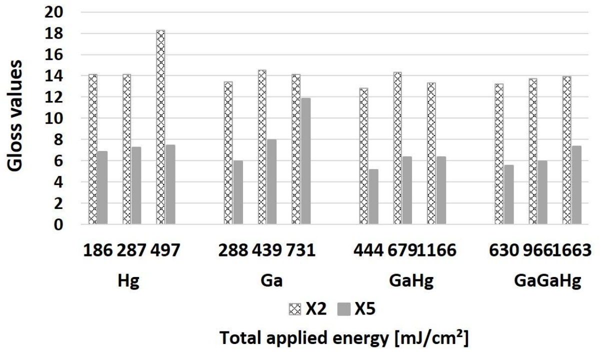

Figure 9 The effect of applied energy on gloss values in pigmented formulations X2 and X5

Moreover, the gloss measurements at all power levels were repeated 5 times. Hence, the t tests show that difference between X2 and X5 formulations in terms of gloss values are significant, since the calculated *t* values are higher than that of the correspondence value at *t* table (95% confidence, 8 degree of freedom) in all power levels excluding 60 and 90 W/cm at single Hg lamp. Figure 10 shows the calculated *t* values versus correspondance *t* value of the table X2 - X5.

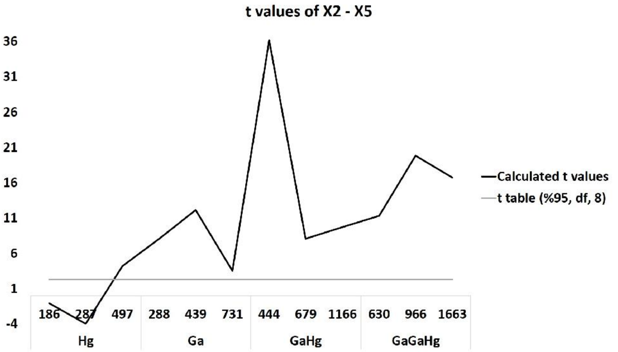

Figure 10 Calculated *t* values of X2 - X5 at all power levels and lamp combinations

The gloss values of the films increased with the increase in the amount of Omnirad® 500 photoinitiator. The highest gloss values were obtained in films prepared with Y4 formulation including Omnirad® 819 DW and Omnirad® 500 at a ratio of 1:4. This can be explained by the fact that surface curing effect of Omnirad® 500 photoinitiator provides high gloss value. At the same time films prepared with Y4 formulation has lowest hardness values. These results cause deterioration and opening of the film surface due to low strength after a certain period of time.

The lowest gloss values obtained with the films prepared with Y2 formulation which have high hardness values when compared with film prepared with Y4 formulation. In Figure 11, the t tests show that difference between Y2 and Y4 formulations in terms of gloss values are significant, since the calculated *t* values are higher than that of the correspondence value at *t* table (95% confidence, 8 degree of freedom) at all power levels (60, 90, 120 W/cm).

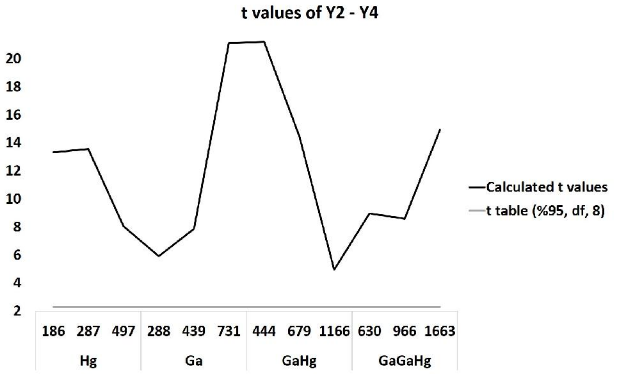

Figure 11 Calculated *t* values of Y2 – Y4 at all power levels and lamp combinations

Gloss values of X1, Y2 and Y4 formulations are given in Figure 12. In terms of film hardness and gloss values, films which are prepared with X1 formulation and cured under *GaHg* lamp combination, could be suggessted.

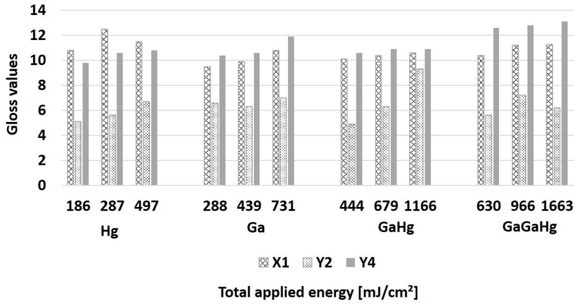

Figure 12 The effect of applied energy on gloss values in pigmented formulations X1, Y2 and Y4

3.3 FTIR spectroscopy

FTIR analysis of the clear films showed that there was a reduction and a disappearance of the twisting peak of $-CH_2=CH_2$ at 810 cm^{-1} wave number and bending peak at 1.410 cm^{-1} wave number, which suggested the development of the cure. Figures 13 and 14 show the FTIR spectrums of clear films prepared with A1 and A3 formulation and cured under *GaHg* lamp at different *power levels* (60, 90 and 120 W/cm), respectively.

Figures 15 to 17 show the FTIR spectrums of pigmented films prepared with X5, Y4 and X1 formulations and cured under *GaHg* lamp at different *power levels* (60, 90 and 120 W/cm). Although FTIR analysis of the clear films showed that there was an evidence for the development of the cure, this could not be observed in the pigmented formulations. This was due to the presence of the pigments, which prevented the observation of the expected scissor deformation peak at wave numbers 1538 cm^{-1}.

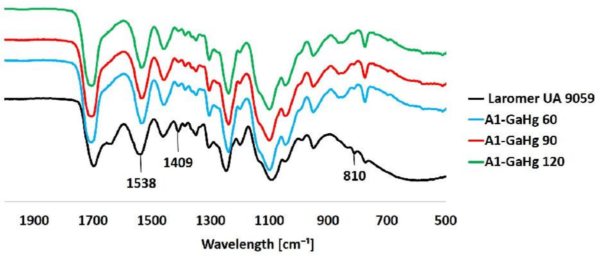

Figure 13 FTIR spectrum of clear film prepared with formulation A1

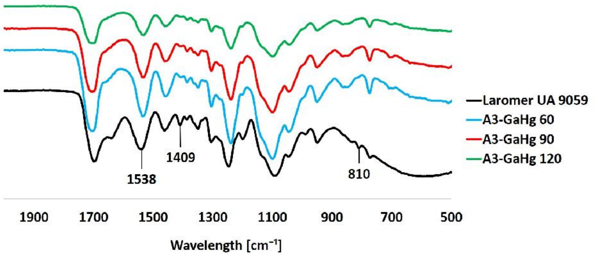

Figure 14 FTIR spectrum of clear film prepared with formulation A3

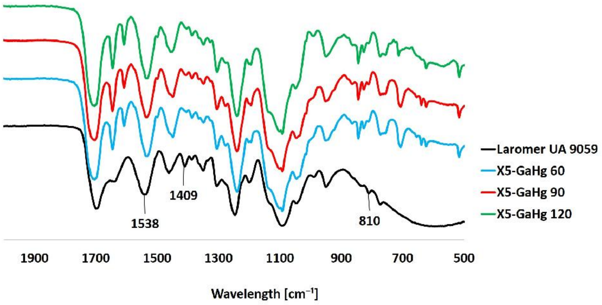

Figure 15 FTIR spectrum of pigmented film prepared with formulation X5

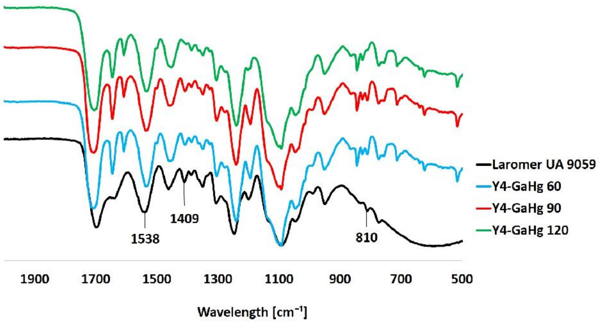

Figure 16 FTIR spectrum of pigmented film prepared with formulation Y4

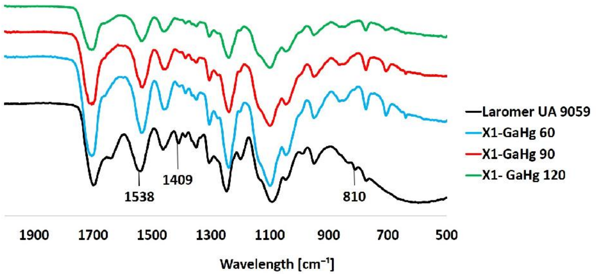

Figure 17 FTIR spectrum of pigmented film prepared with formulation X1

4 CONCLUSION

According to gloss measurement results, the higher gloss values were obtained with clear A3 formulation which includes *Omnirad® 500* and *Omnirad® 819 DW*, photoinitiators at a ratio of 1:2, respectively. The best hardness values were obtained in films prepared with A1 formulation including only *Omnirad® 819 DW*, cured with *GaHg* lamp; however the gloss values of this formulation were the lowest among all formulations. Formulation A3 provided optimum gloss and hardness values. The hardness and gloss values of the films prepared with pigmented formulations showed that photoinitiators should be used in a ratio of (1:1) instead of increasing the amount of the photoinitiators individually. The higher film hardness values were obtained in films prepared with X1 formulation cured under both *GaHg* and *GaGaHg* lamp combinations. In terms of film hardness and gloss values, films prepared with the formulation X1 and cured under *GaHg* lamp combination at high power level (120 W/cm) can be suggested. Although the highest hardness values were obtained with the *GaGaHg* lamp combination, considering the energy efficiency and curing level, *GaHg* lamp combination could be recommended for curing.

ACKNOWLEDGEMENT: The authors acknowledge The Scientific and Technological Research Council of Turkey (TUBITAK) for the financial support (Project No. 215M995).

5 REFERENCES

1. Mikuz M., Turk S.S., Tavcer P.F.: Properties of ink-jet printed, ultraviolet cured pigment prints in comparison with screen-printed, thermo-cured pigment prints, Color. Technol. 126(5), 2010, pp. 249-255, doi: 10.1111/j.1478-4408.2010.00254.x
2. Javadi A., Mehr M.S., Soucek M.D.: Cure-on-command technology: A review of the current state of the art, Progress in Organic Coatings 100, 2016, pp. 2-31, doi: 10.1016/j.porgcoat.2016.02.014
3. Akbulut G., Kayaoğlu K.B., Eren M., Yıldiz B., Orbay M.: The effect of different radiation sources for the UV curing of a screen-printed, water-based polyurethane acrylate binder, Color. Technol. 132(4), 2016, pp. 269-279, doi: 10.1111/cote.12219

4. Jancovicova V., Mikula M., Havlinova B., Jakubikova Z.: Influence of UV-curing conditions on polymerization kinetics and gloss of urethane acrylate coatings, Progress in Organic Coatings 76(2-3), 2013, pp. 432-438, doi: 10.1016/j.porgcoat.2012.10.010
5. Macarie N., Ilia G.: Influence of pigment properties on UV-curing efficiency, Journal of Applied Polymer Science 104(1), 2007, pp. 247-252, doi: 10.1002/app.25563
6. Augusto M., Bardi G., Machado L.D.: Accompanying of parameters of color, gloss and hardness on polymeric films coated with pigmented inks cured by different radiation doses of ultraviolet light, Radiation Physics and Chemistry 81(9), 2012, pp. 1332-1335, doi: 10.1016/j.radphyschem.2011.11.068
7. Green W.A.: Industrial photointiators: A Technical guide, New York: CRC Press, 2010, ISBN: 9781439827451, doi: 10.1002/cphc.201000542
8. Gutjahr H., Koch R.R.: Direct print coloration, In: Miles L.W.C. ed. Textile Printing, Hampshire UK, 2003, 139-196, ISBN: 9780901956798
9. Schwalm R.: UV coatings: basics, recent developments and new applications, Nederlands: Elsevier, 2007, ISBN: 9780080466897
10. Neral B., Sostar-Turk S., Voncina B.: Properties of UV-cured pigment prints on textile fabric, Dyes and Pigments 68(2-3), 2006, pp. 143-150, doi: 10.1016/j.dyepig.2005.01.022

ALTERNATIVE METHOD FOR EXHAUSTED DYE BATH RECYCLING BASED ON REMOVAL OF RESIDUAL DISSOLVED REACTIVE ANIONIC DYES

Barbora Kamenicka and Tomas Weidlich

Chemical Technology Group, Institute of Environmental and Chemical Engineering, Faculty of Chemical Technology,
University of Pardubice, Studentská 95, 532 10 Pardubice, Czech Republic
st38856@student.upce.cz; tomas.weidlich@upce.cz

Abstract: *This work presents precipitation and removal of hydrolyzed reactive dyes by action of liquid ion exchangers in co-action of inorganic flocculant. After addition of cationic surfactant and aqueous aluminium chloride the precipitation occurs and practically decolorized aqueous phase is obtained. The treated water was completely decolorized and purified by addition of powdered charcoal.*

Keywords: *reactive dye, ion exchange, ionic liquid, flocculant*

1 INTRODUCTION

In batch dyeing a certain amount of textile material is loaded into a dyeing machine and brought to equilibrium with a solution containing the dye and the auxiliaries over a period of minutes to hours. In batch dyeing, dye, alkali (sodium hydroxide or sodium carbonate or bicarbonate) and salt are added to the dye bath in one step, at the beginning of the process, or stepwise. Its amount is determined by the reactivity of the system and the desired depth of shade. Salt is added to improve bath exhaustion: the concentration employed depends on the substantivity of the dye and on the intensity of the shade. After dyeing, the liquor is drained off and the material is rinsed and then washed off with the addition of auxiliaries.

Concentrated waste water streams (spent liquors) containing hardly- or non-biodegradable compounds (hydrolyzed reactive dyes, etc.) should be treated at source. For the textile finishing industry, advanced oxidation with a Fenton-like reaction is proposed as a viable pretreatment technique [1]. However, application of strong oxidants causes production of adsorbable organic halogens (AOX) by reaction with NaCl and dissolved organic compounds and moreover oxidation process is not able to remove the dissolved inorganic salts from treated water.

Above mentioned problems could be solved by efficient removal of dissolved dyes from spent dyeing liquors and subsequent re-use of colorless aqueous NaCl solution for next dyeing step. Usually membrane techniques are applied in various ways for the treatment of segregated streams to allow water reclamation and re-use closely integrated with the process. However, membrane separation is very expensive technique. By our opinion, the more cost-effective method for dye bath recycling is based on removal of dissolved dyes using ion-exchange accompanied by flocculation and subsequent action of low quantities of common adsorbent (active carbon).

Effective removal of acid dyes from spent dyeing liquor is based on ion exchange reaction caused by addition of hydrophobic quarternary ammonium chlorides (ionic liquids, $R_4N^+Cl^-$ [2]) into the spent liquor. $R_4N^+Cl^-$ serve as a liquid anion exchanger. We observed that the replacement of chloride anions of $R_4N^+Cl^-$ by larger anions (anions of the acid dyes) proceeds smoothly even at room temperature [3, 4]:

$$R_4N^+Cl^- + \text{dye-}SO_3^-Na^+ \rightarrow \text{dye-}SO_3^-R_4N^+ + Na^+ + Cl^-$$

The interaction of these dyes with suitable $R_4N^+Cl^-$ salts produces slightly soluble ionic salts which can settle after a long contact time or can be removed more efficiently by the action of common inorganic flocculants [3-5].

The aim of this work is to verify possibilities for simple decolorization of model and subsequently industrial aqueous effluents produced in dyeing process. For this purpose decolorization efficiencies of three commonly used reactive dyes by action of five industrially produced and cheap ionic liquids were tested and the most efficient procedure was subsequently applied for treatment of spent industrial dye baths.

2 MATERIALS AND METHODS

2.1 Dyes and reagents

The used dyes Remazol Brilliant Blue R (**RBBR**, CAS No. 2580-78-1), Reactive Blue 4 (**RB4**, CAS No. 13324-20-4), Reactive Black 5 (**RB5**, CAS No. 17095-24-8) and quaternary ammonium salts $R_4N^+Cl^-$ (cetyltrimethylammonium chloride ($cetylNMe_3Cl$), benzalkonium chloride 50 wt.% aqueous solution ($AlkBzNMe_2Cl$), Aliquat 336, Luviquat^{TM} FC 370 (copolymer of poly[(3-methyl-1-vinylimidazolium chloride)-co-(1-vinylpyrrolidone)] (40 wt.% active ingredients) and 20 wt.% aqueous solution of poly(diallyldimethylammonium chloride) (Table 3) and inorganic coagulant $AlCl_3.6H_2O$ were supplied by Sigma-Aldrich Co. Powdered charcoal Silcarbon CW20 was supplied by Silcarbon AktivKohle Gmbh (Germany).

Solid reagents $cetylNMe_3Cl$ and $AlCl_3$ were used as 0.1 M aqueous stock solutions. Mixed aqueous $R_4N^+Cl^-$ based reagent AB consisted of 0.1 M Aliquat 336 and 0.4 M benzalkonium chloride was prepared by dissolution of 10.1 g of Aliquat 336 in concentrated aqueous solution of $AlkBzNMe_2Cl$ (70 g of 50 wt.% aq. $AlkBzNMe_2Cl$ dissolved in 150 mL of water), the obtained solution was diluted to the exact volume of 250 mL by water. Mixed aqueous $R_4N^+Cl^-$ reagent AC containing 50 mM Aliquat 336 and 0.1 M $cetylNMe_3Cl$ was prepared by dissolution of 5.25 g of Aliquat 336 in 0.1 M aqueous solution of cetyltrimethylammonium chloride (8 g of $cetylNMe_3Cl$ dissolved in 200 mL of water under heating), the obtained solution cooled to the room temperature was diluted to the exact volume of 250 mL with demineralized water.

2.2 Exhausted dye baths

Hydrolyzed dye solutions (RB4, RB5 and RBBR) were obtained by addition of sodium carbonate (1 g) to the 250 mL of 10 mM reactive dye aqueous solution and heating at 90°C for 30 minutes (Table 1).

Model exhausted dye bath was prepared by mixing of above mentioned hydrolyzed RB5, RB4 and RBBR aqueous solutions (50 mL of each hydrolyzed dye solution).

Exhausted red dye bath 1 was wastewater after the specific dyeing process obtained from Czech textile Company.

Exhausted red dye bath 2 was wastewater obtained after the same dyeing process using recycled red dye bath 1.

The composition of the (model) exhausted dye baths are given in Table 2.

2.3 Instruments

A UV-visible spectrophotometer Libra S22 (Biochrom, Great Britain) was used to measure the absorbance values of the dyes to establish their λ_{max} and concentrations. A magnetic stirrer HeiTEC (Heidolph Instruments GmbH&Co.) was used for stirring of (model) exhausted dyeing baths.

Chemical oxygen demand (COD) measurements were obtained using the HACH-LANGE apparatus (DR2800) according to standard methods given by the producer. The COD analyses were done with the dichromate (VI) LCK 014 and LCK 914 tests.

Table 1 Description of used dyes

Applied dye (λ_{max})	Structure and molecular weight of studied hydrolyzed dyes
Hydrolyzed Remazol Brilliant Blue R (**hRBBR**) 592 nm	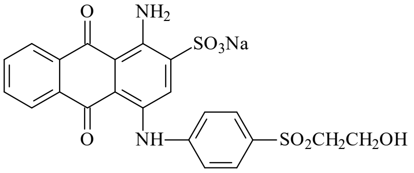 M_r=524.5 g/mol
Hydrolyzed Reactive Blue 4 (X = Cl or OH) (**hRB4**) 597 nm	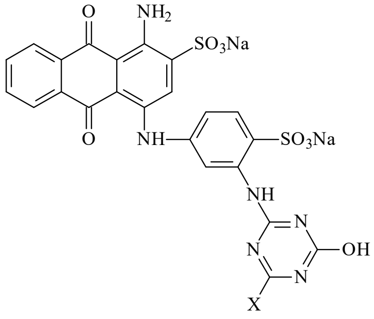 M_r=644.5 g/mol
Hydrolyzed Reactive Black 5 (**hRB5**) 596 nm	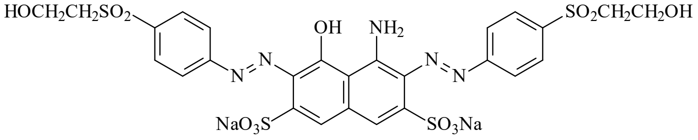 M_r=787.7 g/mol

Table 2 Composition of exhausted dye baths

Exhausted dyeing bath composition	pH	NaCl content [g/L]	Dye content [mmol/L]	COD [mg O_2/L]
Model	11.1	2.8	10	13290
Red 1	11.2	80	approx. 1	8180
Red 2	11.0	76	approx. 0.5	4137

2.4 *Colour removal from (model) dye baths*

Aqueous $R_4N^+Cl^-$ solution (or appropriate amount of ionic liquid $R_4N^+Cl^-$) was added drop wise to 100 mL of (model) spent dyeing bath under stirring until precipitation of ion pairs occurs (optimal molar ratio $R_4N^+Cl^-$:dye-SO_3^- 1:1) and after 15 minutes (or 120 min. in case of Aliquat 336 addition) of vigorous stirring, the sample of obtained mixture was collected, filtered and measurement of absorbance of filtrate was accomplished. To the stirred reaction mixture of produced ion pair dye-$SO_3^-R_4N^+$ in water, 0.1 M aq. $AlCl_3$ was added drop wise until pH value reached pH=6.0-6.4. After 15 minutes of stirring at the speed of 400 rpm and the temperature of 22±2°C, filtration and subsequent measurement of absorbance of filtrate was accomplished. Alternatively, powdered charcoal was added to the obtained filtrate and suspension was filtered after 30 min. of stirring. Absorbance of obtained filtrate and COD were measured.

The decolorization efficiency (*DE %*) of dyes was determined from absorbance measurements, according to the concentration-absorbance standard curves at the respective maximum adsorption wavelength of the individual dye solutions. Afterwards, *DE %* was calculated from (1):

$$DE\ (\%) = [1-(A/A_0) \times 100] \qquad (1)$$

where *A* and A_0 denote the absorbance in the solution after and before precipitation, respectively.

Removal efficiency of chemical oxygen demands (*RECOD*) of dye baths, hydrolyzed dye solutions and obtained filtrates were measured using Hach-Lange cuvette tests LCK 1014 and LCK 914 and the *COD* removal efficiency was calculated using (2):

$$RECOD\ (\%) = [1-(COD/COD_0) \times 100] \qquad (2)$$

where *COD* and COD_0 denote the chemical oxygen demand in the solution after and before precipitation, respectively.

Table 3 Description of used $R_4N^+Cl^-$

Used $R_4N^+Cl^-$	Structure of used $R_4N^+Cl^-$
Cetyltrimethyl-ammonium chloride cetylNMe$_3$Cl $C_{19}H_{42}ClN$ M_r=320.0 g/mol	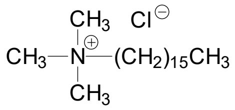
Benzalkonium chloride AlkBzNMe$_2$NCl average M_r=348.4 g/mol	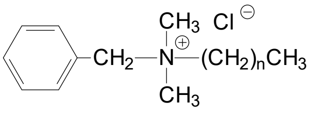 n = 12 and 14
Aliquat 336 average M_r=432.0 g/mol	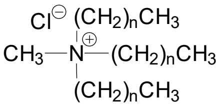 n = 8 and 10
Poly(diallyldimethyl-ammonium chloride) NdiallylMe$_2$Cl monomer unit: $C_{12}H_{26}ClN$ M_r=219.8 g/mol	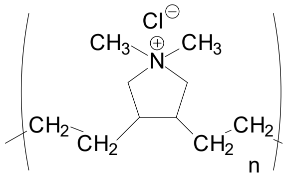
Luviquat^{TM} FC 370 (copolymer of poly[(3-methyl-1-vinylimidazolium chloride)-co-(1-vinylpyrrolidone)] MIM-(CH$_2$)$_4$NMPCl monomer unit: $C_{14}H_{24}ClN_3O$ M_r=285.8 g/mol	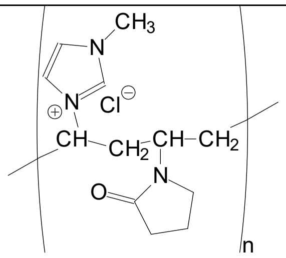

3 RESULTS AND DISCUSSION

Model exhausted dyeing baths were prepared by alkaline hydrolysis of 10 mM reactive dye solutions. In case of vinyl sulfone-type reactive dyes (RBBR and RB5) vinylsulfonyl groups were hydrolyzed to the corresponding inorganic sulphate (Na_2SO_4) and dye-$SO_2CH_2CH_2OH$. In case of chlorotriazine-type reactive dye RB4 chlorotriazine was hydrolyzed to the corresponding hydroxytriazine and NaCl (Table 1).

For practical reasons the cheap $R_4N^+Cl^-$ salts industrially used as cationic surfactants (cetyltrimethylammonium chloride, benzalkonium chloride and Aliquat 336) were tested for the precipitation of hydrolyzed hRBBR, hRB5 and hRB4 in the form of appropriate dye-$SO_3^-R_4N^+$ ion pairs and their *DE* were compared with action of polymeric $R_4N^+Cl^-$ agents poly(diallyldimethylammonium) chloride and Luviquat^{TM} FC 370 (copolymer of poly[(3-methyl-1-vinylimidazolium chloride)-co-(1-vinylpyrrolidone)] (Table 3).

It was proved that optimal dosage of $R_4N^+Cl^-$ into the spent dyeing bath is related to molar quantity of R-SO_3^- groups found in the treated bath [2-4]. As we described earlier, the precipitation of produced ion pair dye-$SO_3^-R_4N^+$ occurred entirely in case, if ion pair of low polarity (substituent R is long alkyl chain preferably) is formed [3-6].

Using mentioned $R_4N^+Cl^-$, the best separation of hydrolyzed dyes was occurred in case of application of water-insoluble Aliquat 336 (ionic liquid composed of 2:1 mixture of methyl trioctyl- and methyl tridecylammonium chloride) [7]. However, the time for effective separation (reactive extraction of dyes into the Aliquat 336 layer) takes hundreds of minutes under vigorous stirring due to the slow mass transfer of dyes from aqueous phase into the lipophilic ionic liquid Aliquat 336 phase. In case of water-soluble $R_4N^+Cl^-$, the precipitation occurred during few minutes of vigorous stirring after addition of appropriate amount of 0.1 M aqueous $R_4N^+Cl^-$ solution (Table 2). Benzalkonium chloride and cetyltrimethylammonium chloride were tested as the most effective water-soluble $R_4N^+Cl^-$. As could be seen, the decolorization efficiency depends more or less on molecular weight of produced ion pair dye-$SO_3^-R_4N^+$. On the other hand (Table 2), in most applications, the polymeric $R_4N^+Cl^-$ failed in separation of dyes based on precipitation of produced dye-$SO_3^-R_4N^+$ ion pairs. This is probably caused by high polarity (aqueous solubility) of these polymers and low molecular weight of obtained dye-$SO_3^-R_4N^+$ ion pair (calculated using mol. weight of monomer unit of Luviquat FC370 or poly(diallyldimethylammonium chloride)) in comparison with above mentioned liquid ion exchangers $R_4N^+Cl^-$ (Table 4).

We observed that even though Aliquat 336 is not water soluble. It is soluble in concentrated aqueous solutions of benzalkonium chloride or cetyltrimethylammonium chloride. To solve the problems with required long reaction time essential for achievement of high *DE* in case of Aliquat 336 application and difficulties with precise dosing of highly viscous Aliquat 336, mixed $R_4N^+Cl^-$ aqueous solutions of benzalkonium chloride or cetyltrimethylammonium chloride with Aliquat 336 were prepared and tested for the removal of hydrolyzed reactive dyes from exhausted dye baths. These mixtures enable simple and precise dosage of $R_4N^+Cl^-$ into the treated hydrolyzed dye solution (model) spent dyeing baths and rapid separation of produced insoluble dye-$SO_3^-R_4N^+$ ion pairs from the aqueous mixture (Table 4).

Table 4 Changes in relative molar mass (*M_r*) of dyes caused by ion exchange of cations and determined *DE* related to aqueous solubility of obtained dye(SO_3NR_4)$_n$ ion pairs

Used anionic dye dye(SO_3Na)$_n$	Applied $R_4N^+Cl^-$	Produced ion pair	M_r of ion pair [g/mol]	DE [%]
hRB5	$C_{16}Me_3NCl$	hRB5($SO_3NMe_3C_{16}$)$_2$	1310.8	79.1
hRB5	$AlkBzMe_2NCl$	hRB5($SO_3NAlkBzMe_2$)$_2$	1463	68.6
hRB5	$MeOct_3NCl$	hRB5($SO_3NMeOct_3$)$_2$	1282.8	86.1
hRB5	Luviquat^{TM}FC370 MIM-(CH_2)$_4$NMPCl	hRB5(SO_3MIM-(CH_2)$_4$NMP)$_2$	1136.3	44.6
hRB5	polydiallyldiMeNCl	hRB5($SO_3NdiallylMe_2$)$_2$	994.2	36.8
hRB4	$C_{16}Me_3NCl$	hRB5($SO_3NMe_3C_{16}$)$_2$	1167.6	97.2
hRB4	$AlkBzMe_2NCl$	hRB5($SO_3NAlkBzMe_2$)$_2$	1319.8	99.92
hRB4	$MeOct_3NCl$	hRB5($SO_3NMeOct_3$)$_2$	1335.9	99.95
hRB4	Luviquat^{TM}FC370 MIM-(CH_2)$_4$NMPCl	hRB5(SO_3MIM-(CH_2)$_4$NMP)$_2$	993.1	11.5
hRB4	polydiallyldiMeNCl	hRB5($SO_3NdiallylMe_2$)$_2$	851	-
hRBBR	$C_{16}Me_3NCl$	hRB5($SO_3NMe_3C_{16}$)	786	62.2
hRBBR	$AlkBzMe_2NCl$	hRB5($SO_3NAlkBzMe_2$)	862.2	76
hRBBR	$MeOct_3NCl$	hRB5($SO_3NMeOct_3$)	870.2	97
hRBBR	Luviquat^{TM}FC370 MIM-(CH_2)$_4$NMPCl	hRB5(SO_3MIM-(CH_2)$_4$NMP)	721.8	66.5
hRBBR	polydiallyldiMeNCl	hRB5($SO_3NdiallylMe_2$)	627.7	50.5

Table 5 Effect of $R_4N^+Cl^-$ mixtures, addition of $AlCl_3$ and adsorption on charcoal *DE* and *RECOD*

Exhausted dye bath	Applied $R_4N^+Cl^-$ mixture	DE [%]	Quantity of 0.1M aq. $AlCl_3$ solution	DE [%]	Quantity of added charcoal	DE [%]	RECOD [%]
Model	AB (13 mL/L)	99.7	50 mL/L	99.9	1 g/L	99.99	98.0
Model	AC (40 mL/L)	90.5	50 mL/L	92.3	1 g/L	99.8	97.1
Red 1	AB (5 mL/L)	61.8	10 mL/L	96.7	1 g/L	97.0	41.9
Red 1	AC (5 mL/L)	51.5	10 mL/L	92.5	1 g/L	96.5	36.3
Red 1	-	-	-	-	20 g/L	97.9	31.2
Red 2	AB (2.5 mL/L)	58.8	38 mL/L	94.5	0.5 g/L	96.7	31.6
Red 2	AC (2.5 mL/L)	36.9	42 mL/L	71.3	0.5 g/L	95.9	42.3
Red 2	-	-	-	-	20 g/L	98.4	22.9

Subsequent addition of 0.1 M $AlCl_3$ in quantity ensuring neutralization of exhausted dye bath treated with $R_4N^+Cl^-$ mixture was accompanied by coagulation and flocculation of $Al(OH)_3$. The produced dye-$SO_3^-R_4N^+$ ion pairs were well removable by adsorption on the rapid sedimented flocs of $Al(OH)_3$ (Table 5).

The subsequent short time mixing of obtained filtrates with charcoal enables complete decolorization of filtered treated dye baths in optimal cases (Table 5).

As could be seen in Table 5, the obtained decolorization efficiency (DE) and removal efficiency of chemical oxygen demand (RECOD) using combination of dye-$SO_3^-R_4N^+$ ion pair formation with subsequent neutralization and flocculation using $AlCl_3$ is higher than in case of simple action of large-quantity powdered charcoal.

4 CONCLUSIONS

In this study, the model (laboratory prepared) and real exhausted reactive dye baths after the industrial reactive dyeing process were decolorized for re-use in the next dyeing step. Due to high salinity, high pH and intense color, it is the most problematic textile wastewater type from an environmental point of view. However, using appropriate mixture of hydrophobic and hydrophilic ionic liquids combined with coagulation/flocculation enables simple separation of precipitated hydrolyzed dyes and subsequent final treating with low quantity (0.5-1.0 g/L) of powdered charcoal results in excellent decolorization of original exhausted dye baths which enables complete re-use of obtained filtrate in next dyeing step (Figure 1).

We verified in this study that especially mixture of cheap and commercially simply available ionic liquids benzalkonium chloride and Aliquat 336 prepared in the form of the easy to handle aqueous mixture with subsequent addition of $AlCl_3$ as neutralizing and flocculating agent can be more efficient, economically reasonable and cheaper than decolorization using high quantity (20 g/L) of charcoal. In addition, application of aluminium chloride for neutralization of treated exhausted dye baths enables not only additional decolorization but also simple removal of precipitated dye-$SO_3^-R_4N^+$ by flocculation and sedimentation.

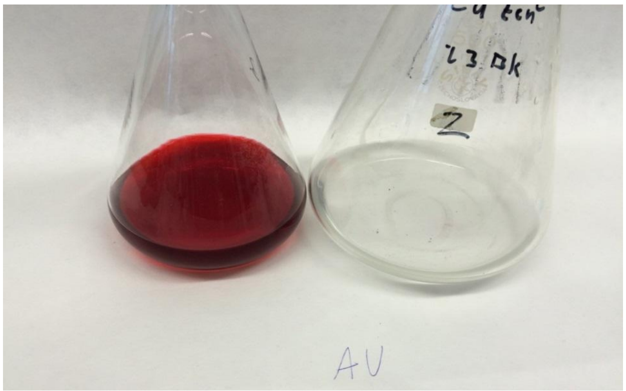

Figure 1 Red dye bath 2 (recycled) before and after treatment

The treated exhausted red dye bath 1 was recycled efficiently in dyeing process and subsequently treated using described combined method based on application of benzalkonium chloride and Aliquat 336 mixture with $AlCl_3$ and subsequent simple adsorption using low quantity of powdered charcoal (Figure 1).

Acknowledgement: *This work was supported by Technology Agency of the Czech Republic, project No. TG02010058-GAMA01/007.*

5 REFERENCES

1. Dušek L., Kočanová V.: Decolourization of wastewater from the production and application of Acid Blue 62, Vlakna a Textil (Fibres and Textiles) 23(3), 2016, pp. 51-55
2. Welton T.: Room-temperature ionic liquids. Solvents for synthesis and catalysis, Chemical Review 99(8), 1999, pp. 2071-2084, doi: 10.1021/cr980032t
3. Weidlich T., Martinková J.: Dye precipitation process from aqueous solutions, Czech Patent No. CZ303942 (B6), 2013
4. Weidlich T., Martinkova J.: Removal of acid dyes from aqueous effluents using ionic liquids, Vlakna a Textil (Fibres and Textiles) 23(3), 2016, pp. 219-223
5. Šimek M., Mikulášek P., Kalenda P., Weidlich T.: Possibilities for removal of chlorinated dye Mordant Blue 9 from model waste water, Chemical Papers 70(4), 2016, pp. 470-475, doi:10.1515/chempap-2015-0225

6. Weidlich T., Martinková J.: Application of tetraphenyl- and ethyltriphenylphosphonium salts for separation of reactive dyes from aqueous solution, Separation Science and Technology 47(9), 2012, pp. 1310-1314, doi: 10.1080/01496395.2012.672527
7. Mikkola J.P., Virtanen P., Sjoholm R.: Aliquat 336 - a versatile and affordable cation source for an entirely new family of hydrophobic ionic liquids, Green Chemistry 8, 2006, pp. 250-255, doi: 10.1039/B512819F

EFFECTS OF MULTILAYER CLOTHING SYSTEM ON TEMPERATURE AND RELATIVE HUMIDITY OF INTER-LAYER AIR GAP CONDITIONS IN SENTRY COLD WEATHER CLOTHING ENSEMBLE

Andrii Kurhanskyi[1], Sergij Bereznenko[1], Dmitriy Novak[1], Myroslava Kurganska[1], Vasyl Sakovets[2], Natalia Bereznenko[1] and Olga Haranina[1]

[1]Kyiv National University of Technologies and Design, N.-Danchenko 2, 01011 Kyiv, Ukraine
[2]Ministry of Defence of Ukraine, Melnykova 81, 04050 Kyiv, Ukraine
novak.knutd@gmail.com, kurganskij.av@knutd.edu.ua

Abstract: *The cold effects on sentry and the inter-layer air gaps microclimate conditions in cold weather multi-layer clothing ensembles used by the Armed Forces of Ukraine was analyzed. Comparative testing of two outer item variations for sentry cold weather clothing ensembles was conducted by human trials (n=10) and wireless body area network IBK3.4 in real time at a temperature of -18±1°C, a relative humidity of 15±10% and a wind speed of 5-10 m/s. The basic parameters of the upper inter-layer air gap microclimate of multilayer clothing system were obtained under real usage conditions. In order to improve outer item design and material the optimization of temperature and relative humidity sensor measurement points suggested. The results are significant for predicting of the maximum sentry comfort time and for optimization of a quantitative and qualitative composition of the wireless body area network sensors.*

Keywords: *multi-layer, clothing ensembles, sentry, cold, temperature, relative humidity, membrane, wireless body area network, microclimate.*

1 INTRODUCTION

A significant effect on reducing sanitary losses of dismounted soldiers from cold injuries (e.g., frostbite and hypothermia) are given by the use of multi-layer cold weather clothing ensembles as part of united personal combat ensembles (UPCE) which includes various item types of clothing, footwear and combat body armor etc.

The cold weather clothing ensembles ensures fulfillment of two tasks: increase of the effectiveness of soldier actions on the battlefield and lifesaving measures for the soldier. The concept of separation of combat and auxiliary equipment is the soldier must have with him all necessary equipment for a successful battle. The application of the concept of combat and auxiliary equipment separation has allowed reducing the equipment weight and increasing the soldier mobility. In addition, be able to combine different types of ammunition depending on the task type.

The modern UPCE for the Armed Forces of Ukraine (AFU) is modular and composed of standardized units to achieve maximum single soldier adaptability to various mission needs and environmental conditions [1]. The modern cold weather clothing ensemble (CWCE) is the part of UPCE used be AFU. Furthermore, improving the structure and requirements for CWCE had not scientifically justified, the most outdated USSR GOSTs and material manufacturer experience used [2]. The developers of existing military cold clothing systems was not reliably assessed the consumer attitudes about fabrics and clothing with appropriate psychometric techniques or conjoint analysis [3].

Additionally, the participation of people as subjects in the human trials requires their appropriate selection and requirements consideration for the repeated cycle of studies. The characterization of human traumas associated with cold processes is rather complicated; reactions to cold have a higher individual variability than reactions associated with heat transfer [4]. The clothing parameters are static and do not sufficient to describe the processes of heat and mass transfer from the skin through clothing to the environment. In addition, changing environmental conditions, human physical activity, moisture absorption, condensation, and vice-versa processes in clothing take affect the transfer processes [5, 6]. Also, modified textile materials exhibit improved functional properties as for example in [7]. In view of this, the further interest to implement such type textile materials in the manufacture of modern clothing systems.

Therefore, the integration of monitoring elements into clothing allows correcting the prediction and monitoring of the temperature state of the human body and its estimation in real time, which in turn can be a complement to the open body area network of physiological status monitoring (PSM) [8] and Warfighter Physiological and Environmental Monitoring [9, 10]. The CWCE items should be assembled as a complete ensemble designed for the specific conditions to be encountered such as environmental conditions and level of the physical activity [11, 12] spatially on the battle-field for frontline troops. The development of modular multi-layer ensemble for maximum protection requires the availability of heat and moisture transfer, biophysical and mechanical layer data variation for each ensemble entirely and for clothing items separately. An effective clothing ensemble is one that body could lose sufficient heat as the clothing design and the type of fabric does not restrict heat loss in some way [13].

2 EXPERIMENTAL PART

2.1 Setting the task

Certain types of duties of sentry and officers are required to stationed to keep guard with significant adverse effects of cold and wind on guard. The cold exposure effects on dismounted soldier performance are not entirely known [14]. For this purpose, a personal cold weather clothing system should offer greater protection against the elements whilst on guard. Currently, the fur coat, also well known as tulup, was developed for sentry protection. Fur coat is not a product of mass production, due to the curtailment of production at the base enterprises in the period 2014-2017. Therefore, the question of finding alternative clothing for protection of low-activity sentry from the cold has arisen.

3 MATERIALS AND METHODS

The fur coat alternative was chosen a waterproof and windproof long winter jacket X9.2 with a direct silhouette, hood, membrane laminated basic fabric, thermal insulation and sentry coat X9.1 with a direct silhouette, artificial fur insulation. Table 1 shows the characteristics of the entire AFU cold weather ensembles E1 and E2, its items and segmental division.

Total 10 cold weather ensemble items were selected in the established order. The upper layer items X9.1 and X9.2 are variable. Fabric characteristics of outer CWCE item are shown in Table 2.

The human trials were used to simulate the outdoor exercises for the sentry in the climate chamber. The research conducted in two steps according to the protocol (Figure 1) during the time 80 min, of which: 20 min - seats at a temperature of 20±0.5°C and a relative humidity of 58±4%; 60 min - walking up to 2 km/h at a temperature of -18±1°C, a relative humidity of 15±10% and a wind speed of 5-10 m/s.

Table 1 Characteristics of AFU cold weather ensembles and segmental division

Item code	Type of ensemble item	Structure of the ensembles		Segment number [15]
		E1	E2	
X4	Winter hat	+	+	S1
X10	Winter waterproof and windproof trousers	+	+	S6-S10-S11-S12
X13	Winter gloves	+	+	S9
X15	Winter scarf-pipe	+	+	S2-S3
X18, X19	Linen for cold weather (winter shirt and winter pants)	+	+	S4-S5-S6-S7-S8-S10-S11-S12
X21	Winter socks (trekking)	+	+	S13
X28	Winter combat boots	+	+	S12-S13
X7	Insulation suit jacket (fleece jacket)	+	+	S3-S4-S5-S6-S7-S8
X27	Ballistic helmet	+	+	S1
X9.1	Sentry coat	+	-	S3-S4-S5-S6-S7-S8
X9.2	Long winter jacket	-	+	S1-S3-S4-S5-S6-S7-S8

Table 2 Fabric characteristics of outer layer items of AFU cold weather clothing ensembles

Code of the ensemble	Type and code of the item	Type of fabric	Fibrous composition [%]	Normative values		
				Surface density [g / m^2]	Air permeability [dm^3/m^2.s]	Hygroscopicity [%]
E1	Sentry coat X9.1	Basic	65 CO, 35 PES	260	> 20	> 10.0
		Lining: Hair material Basis material	Artificial fur: 20 PE, 80 PAN 100 PES	320	-	> 1.5
E2	Long winter jacket X9.2	Basic	100% PA 6.6 +membrane 100% PTFE+PU	220	> 20	> 6.0
		Thermal insulation	100 PES	135	> 50	> 6.0
		Lining	100 PES	110	-	-

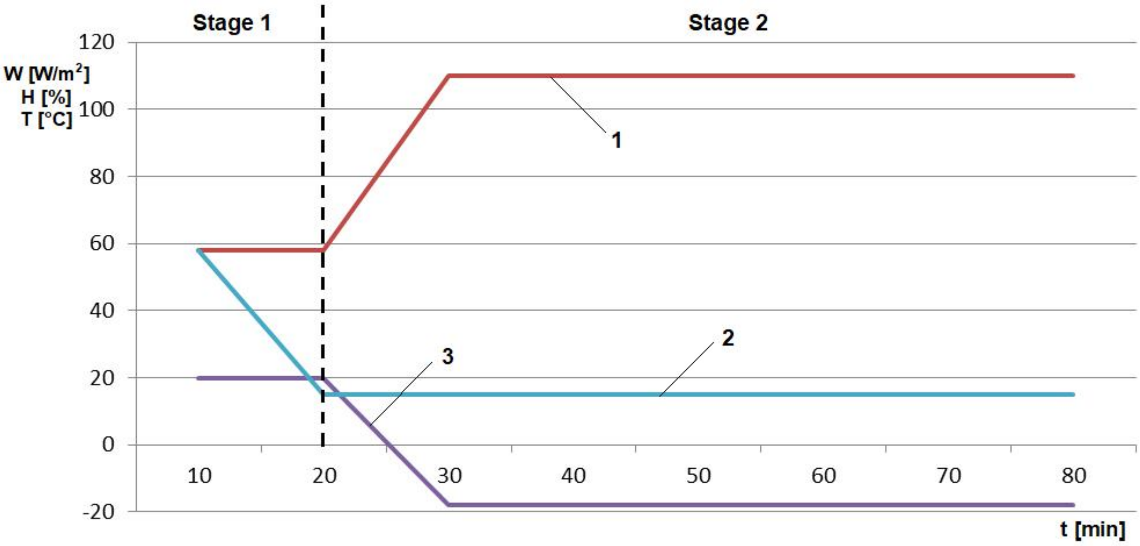

Figure 1 The protocol of comparative testing:
1 - energy costs of the subject *W*; 2 - relative humidity of the environment *H*; 3 - ambient temperature *T*

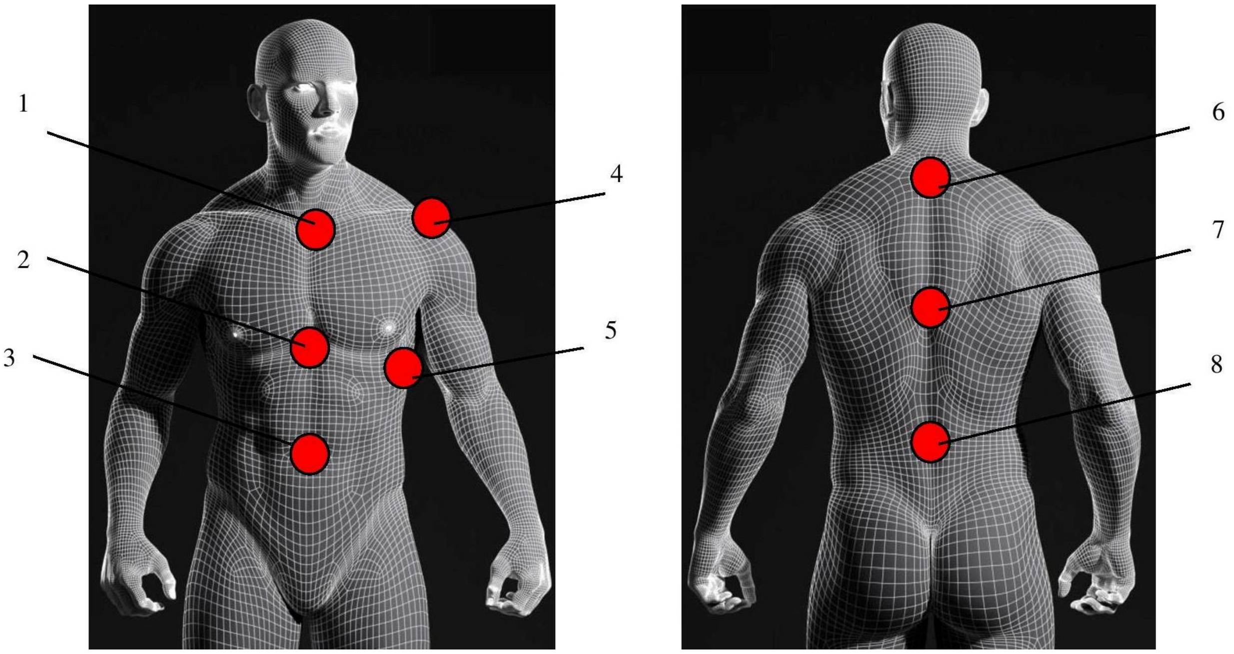

Figure 2 Schematic of the eight-point DT sensors location for IBK3.4 modules

The human trials were conducted with 10 volunteers (n=10). The volunteers are characterized by: age 45.5±1.5 years (16650.5±560.5 days), height 179.5±3.5 cm, weight 95.5±5.5 kg, breast circumference 110±1 cm, waist circumference 109.5±4.5 cm. The research and methodology have been selected in such a way that it is possible to use personal wireless systems in a reliable space to evaluate the biophysical properties of new CWCE samples [16]. According to the protocol, the volunteers were dressed in the ensemble for 20 minutes to stabilize the upper inter-layer air gap microclimate conditions.

The wireless measurement system (WBAN) IBK3.4 and software WBIM Soft 6.0 and WBIMSoft Core Analytics was chosen to conduct the research [16]. The system is easy to use and rugged enough to sustain the harshest environments.

The structure of the wireless body area network (WBAN) consisted of 4 remote modules with 4 dual-type sensors (DT sensors) in each [17]. The use of the system allows obtaining parameters of the inter-layer air gaps such as temperature and relative humidity in real time. The 8-point model of the location of DT sensors was selected for the studies (Figure 2) [18]. Additionally, further expansion of areas for measuring of the inter-layer air gaps microclimate parameters is possible due to the wider use of conductive polymers in the structure of fabric layer [19].

A multi-layer clothing system is developed and integrated with the human model based on [20, 21] with a coupled heat and moisture model of clothing materials for body element S4 (Figure 3).

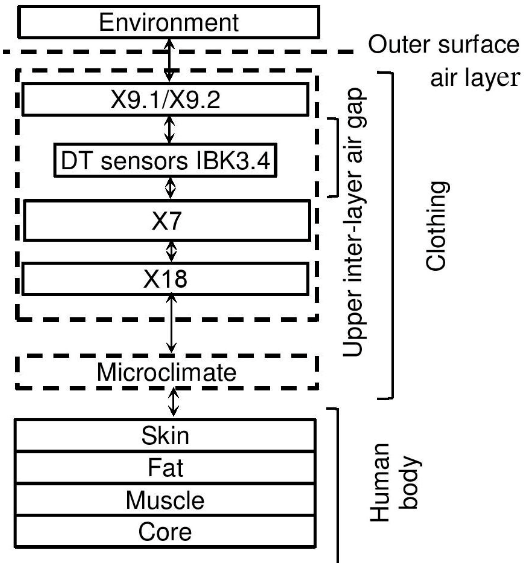

Figure 3 Human body-clothing-environment system for covered body segment S4 by cold weather clothing ensemble and for point 2 of DT sensors location

4 RESULTS AND DISCUSSION

Accordingly to [22] the classification of effects air gap characteristics for each point of DT sensors IBK3.4 were evaluated in Table 3.

The DT sensors (temperature and relative humidity) of the selected system were located over a thermal or sweat-wicking layer on insulation suit jacket X7 [18].

The second half part (30 min.) of step 2 in the research is determining according to the established procedure. The averages and standard deviation diagrams of temperature and relative humidity in the eight sensor points of the ensemble upper inter-layer air gap were plotted in the Figures 4 and 5.

As is shown in Figures 4 and 5, the average temperature values in eight points of the upper inter-layer air gap varied in the range 14-24°C for the E1 ensemble and 21-25°C for the E2 ensemble. The average relative humidity values varied in the range of 25-75% and 15-73% accordingly. The magnitude of the root-mean-square deviation of temperature and relative humidity for the E2 ensemble is significantly smaller than for E1 ensemble. The long winter jacket, unlike the sentry coat, creates conditions that are more comfortable and minimizes the temperature and relative humidity drops at different points of the upper inter-layer air gap.

The step 2 analysis shows that the presence of waist drawstrings in the long winter jacket allowed increasing the temperature for 47.94% at points 1, 2, 3 and 7 that completely leveled in the jacket design. Also, the temperature was 25% higher for the jacket due to the rack collar in the point 8 of the long winter jacket. The considerable elongation of the sentry coat and the absence of constructive restriction of air movement led to temperature decrease at the lower measurement points, which was not compensated by the heat production of the subject's movements. As is shown in Table 4, the moisture accumulation was decreased by 11% due to the use of the basic fabric laminated by the membrane for the jacket.

Table 3 The classification of air gap characteristics for each point of DT sensors IBK3.4

Code of point	Traits			Orientation	Dynamics
	Thickness	Location	Heterogeneity		
1	Variable	In clothing layers	Non-uniform thickness	Horizontal	Induced by human body motion
2	Constant		Non-uniform thickness		Induced by human body motion
3	Variable		Contact area		Induced by human body motion
4	Variable		Contact area	Vertical / Inclined	Induced by fabrics
5	Variable		Contact area	Horizontal	Induced by human body motion
6	Constant		Non-uniform thickness		Induced by fabrics
7	Constant		Contact area		Induced by fabrics
8	Variable		Non-uniform thickness		Induced by human body motion

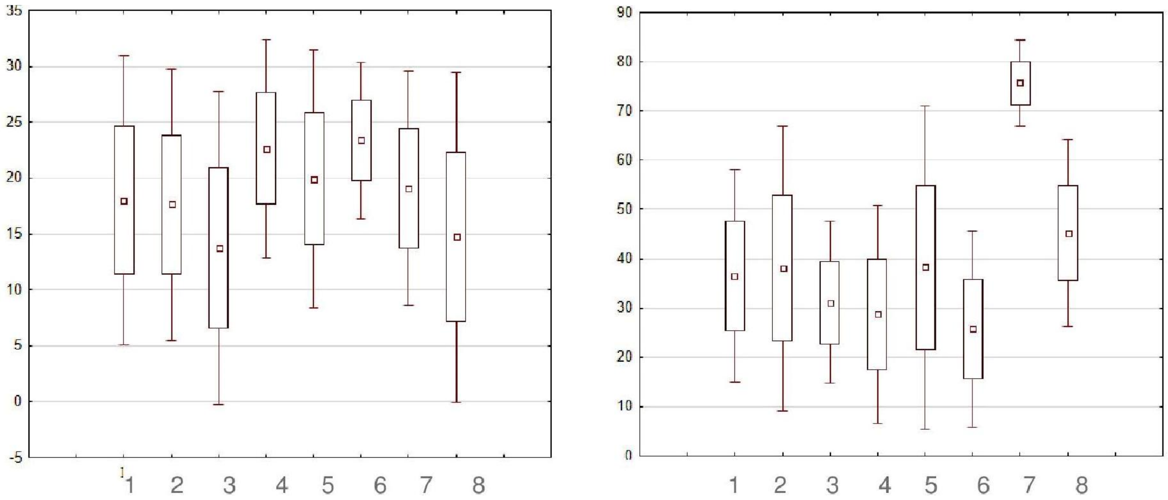

a) b)

Figure 4 Comparison of mean values and root-mean-square deviation of temperature T (a) and relative humidity H (b) in eight sensor points of the upper inter-layer air gap in the E1 ensemble

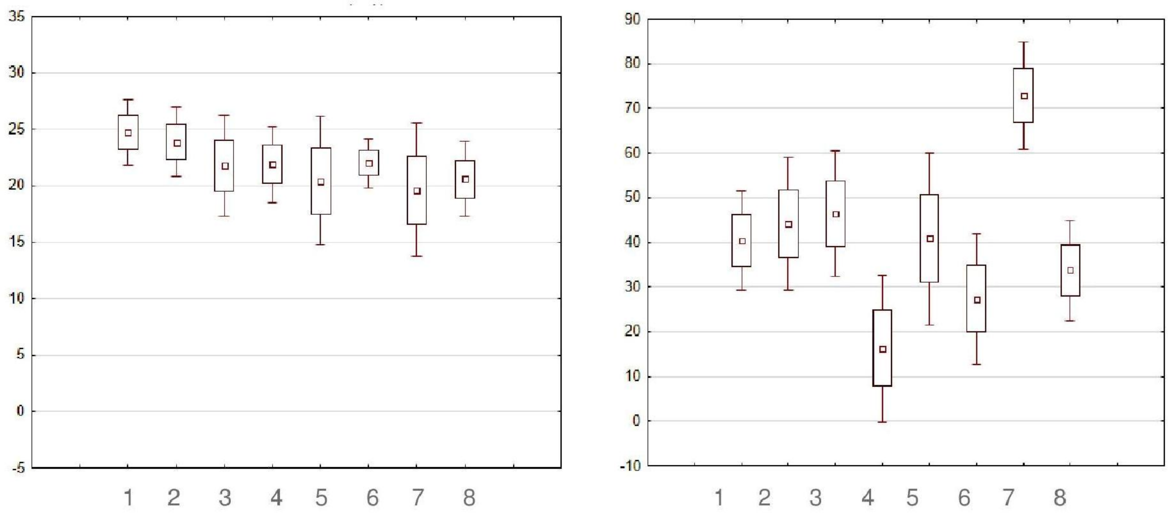

a) b)

Figure 5 Comparison of mean values and root-mean-square deviation of temperature T (a) and relative humidity H (b) in eight sensor points of the upper inter-layer air gap in the E2 ensemble

Table 4 Comparison of E1 and E2 ensemble

Code of the ensemble	The number of the sampled signals obtained from sensors	The average value		The minimum value	
		T [°C]	H [%]	T [°C]	H [%]
E1	19688	14.4	34.1	7.52	11
E2	12000	17.7	32.5	10.3	12

4.1 Optimization of the quantitative composition of the microclimate dynamics indicators

The Pearson correlation matrix was constructed to establish the relationship between temperature and relative humidity. The matrix analysis showed that some parameters were correlated at a significance level of 0.95. Therefore, it is advisable to minimize the number of sensor measurement points to reduce the required time to perform measurements and calculations. Conditionally we divide the upper inter-layer air gap into three groups: front (1, 2 and 3 points), side (4 and 5 points) and back (6, 7 and 8 points).

The DT sensors located in the front of the jacket and sentry coat correlate with each other in temperature and relative humidity. Therefore, points 1 and 3 cannot be used and we focus on the point 2, which is located in the middle of the front upper inter-layer air gap.

The side-sensors have a temperature correlation for the jacket and sentry coat but do not correlate with the relative humidity for the sentry coat, so it is necessary to use points 4 and 5 of sensor data. The sensor point 6 for temperature and relative humidity correlate with point 8 for the back of the jacket and sentry coat. The points 7 and 8 do not have correlation dependence with the relative humidity index for the jacket; therefore, it is advisable to use the points 7 and 8. Therefore, for further research on the eight points that were used in the previous step, we can use the points 2, 4, 5, 7 and 8. The regression equations were determined for sensors 1, 3 and 6, which have been eliminated (Figures 6 and 7).

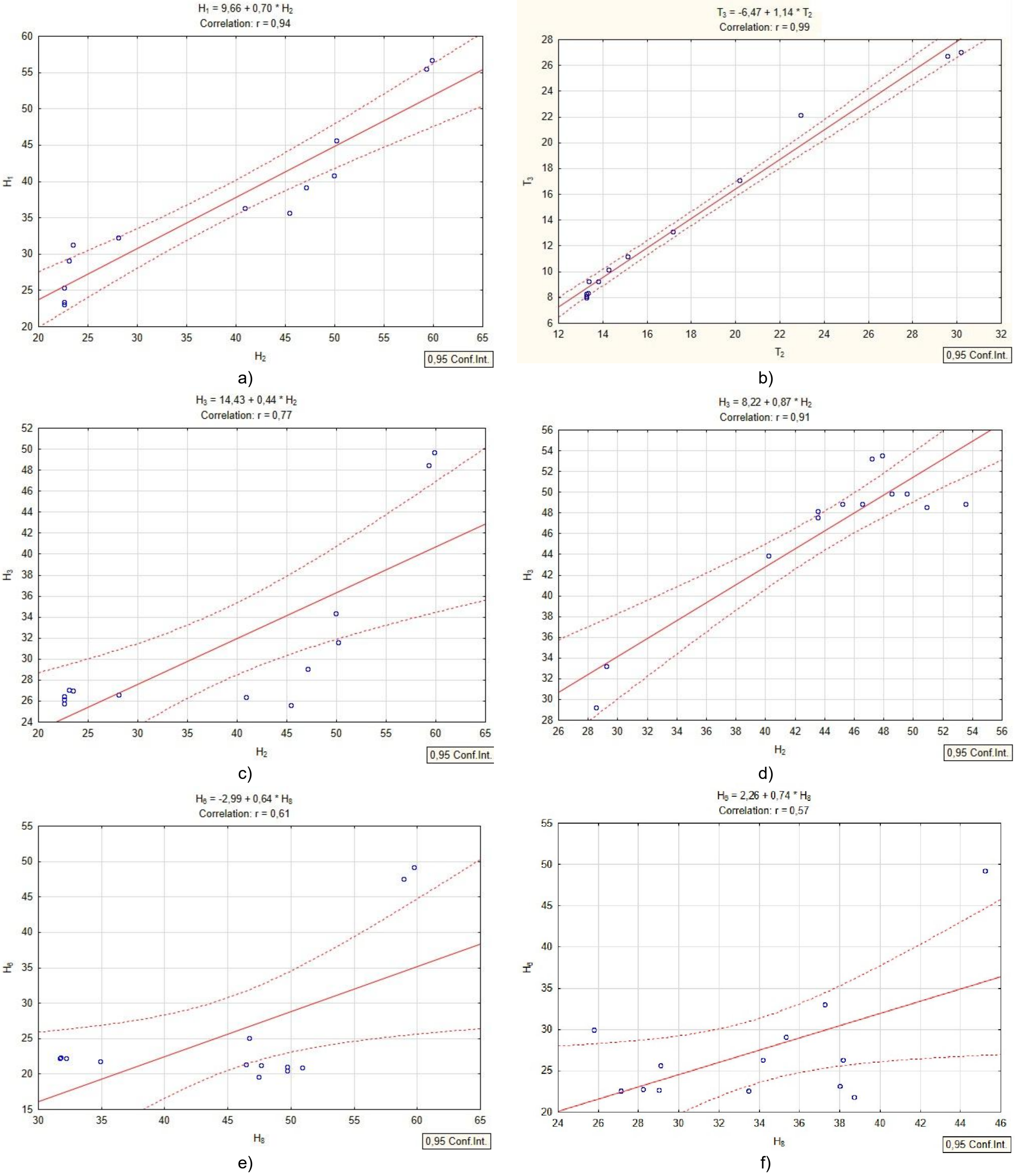

a)

b)

c)

d)

e)

f)

Figure 6 The regressive models of the relative humidity at given measurement points: a, c, e - E1 ensemble; b, d, f - E2 ensemble

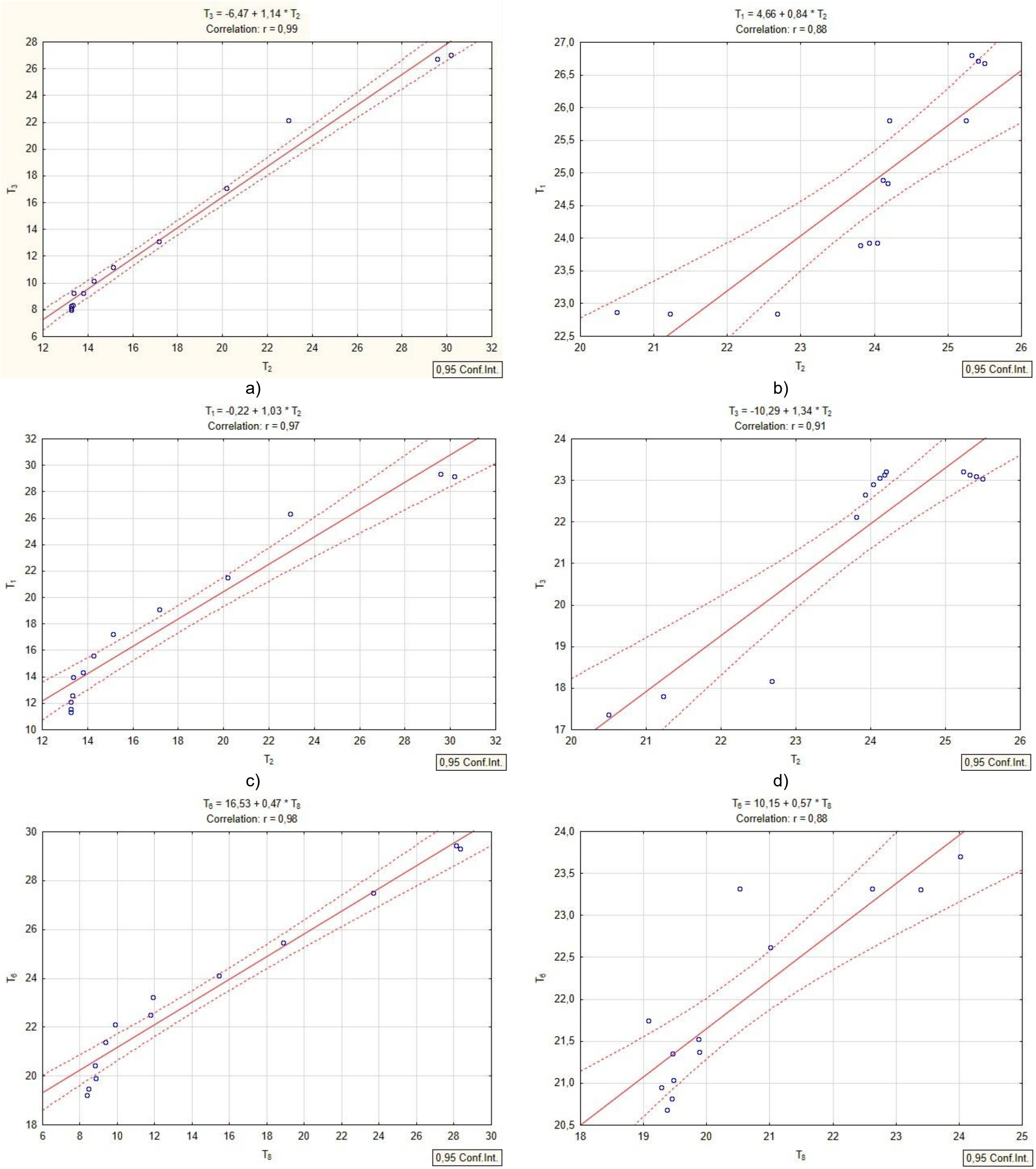

a) b) c) d) e) f)

Figure 7 The regressive models of the temperature dependencies at given measurement points: a, c, e - E1 ensemble; b, d, f - E2 ensemble

5 CONCLUSIONS

To conclude, the tests of studies of various samples of the upper layer of the cold weather clothing ensemble on volunteers in a climate chamber showed a significant influence of the outer_layer item on the temperature dynamics and relative humidity of the inter-layer air gaps microclimate. The E2 ensemble has an average temperature value of 18.6% and a relative humidity 4.9% lower in the upper inter-layer air gap compared to the sentry coat. The minimum value of the temperature for E1 ensemble is 27% lower and the relative humidity is 8.3% lower than for the E2 ensemble.

The finding reported can be used by developers of military clothing systems to better understand microclimate dynamics (e.g., temperature and relative humidity) of inter-layer air gaps. Thus, in future studies, it is advisable to pay considerable attention to the volume and mass optimization of the cold weather clothing ensemble and influence on inter-layer air gaps parameters.

***Acknowledgment**: The research was supported by the project through the financial support of the Ministry of Education and Science of Ukraine registration number 0117U007237. In addition, the views, opinions, and findings in this paper are those of the authors and should not be construed as an official Ministry of Defence of Ukraine position or decision unless so designated by other official documentation.*

6 REFERENCES

1. Giesbrecht G.: Cold weather clothing, Accessed: 2018-07-18, Available from: https://www.umanitoba.ca/faculties/kinrec/hlhpri/media/Cold_Weather_Clothing.pdf
2. Kurhanskyi A., Sakovets V.: Predicting thermophysiological comfort limits to simulate the personal protective equipment abilities, Proceedings of Naukovi rozrobky molodi na suchasnomu etapi, September 2017, KNUTD, Kyiv, pp. 97-98
3. Schutz H.G., Cardello A.V., Winterhalter C.: Perceptions of fiber and fabric uses and the factors contributing to military clothing comfort and satisfaction, Textile Research Journal 75(3), 2005, pp. 223-232, https://doi.org/10.1177/004051750507500307
4. Potter A. W. et al.: Comparison of cold weather clothing biophysical properties, US Army, Canadian Department of National Defence, and Norwegian Military, US Army Research Institute of Environmental Medicine Natick United States, 2018
5. Xu X., Werner J.A.: A dynamic model of the human/clothing/environment-system, Applied Human Science 16(2), 1997, pp. 61-75
6. Kurganska M., Bereznenko S., Pavlova M.; Vasylenko V.: Effects of physical properties of clothes on parameters of the microclimate layer, Bulletin of KNUTD 110(3), 2017, pp. 77-82
7. Garanina O.: The development of scientific foundations for the finishing of textile materials, taking into account the nanostate of dyes, Qualifying scientific work on the manuscript, The dissertation for the degree of doctor of technical sciences, specialty 05.18.19 - technology of textile, garment and knitwear, Kyiv National University of Technology and Design, Kyiv, 2017
8. Tharion W.J., Hoyt R.W.: Form Factor Evaluation of Open Body Area Network (OBAN) Physiological Status Monitoring (PSM) System Prototype Designs, US Army Research Institute of Environmental Medicine Natick United States Vol(18-06), 2018
9. Oviatt C.M.: Perception vs. Reality: Improving Mission Commander Decision Making Capabilities by use of Heart Rate Zone Feedback in Training Environments, Air Force Institute of Technology Wright-Patterson AFB United States, 2017
10. Kutilek P. et al.: Wearable systems and methods for monitoring psychological and physical condition of soldiers, Advances in Military Technology 12(2), 2017, pp. 259-280
11. Das A., Alagirusamy R., Kumar P.: Study of heat transfer through multilayer clothing assemblies, AUTEX Research Journal 11(2), 2011, pp. 54-60, http://www.autexrj.org/No2-2011/5_0013_11.pdf
12. Marszałek A., Bartkowiak G., Dąbrowska A.: Assessment of the effectiveness of modular clothing protecting against the cold based on physiological tests, International Journal of Occupational Safety and Ergonomics, 2018, pp. 1-12, DOI:10.1080/10803548.2017.1376927
13. Birnbaum R.R., Crockford G.W.: Measurement of the clothing ventilation index, Applied Ergonomics 9(4), 1978, pp. 194-200, https://doi.org/10.1016/0003-6870(78)90079-0
14. Tikuisis P., Keefe A.: Effects of cold strain on simulated sentry duty and marksmanship, Aviation, space, and environmental medicine 78(4), 2007, pp. 399-407
15. Lotens W.A., Havenith G.: Calculation of clothing insulation and vapour resistance, Ergonomics34(2), 1991, pp. 233-254, https://doi.org/10.1080/00140139108967309
16. Kurhanskyi A.V., Vasylenko V.M., Kurganska M.M., Sakovets V.V.: Remote monitoring system for microclimate and pressure in real time based on native touch networks, Bulletin of the Kyiv National University of Technologies and Design 108(2), 2017, pp. 114-119
17. Kurganska M.M., Vasylenko V.M., Kurhanskyi A.V., Sakovets V.V., Maliy A.O., Opanasenko K.V.: Prediction of dynamic characteristics of thermal insulation properties of winter clothing sets, Bulletin of the Kyiv National University of Technologies and Design 112, 2017, pp. 82-88
18. Bogdan A., Zwolińska M.: Future trends in the development of thermal manikins applied for the design of clothing thermal insulation, Fibres & Textiles in Eastern Europe 20(4), 2012, pp. 89-95
19. Novak D., Budash Y., Bereznenko N.: Graphic modeling of conductive filler spatial distribution in polymer matrix, Vlakna a Textil (Fibres and Textiles) 23(2), 2016, pp.37–42
20. Stolwijk J., Hardy J.: Control of body temperature, Comprehensive Physiology, 2010, pp.45-68, https://doi.org/10.1002/cphy.cp090104
21. Wan X., Fan J.: A transient thermal model of the human body–clothing–environment system, Journal of Thermal Biology 33(2), 2008, pp. 87-97, https://doi.org/10.1016/j.jtherbio.2007.11.002
22. Deng M., Wang Y., Li P. Effect of air gaps characteristics on thermal protective performance of firefighters' clothing: A review, International Journal of Clothing Science and Technology 30(2), 2018, pp. 246-267, https://doi.org/10.1108/IJCST-07-2017-0103

SCREEN PRINTING ON SILK FABRIC USING NATURAL INDIGO

Rattanaphol Mongkholrattanasit[1], Charoon Klaichoi[1], Nongnut Sasithorn[1], Wasana Changmuang[1], Kasem Manarungwit[1], Kongkiat Maha-In[1], Photsathon Ruenma[1], Nuttapong Boonkerd[1], Nutthamon Sangaphat[1] and Manat Pangsai[2]

[1]Faculty of Industrial Textiles and Fashion Design, Rajamangala University of Technology Phra Nakhon,
No. 517 Nakhon Sawan Road, Suanchitladda Sub-district, Dusit District, Bangkok, 10300 Thailand
[2]Department of Mechanical Engineering, Faculty of Engineering, Srinakharinwirot University,
Ongkharak, Nakhonnayok 26120, Thailand
rattanaphol.m@rmutp.ac.th; jaroon.k@rmutp.ac.th; nongnut.s@rmutp.ac.th; wasana.c@rmutp.ac.th; kasem.m@rmutp.ac.th; kongkiat.m@rmutp.ac.th; thon_r@hotmail.com; nuttapongss_55@hotmail.com; dew95_9@hotmail.com; manat@swu.ac.th

Abstract: *The purpose of this research was to study the printing silk fabric with natural indigo, using a modified starch produced from wild taro (Colocasia esculenta (L.) Schott) corm as thickening agent. The effects from the concentration of the natural indigo dye, added to the modified starch of wild taro corm, in recording the results of thiourea dioxide and sodium hydroxide were examined, after combining the printing paste. The colour values, colour strength, and the fastness properties of printed silk fabric were investigated and the results recorded in the following study. The optimal formula of printing silk fabric using natural indigo paste was prepared by mixing 50% natural indigo paste, 5% thickening agent from modified starch of wild taro corm, 6% thiourea dioxide, 0.4% sodium hydroxide and 38.6% water. The pattern design produced from these combinations in the printing areas on fabrics showed an excellent standard of printing quality and satisfactory colour fastness results were recorded at a level of good to very good.*

Keywords: *printing, natural indigo, silk, thickening agent, wild taro*

1 INTRODUCTION

Natural colourants are generally eco-friendly and have many advantages over synthetic dye [1]. Natural dyes have been an integral part and parcel of human lives since time immemorial [2]. Natural dyes are derived from naturally occurring sources such as animals, insects, bacteria, fungi, minerals and various parts of plants, including roots, bark, leaves, flowers, and fruit, etc. [3-5]. Natural dyes are currently undergoing a revival in craft, food, cosmetic, leather, dye sensitizer, medical plants and textile dyeing and printing [4-5]. In recent years, the ban on toxic azo and benzidine synthetic dyes with 24 carcinogenic aromatic amines set by many countries worldwide has increased the scope for the reintroduction of colourants from natural sources once again, with positive cause and effect to our environment [6-7]. Natural dyes produce very lustrous soft and soothing shades as compared to synthetic dyes [8]. Natural dyes have become quite popular amongst environmentally conscious consumers and are receiving more and more attention in the market of ethical conscious environmentally friendly sales [9]. Nowadays, the market for natural dyes in the textile industry is experiencing a positive resurgence, as Western consumers have become more concerned about the possible health and environmental impact of synthetic dyes [4, 10].

Silk is a natural fiber produced by the silk worm and has been used as a fiber material for over thousands of years [11]. Silk fiber contains an amount of amino ($-NH_2$) and carboxylic ($-COOH$) groups, at either ends of its chemical structure, this combination makes it possible to be able to dyed the silk with acid dyes, reactive dyes, metal complex dyes, etc. [11].

Natural indigo, known in different names in different parts of the world, has been in use since around 7000 BC for the dyeing of cotton in attractive and bright blue shades [12]. Plants belonging to the genus *Indigofera* species are most valuable for producing natural indigo. The leaves of these species are usually divided into smaller leaflets. The small rose, purple or white flowers are grown and developed naturally into spikes. The fruit is a type of pod, usually with a thin partition between the seeds [13]. The leaves, flowers and pod of the indigo plant are shown in Figure 1. The colouring matter in the plant leaves are present as a glucoside of indoxyl, known as indican, an organic compound, which is hydrolysed to the indoxyl, by enzymatic action, of which an indigo blue dye is then obtained by a subsequent oxidation process (Figure 2) [14]. In ancient times, reduction of indigo was carried out by a fermentation technique, which included use of ripe fruit and stale urine mixed together, then assisted by wood ash or lime as an alkaline, to produce the desired results.

The solution prepared in this way was left overnight for reduction and solubilization of the indigo dye produced from this process. The reduction of indigo dye into its leuco from is shown in Figure 3 [14].

Wild taro (*Colocasia esculenta* (L.) Schott) is a vegetative propagated root crop species of the monocotyledonous family *Araceae*. It is grown in almost all tropical regions of the world [15, 16]. Wild taro tubers or corms contain considerable amounts of starch (70-80 g/100 g dry taro) [17]. The corm of wild taro is shown in Figure 4. Wild taro tubers contain an oxalic acid crystal in the form of a soluble oxalic acid and insoluble oxalate salts, which cause a skin irritation and pungent odor in unwashed wild taro corms [16].

Figure 1 Indigo plant: (left) leaves and pod (right) flowers

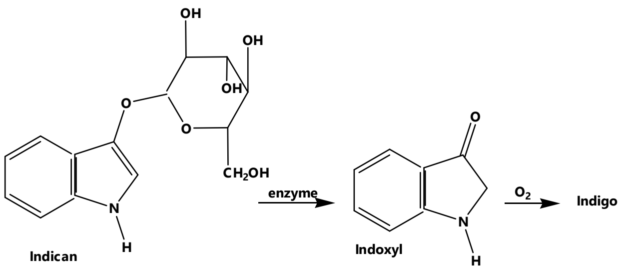

Figure 2 Natural synthetic route to indigo from indicant in *Indigofer tinctoria* [14]

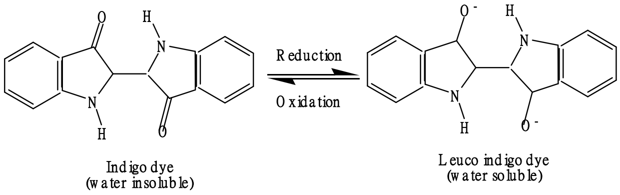

Figure 3 The reduction and oxidation of indigo dye [14]

Figure 4 Wild taro tubers or corm

The aim of this present work was to study the printing of silk fabric with the effects created from the use of natural indigo dye, using a new thickening agent from the modified starch of wild taro corm. The printing and fastness properties were investigated and recorded.

2 EXPERIMENTAL

2.1 Materials and chemicals

A commercially produced plain-weave silk fabric was purchased from market. Silk fabric was scoured with an aqueous nonionic surfactant solution at a temperature of 50°C for 30 mins, then thoroughly rinsed and air dried at room temperature. Fresh materials of *Indigofera tinctoria* Linn were collected from Nakhon Phanom province, Thailand. The following chemicals of laboratory grade were used in the experiment: thiourea dioxides ($(NH_2)_2CSO_2$), sodium hydroxide (NaOH) and hydrogen peroxide (H_2O_2), supplied by Star Tech Chemical Industrial Co., Ltd. A nonionic soaping agent was purchased from Boonthawee Chemephan Co, Ltd. (Thailand). Wild taro corms used in this experiment was collected from Chantaburi province, Thailand.

2.2 Extraction of indigo dye

Plant materials were cut to small pieces, fermented in water for one night and then added twice in volume of $Ca(OH)_2$ solution (pH~11), blew the air for 15 mins to precipitate indigo [18]. The precipitated indigo or indigo paste was used for printing as such without any further purification.

2.3 Preparation modified starch of wild taro corms

The wild taro corms were dried in sunlight for 1 month and then crumbled using a blender; the corms were then milled and ground through a 355 µm mesh sieve. The resulting powder produce from the wild taro corm was dispersed in alkaline aqueous methanol at 80%v/v. Then, monochloro-acetic acid (MCA) was added in solid form to the (above mentioned) solution and mixed for 10 min. The temperature was adjusted and raised to 70°C for a further 60 min. The mixture paste was cooled in room temperature and then filtered through a suck funnel, to resolve in water. An added amount at 50% of HCl was added drop by drop until it became neutral. The development reaction of this product through all of the above processes and methods was then precipitated and washed with ethanol to remove ionic salts. The carboxymethylated wild taro corm (or modified starch of wild taro) was removed by filtration and an added process of washing three times with methanol. The washed product was dried at 40°C for 4 h. The milling was size reduced to 355ve size. The powder was stored in a desiccator.

Table 1 Recipe of natural indigo printing paste

Parameters	Recipe [g/kg]				
	Indigo paste [g]	**Modified starch [g]**	**Thiourea dioxide [g]**	**NaOH [g]**	**50°C water [ml]**
Effect of indigo paste conc.	500-900	50	60	10	X
Effect of modified starch conc.	500	0-90	60	10	X
Effect of thiourea dioxide conc.	500	50	0-120	10	X
Effect of NaOH conc.	500	50	60	0-10	X

2.4 Preparation of printing paste

The printing paste was prepared using the following recipe as shown in Table 1. It was prepared by mixing concentrations of indigo, modified starch of wild taro, thiourea dioxides and sodium hydroxide in water, then continual stirring for 20 min to produce a homogenous paste until the reduction was completed. With indigo the colour of the leuco indigo solution is yellow green when reduced with thiourea dioxide.

2.5 Printing process

The printing process consisted of forcing a various print paste through the open areas of the screen with a flexible synthetic rubber squeegee. The rubber blade, which is contained in a wooden support, is drawn steadily across the screen at a constant angle and pressure. The pressures exerted must be as similar as possible [11]. The fixation was done by hot air at 60°C for 10 mins. Following these steps, the fabric was then immersed with 5 g/L of H_2O_2 for 15 min and finally the samples were washed in 1 g/L of a soaping agent at 60°C for 15 min and then air-dried at room temperature.

2.6 Measurement of the viscosity of the printing paste

The rheological properties of the printing pastes were measured at 25°C using a viscometer (BROOKFIELD DV-II+Pro). The apparent viscosity (η) of the printing pastes at various rates of shear was calculated from the shearing stress (τ) [dyne/cm^2] and rate of shear (D) as follows [19-20]:

$$\eta = \tau / D \qquad (1)$$

2.7 Evaluation of colour value and colour strength

The colour value (*CIE L**, *a**, *b**) and color strength (*K/S*) of the printed samples were evaluated using a spectro-photometer (Hunter Lab Color Quest XE, USA). The *K/S* value and colour value (*CIE L*, a*, b**) of all printed fabrics were determined at 650 nm (λ_{max}) and measured for five different locations for each sample. The average of these values were reported and showed a standard deviation within the order of ±0.04 in all cases. The *L** value indicates perceived lightness in CIELAB colour space. The *L** scale ran from 0 (black) to 100 (white); the higher the *L** reading the lighter the colour. The *a** value indicates red (+*a**) and green (-*a**) while the *b** value indicates yellow (+*b**) and blue (-*b**) [21-22]. The colour strength in terms of *K/S* values were calculated using the Kubelka-Munk equation:

$$K/S = (1-R)^2/2R \qquad (2)$$

where R is representative of reflectance, K is the sorption coefficient and S is the scattering coefficient [21-22].

2.8 Colour fastness evaluation

The color fastness to washing, light, rubbing, water, perspiration of the printed samples was determined according to ISO 105-C06 A1S: 2010, ISO 105-B02: 1994, ISO 105-X12: 2001, ISO 105-E01: 2010, and ISO 105-E04: 2008 respectively.

3 RESULTS AND DISCUSSION

3.1 Effect of dye concentration on colour value

Silk fabric samples printed with natural indigo at different natural indigo dye concentrations is shown in Table 2. It can be observed that the colour strength increased when the natural indigo concentration ranged from 500 to 800 g. The changes of *K/S* values are not obvious when the concentration of dye is above 800 g. The reason was that the penetration of natural indigo has reached in it saturated state when the concentration was more than 800 g. The *b** values varied from about -8 to -12 when the natural indigo dye concentration ranges from 500 to 900 g. From the results, it is promising that the silk fiber has various carboxylic (-COOH) groups in its structure. The carboxylic groups helped to interact very well to the amine (-NH) or carbonyl (C=O) groups of the natural indigo via hydrogen bonds resulted to easy printed with natural indigo [23]. The silk with these measurements when printed with natural indigo paste showed a blue shade.

Table 2 Colour values, colour strength, viscosity and colour obtained at varying dye concentrations

Dye conc. [g]	L*	a*	b*	K/S	Viscosity [cpi]	Colour obtained
50	50.10	-4.22	-8.84	3.04	18.476	
60	49.95	-4.37	-8.69	3.45	19.109	
70	48.30	-4.59	-12.86	4.19	20.823	
80	47.57	-4.70	-12.70	4.26	21.723	
90	46.06	-4.29	-12.37	4.29	22.874	

Table 3 Colour values, colour strength, viscosity and colour obtained at varying modified starch of wild taro concentrations

Modified starch conc. [g]	L*	a*	b*	K/S	Viscosity [cpi]	Colour obtained
0	52.23	-5.50	-8.22	2.63	9.598	
30	51.97	-4.88	-9.35	2.72	9.838	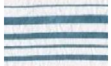
50	50.10	-4.22	-9.84	3.04	18.476	
70	50.28	-5.47	-10.45	3.01	18.956	
90	49.19	-4.96	-9.94	3.09	19.036	

3.2 Effect of modified starch of wild taro concentration

The colour value, colour strength and viscosity of the effect from the modified starch of wild taro concentration results are obtained and presented in Table 3. Table 3 shows that increasing the modified starch of wild taro concentration from 0 to 50 g resulted in an improvement in the *K/S* values of the natural indigo print, which could be discussed in terms of higher paste viscosity and minimum undue penetration or flashing of the dye. A further increase in the concentration of the modified starch of wild taro has practically no effect on the depth of the obtained print and was accompanied with the negative impact on softness [20].

3.3 Effect of thiourea dioxide and sodium hydroxide concentration

The effect of thiourea dioxide concentration on silk fabric printed with the natural indigo in a print paste including thiourea dioxide and sodium hydroxide is shown in Table 4. At a constant concentration of 10 g sodium hydroxide, the *K/S* value increased with an increasing concentration of thiourea dioxide. This increase almost saturated over the concentration of 90 g thiourea dioxide. The effect of the sodium hydroxide concentration on silk fabrics printed with natural indigo is shown in Table 5. The total *K/S* value decreased with the added increasing concentration of sodium hydroxide over the range of 4 g. The effect and use of the amount of sodium hydroxide used in its concentrated form was not enough at 6 g sodium hydroxide. The effect of the thiourea dioxide and sodium hydroxide on the *K/S* value of the dye indicates clearly that the solubilization of the dye from the *Indigofer tinctoria* leaves is very similar to that found in vat dyes which ordinarily is initiated by the reduction of the insoluble dye species in the plant tissue into soluble leuco forms which are sparingly soluble [24].

3.4 Fastness properties of printed silk

The fastness properties of silk fabric printed with 500 g of natural indigo dye, 50 g of modified starch of wild taro corm, 60 g of thiourea dioxide and 10 g of sodium hydroxide are presented in Table 6. Table 6 indicates that the washing and water fastness rating of silk fabrics printed with the natural indigo were good to very good (4 to 4-5). The results indicated that the silk fibers much be reached to the indigo dye via strongly chemical bonds. The formed bond should be enhanced the stability of dye when exposed to wash and water. Colour fastness to light was fair (5). Colour fastness to perspiration of all printed silk fabrics showed good to very good (4 to 4-5). The results showed that indigo dye and silk fibers interacted very well via the hydrogen bonds which helped to sustain the colour of dye. Colour fastness to rubbing was found to be in the range of 4-5 (good to very good). This result can be also attributed to the insolubility of the indigo characteristics [25].

Table 4 Colour values, colour strength, viscosity and colour obtained at varying thiourea dioxide concentrations

Thiourea dioxide conc. [g]	L*	a*	b*	K/S	Viscosity [cpi]	Colour obtained
0	67.66	-3.67	0.09	0.74	8.548	
30	60.35	-3.20	-4.17	1.20	15.490	
60	50.10	-4.22	-8.14	3.04	18.476	
90	49.09	-4.16	-8.13	3.10	19.101	
120	48.98	-4.17	-8.25	3.13	19.116	

Table 5 Colour values, colour strength, viscosity and colour obtained at varying sodium hydroxide (NaOH) concentrations

NaOH conc. [g]	L*	a*	b*	K/S	Viscosity [cpi]	Colour obtained
0	48.78	-4.35	-8.33	2.01	18.670	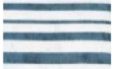
2	48.58	-4.66	-9.63	2.30	18.754	
4	48.14	-5.46	-10.12	3.34	18.695	
6	49.62	-5.02	-9.03	3.10	18.800	
10	50.10	-4.22	-8.84	3.04	18.476	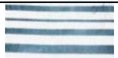

Table 6 Colour fastness to washing, water, perspiration and light

Colour fastness to	Colour change	Colour staining					
		Acetate	Cotton	Nylon	Polyester	Acrylic	Wool
washing	4	4-5	4-5	4-5	4-5	4-5	4-5
water	4-5	4-5	4-5	4-5	4-5	4-5	4-5
perspiration (acid)	4	4-5	4-5	4-5	4-5	4-5	4-5
perspiration (alkaline)	4	4-5	4-5	4-5	4-5	4-5	4-5
light	5	-	-	-	-	-	-

4 CONCLUSION

It is evident from the results that silk fabric can be successfully screen printed with natural indigo using modified starch of wild taro corms. The investigation shows that the recipe is suitable for printing. The modified starch of wild taro corms could be used as a thickening agent for natural indigo printing on silk fabric. Printed silk fabric exhibited good to very good colour fastness.

ACKNOWLEDGEMENTS: This research was financially supported by The National Research Council of Thailand and Rajamangala University of Technology, Phra Nakorn.

5 REFERENCES

1. Wang H., Li P., Zhou W.: Dyeing of silk with anthocyanins dyes extract from Liriope platyphylla fruits, Journal of Textiles, 2014, 9 p., doi: 10.1155/2014/587497
2. Sheikh J., Jagtap P.S., Teli M.D.: Ultrasound assisted extraction of natural dyes and natural mordants vis a vis dyeing, Fibers and Polymers 17(5), 2016, pp. 738-743, doi: 10.1007/s12221-016-5031-0
3. Saikhom J.D., Potsangbam K.S., Choudhury M.D.: Effect of various mordants in Kum dyed cotton, silk and woollen yarns, Indian Journal of Fibre and Textile Research 40(2), 2015, pp. 184-189
4. Mongkholrattanasit R., Saiwan C., Klaichoi C. Rungruangkitkrai N., Punrattanasin N., Sriharuksa K., Nakpathom M.: Ecological dyeing of silk fabric with lac dye by using padding techniques, Journal of the Textile Institute 106(10), 2015, pp. 1106–1114, doi: 10.1080/00405000.2014.976957
5. Mongkholrattanasit R., Saiwan C., Klaichoi C., Rungruangkitkrai N., Punrattanasin N., Sriharuksa K., Nakpathom, M.: Eco-dyeing of silk fabric with Garcinia Dulcis (Roxb.) Kurz bark as a source of natural dye by using the padding technique, Journal of Natural Fiber 13(1), 2016, pp. 65-76, doi: 10.1080/15440478.2014.984056

6. Yusuf M., Khan M. A., Mohammad, F.: Investigations of the colourimetric and fastness properties of wool dyed with colorants extracted from Indian madder using reflectance spectroscopy, Optik 127(15), 2016, pp. 6087-6093, doi: 10.1016/j.ijleo.2016.04.084
7. Rather L.J., Shabbir M., Bukhari M.N., Shahid M., Khan M.A., Mohammad F.: Ecological dyeing of woollen yarn with Adhatoda vasica natural dye in the presence of biomordants as an alternative copartner to metal mordants, Journal of Environmental Chemical Engineering 4(3), 2016, pp. 3041-3049, doi: 10.1016/j.jece.2016.06.019
8. Mulec I., Gorjanc M.: The influence of mordanting on the dyeability of cotton dyed with turmeric extract, Tekstilec 58(3), 2015, pp. 199-208, doi: 10.14502/Tekstilec2015.58.199-208
9. Čuk N., Gorjanc M.: Natural dyeing and UV protection of raw and bleached/mercerised cotton, Tekstilec 60(2), 2017, pp. 126-136, doi: 10.14502/Tekstilec2017.60.126-136
10. Samanta A.K., Agarwal P.: Application of natural dyes on textiles, Indian Journal of Fibre and Textile Research 34(4), 2009, pp. 384-399
11. Babel S., Gupta R.: Screen printing on silk fabric using natural dye and natural thickening agent, Journal of Textile Science & Engineering 6, 2016, pp. 1-3, doi: 10.4172/2165-8064.1000230
12. Chakraborty J.N., Chavan, R.B.: Dyeing of denim with indigo, Indian Journal of Fibre and Textile Research 29(1), 2004, pp. 100-109
13. Nisachon N.: Indigo natural dye and hand-woven textile in Thailand, Proceedings of Revival of Natural Indigo Dye, 1998, pp. 109-112
14. Głowacki E.D., Voss G., Leonat L., Irimia-Vladu M., Bauer S., Sariciftci N.S.: Indigo and Tyrian purple– from ancient natural dyes to modern organic semiconductors, Israel Journal of Chemistry 52(6), 2012, pp. 540-551, doi: 10.1002/ijch.201100130
15. Klaichoi C., Mongkholrattanasit R., Rungruangkitkra N.: Printing of silk fabric with reactive dye using flour of wild taro corm as a resist printing paste, Materials Science Forum 857, 2016, pp. 503-506, doi: 10.4028/www.scientific.net/MSF.857.503
16. Klaichoi C., Mongkholrattanasit R., Rungruangkitkrai N.: Application of pigment dye and resist printing paste from flour of wild taro (Colocasia esculenta (L.) Schott) for printing of silk fabric. Advanced Materials Research 1030-1032, 2014, pp. 410-413, doi: 10.4028/www.scientific.net/AMR.1030-1032.410
17. Klaichoi C., Mongkholrattanasit R., Rungruangkitkrai N.: Silk fabric painted with natural dye from Acacia Catechu Willd. by using flour of wild taro (Colocasia Esculenta (L.) Schott) as resist printing paste, Advanced Materials Research 1030-1032, 2014, pp. 434-437, doi: 10.4028/www.scientific.net/AMR.1030-1032.434
18. Chanayath N., Lhieochaiphant S., Phutrakul S.: Pigment extraction techniques from the leaves of Indigofera tinctoria Linn. and Baphicacanthus cusia Brem. and chemical structure analysis of their major components, CMU J 1, 2002, pp. 149-160
19. Abd E.I., Rekaby M., Abdel-Rahman A.H., El-khabery Sh.A.: Preparation and characterization of phosphorylated Sesbania Galactomannan gum derivatives and their applications in textile printing, Research Journal of Textile and Apparel 16(1), 2012, pp. 68-76, doi: 10.1108/RJTA-16-01-2012-B007
20. El-Zairy E.M.R.: New thickening agent based on Aloe vera gel for disperse printing of polyester, Autex Research Journal 11(2), 2011, pp. 66-70
21. Giles C.H.: A Laboratory course in dyeing, West Yorkshire: Society of Dyers and Colourists, 1974
22. Duff D.G., Sinclair R.S.: Giles's Laboratory course in dyeing, West Yorkshire: Society of Dyers and Colourists, 1986
23. Wannajun S., Srihanam P.: Development of Thai textile products from bamboo fiber fabrics dyed with natural indigo, Asian Journal of Textile 2, 2012, pp. 44-50, doi: 10.3923/ajt.2012.44.50
24. Oduro W.O., Addo-Yobo F.: Enhancing the value of indigo-blue dyes from Lonchocarpus cyanescens leaves, International Journal of Applied Science and Technology 3(5), 2013, pp. 78-86
25. Son Y.A., Hong J.P., Tim T.K.: An approach to the dyeing of polyester fiber using indigo and its extended wash fastness properties, Dyes and Pigments 61(3), 2004, pp. 263-272, doi: 10.1016/j.dyepig.2003.11.001

IMPACT OF CARBONIZATION TEMPERATURE ON ACTIVATED CARBON WEB FOR EMI SHIELDING AND OHMIC HEATING

M. Salman Naeem[1], Vijay Baheti[1], Jiri Militky[1], Veronika Tunakova[1], Qummer Zia Gilani[1], Saima Javed[2] and Promoda Behera[1]

[1]Department of Materials Engineering, Faculty of Textile Engineering, Technical University of Liberec
Studentská 2, 46117 Liberec, Czech Republic
[2]Department of Microbiology and Molecular Genetics, Punjab University Lahore, Pakistan
Muhammad.salman.naeem@tul.cz

Abstract: *In this work porous and electrically conductive activated carbon webs were produced by using acrylic fibrous waste followed by carding and needle punching. The physical activation of acrylic webs was performed by using high temperature muffle furnace at different temperatures (800, 1000 and 1200°C). These activated carbon webs were characterized by using energy dispersive X-rays, scanning electron microscopy and X-ray diffraction analysis. Further the utility of prepared activated carbon webs was checked for electromagnetic shielding ability. Activated carbon webs prepared at 800, 1000 and 1200°C showed the electromagnetic shielding effectiveness of 3.34, 26.06 and 28.29 dB at a frequency of 2.45 GHz. This behavior was attributed because of increased multiple internal reflections and stronger absorption of electromagnetic radiations in activated carbon webs. At the end these activated webs were checked for ohmic heating application. The web prepared at 800°C showed higher generation of heat (185°C) after 60 seconds at 1.5 volt.*

Keywords: *Activated carbon, acrylic fibrous wastes, electromagnetic shielding, textile recycling.*

1 INTRODUCTION

Nowadays electrically conductive textiles are gaining interest because of their possible applications in different fields like military, electromagnetic shielding as well as in sensors and actuators. The electrically conducting textiles can be obtained through different methods like metallization, electroless deposition, chemical coating, insertion of metallic yarns and deposition of thin layers having electrically conductive fillers such as carbon black particles [1]. For electromagnetic shielding (EM) application the surface electrical resistivity should be lower than 10^2 Ω/cm^2, however most of the synthetic fibres used in textiles are insulating materials having resistivity around 10^{14}-10^{15} Ω/cm^2 [2]. Therefore, in this age of telecommunication the widespread usage of electrical devices attracts attention towards electromagnetic interference shielding. The radiant electromagnetic signals emitting from electrical instruments not only can cause interference with the proper working of other instruments [3, 4]. In this context the idea of using conductive fabric to counter electromagnetic shielding is not a preferred choice because electromagnetic shielding inference is controlled by absorption, reflection and multiple internal reflections of EM radiations [5, 6]. However like metals, conductive fabrics are also accompanied with the lack of absorption of EM shielding and reflection is the only mechanism of EM shielding [7]. But for eco-friendly advancement in the field of EM shielding it is preferred to use light weight shielding materials having more absorption and weak secondary reflection. This is possible by a material having porous structure, high bulk and above all higher values of electrical conductivity. Although the much work was done for the development of carbon based porous structures having effective EM shielding ability [8, 9], however, the construction of light weight carbon structures with good EM shielding application is still a problem. In this paper the simple and affordable solution for the development of electrically conductive and porous carbon structures from acrylic fibrous waste is presented and basic properties together with functionality (electromagnetic shielding, ohmic heating) are evaluated.

2 MATERIALS AND METHODS

2.1 Materials

The acrylic fibrous waste used in this study was provided by Grund Industries, Czech Republic. The acrylic fibres were in the form of bath mats. These fibres have acrylonitrile copolymer 85-89%. The physical characteristics of acrylic fibres are shown in Table1.

Table 1 Physical properties of acrylic fibres

Fineness [tex]	117
Tenacity [cN/tex]	23.8
Elongation [%]	45
Wet shrinkage [%]	2.5

2.2 Preparation of activated carbon nonwoven web

The acrylic fibers were separated from bath mats by using mechanical cutting method. The fibers were further opened on laboratory roller card (Befama, Poland) and converted into compact structure of non-woven web by using needle punching machine. Carding is a mechanical process which cleans, disentangles and intermixes fibers to produce a continuous web for further processing and is achieved by passing fibers through differentially moving surfaces covered with card clothing. After carding, the web was transferred to needle punching machine to form a compact structure of non-woven web. The speed of feeding the carded web to needle punching machine was at the rate of 0.4 m/sec. The frequency of strokes was maintained at 200 (strokes per minute) with the depth of needle penetration is 5 mm produced the web having thickness of 11.6 mm and density 2.78 g/cm^3. The acrylic fibrous web was then cut into 30 cm (length) and 20 cm (width) and was stabilized by heating at a rate of 50°C.hr^{-1} under the application of heat. Later these stabilized webs were carbonized and physically activated in single stage at 800, 1000 and 1200°C at a heating rate of 300°C.hr^{-1}.

2.3 Characterization of activated carbon web

The physical properties of acrylic web and activated carbon web were characterized in terms of flexibility, shrinkage, yield and dusting tendency. The shrinkage was evaluated from change in length of web before and after carbonization. Similarly like shrinkage, yield of activated carbon before carbonization and after carbonization at different temperatures was calculated by using the eq. 1:

$$Yield = \frac{\text{Final weight of activated carbon web}}{\text{initial weight of acrylic web}} \times 100 \qquad (1)$$

The taber fabric stiffness tester (model 112) was used for measuring flexibility or stiffness by employing the principle of cantilever bending of the web under its own weight as per ASTM D 1388 standard. The dusting tendency was evaluated from amount of generated dust particles after rubbing the surface of web on Taber wear and abrasion tester as per ASTM D 3884 standard.

X-ray diffraction (XRD) analysis

It was carried out on a PANalytical X_0 Pert PRO MPD diffraction system. The development of crystalline and amorphous regions in prepared activated carbon web was investigated with respect to change in carbonization temperature. X-ray diffraction (XRD) is a technique used for the identification of crystalline material and analysis of unit cell dimensions. Degree of crystallinity can be calculated by using equation 2:

$$I_c = 1 - \frac{I_1}{I_2} \qquad (2)$$

where I_1 is intensity at minimum peak and I_2 is intensity at maximum peak [10].

Energy dispersive x-ray (EDX) analysis

EDX analysis was performed on Oxford Instruments, LZ 5 EDX detector, UK, to know the change in relative proportion of different elements with respect to change in carbonization temperature. EDX analysis is an analytical technique used for the chemical characterization or elemental analysis of a sample.

Scanning electron microscopy (SEM)

The field emission scanning electron microscope Sigma, Zeiss, Germany, was employed to investigate the morphology of prepared activated carbon web of 800, 1000 and 1200°C carbonization temperature. As the carbon was electrically conductive so no need to be metalized before conducting the test. The micrographs were taken at 2 kV accelerated voltage and 1000 magnification.

Electrical resistivity of activated carbon webs

The surface resistivity of AC webs prepared at 800, 1000 and 1200°C was measured at relative humidity 40% and at temperature 22°C according to ASTM D 257-14 with the help of Prostat PRF-911 concentric ring set. The specific voltage of 1 V using direct current was applied across opposite ends of activated carbon web and resultant current flowing across the sample was measured after 15±1 s. Surface electrical resistivity of activated carbon webs was measured by concentric electrode and parallel electrode method.

Electromagnetic shielding effectiveness of activated carbon web

The electromagnetic shielding effectiveness of activated carbon webs was determined by using waveguide method [11]. By using this method, the shielding effectiveness was calculated in high frequency range (i.e. at 2.45 GHz). This device comprises on a hollow cylinder in which receiving antenna was placed, however the sample was placed at the entrance of waveguide. From equation (3), the electromagnetic shielding effectiveness *SE* [dB] was calculated:

$$SE = 10 \log \frac{P_t}{P_i} \qquad (3)$$

where P_t and P_i is power density [W/m^2] measured in presence of sample (transmitted), and without the sample (incident) respectively.

Ohmic heating of activated carbon webs

For calculating the evolution of heat by activated carbon webs prepared at different temperatures, 0.5, 1.0 and 1.5 V, DC electromotive forces by DC voltage supplier NZ-2229.2 from Statron, Czech Republic, was applied via stainless steel clamp type electrodes. The rise in temperature was determined by the help of infrared thermal camera by Fluke.

3 RESULTS AND DISCUSSION

3.1 *Effect of temperature on physical characteristics of AC web*

When the temperature was increased from 800 to 1000°C and finally to 1200°C, the reaction of forming carbon with oxygen increased which resulted in decreasing yield of carbon and consequently shrinkage was increased and more rigid structure of activated carbon was achieved. Because of this reason, activated carbon web at high temperature showed poor flexibility and dusting behavior as can be seen from Table 2. However as far as thickness is concerned it decreased from 11.6 mm (thickness of acrylic web) to 6.87 mm, 6.11 mm and 5.23 mm when the carbonization temperature was increased from 800 to 1000°C and finally to 1200°C.

Table 2 Effect of carbonization temperature on physical properties of activated carbon webs

Temperature [°C]	Yield [%]	Shrinkage	Flexibility	Dusting
800	61.27	Good	Good	Good
1000	57.12	Good	Average	Average
1200	45.11	Average	Poor	Poor

3.2 *Energy dispersive x-ray (EDX) analysis*

The EDX analysis helped to determine the relative proportion of different elements in activated carbon web prepared at different temperatures. From Table 3, the increase in carbon content and reduction in oxygen content was found with increase in carbonization temperature from 800 to 1200°C. The activated carbon web produced at 1200°C exhibited 92.49% carbon content and 6.61% oxygen content. This behavior was attributed to removal of hydrogen, sulphur, nitrogen and other elements due to decomposition at higher temperature [8].

Table 3 Effect of carbonization temperature on elemental composition of activated carbon web

Element	App conc.	Intensity	Weight [%]	Atomic [%]
		800°C		
C K	0.26	2.12	0.13	91.76
O K	0.01	0.761	0.01	8.24
		1000°C		
C K	0.37	2.12	0.18	91.87
O K	0.02	0.760	0.02	8.13
		1200°C		
C K	0.18	2.10	0.09	92.49
O K	0.01	0.744	0.01	6.61
Ca K	0.00	0.902	0.00	0.90

3.3 *X-ray diffraction (XRD) analysis*

In order to know the development of crystallinity with increase in carbonization temperature, the XRD analysis was carried out. Figure 1 shows the XRD pattern of different activated carbon samples prepared at 800, 1000 and 1200°C temperature. The degree of crystallinity is increased from 82.21% to 86.7 and then finally reached to 92.41% by increasing temperature from 800 to 1000°C and then finally to 1200°C. The higher degree of crystallinity at higher temperature indicates more parallel orientation of chains.

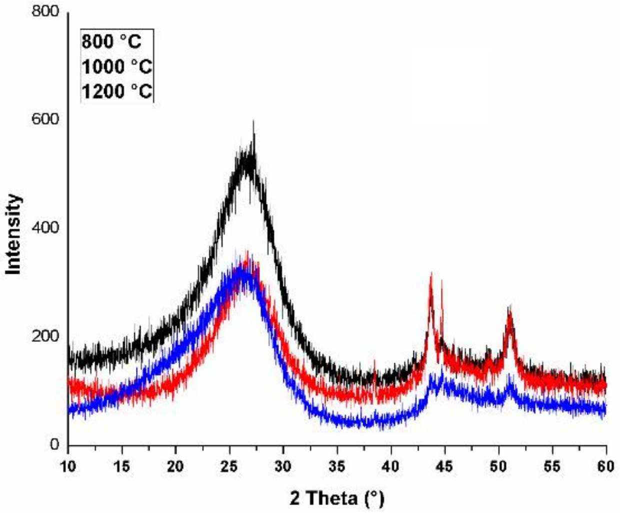

Figure 1 Effect of carbonization temperature on crystallinity of activated carbon web

3.4 *SEM morphology*

The surface morphology of acrylic web before and after carbonization was studied from SEM images. Figure 2(a-d) show the SEM images of acrylic fibrous web and activated carbon web produced at temperature of 800, 1000 and 1200°C respectively.

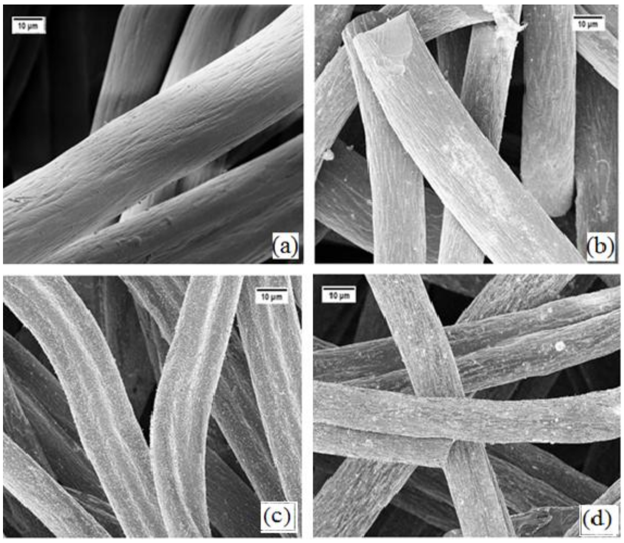

Figure 1 SEM images of (a) acrylic fibrous web (b) 800°C activated carbon web (c) 1000°C activated carbon web and (d) 1200°C activated carbon web

The activated carbon web showed noticeable rough surface as compared to acrylic fibrous web. The surface roughness was found to increase with increase in carbonization temperature, which indicated the development of more porous structure after physical activation of acrylic fibrous wastes. Further at high temperature carbonization due to more elimination of gases from acrylic fibers the diameters of fibers keep on decreasing as can be seen from Figure 2(a-d).

3.5 Results of electrical resistivity of activated carbon webs

The knowledge of electrical resistivity is very important for the selection of material to be used for electromagnetic shielding applications. The results of surface resistivity of activated carbon webs are shown in Table 4. The electrical resistivity was found to decrease with increase in carbonization temperature. The lower resistivity in activated carbon web at 1200°C was attributed due to more graphitization, which was confirmed from presence of sharp diffraction peak observed in XRD spectra and higher degree of crystallinity. As the temperature during carbonization was increased, the degree of crystallinity also increased. The degree of crystallinity was found to be 82.21%, 86.7% and 92.1% at carbonization temperature 800, 1000 and 1200°C. Further at higher temperature the content of carbon also increased which is also another cause for decrease of electrical resistivity by increasing carbonization temperature as can be seen from Table 4.

Table 41 Surface resistivity of activated carbon webs

800°C	1000°C	1200°C
Parallel electrode (surface resistivity Ω)		
3.33×10^2	1.28	0.27×10^{-1}
Concentric electrode (surface resistivity Ω)		
10	2.85	0.09

3.6 EMI shielding effectiveness by wave guide method

Figure 3 shows the electromagnetic shielding effectiveness of activated carbon web measured at 2.45 GHz frequency. The shielding effectiveness was found to increase with increasing carbonization temperature. The electromagnetic shielding effectiveness of 28.29 dB, 26.06 dB and 3.34 dB was exhibited by activated carbon web produced at 1200, 1000 and 800°C, respectively. At very low carbonization temperature, the shielding effectiveness remained similar to that of non-carbonized polyacrylonitrile substrate (i.e. zero). Then, the shielding effectiveness was found to increase dramatically over a very narrow range of carbonization temperature, which was connected to the amount of carbon/graphite phase present in the structure. This point is called the percolation threshold [12], which showed minimum carbonization temperature required for maximum increase in conductivity for higher shielding effectiveness. In present study, the percolation threshold was found between the range of 800 and 900°C carbonization temperature. The maximum shielding effectiveness in this range was attributed not only due to absorbance but also due to increased multiple internal reflections due to higher electrical conductivity, higher porosity and higher surface area. The dramatic increase of shielding ability could not be expected with further increase of carbonization temperature (T>1100°C). Therefore, the usage of 1000°C carbonization temperature was considered optimal with regard to its relatively high electromagnetic shielding ability and satisfactory mechanical properties [6].

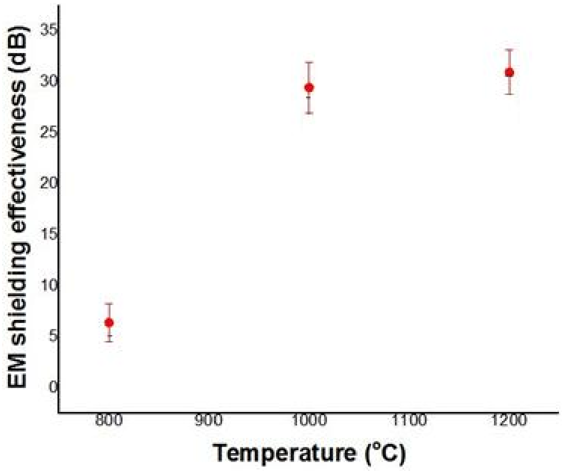

Figure 3 Effect of carbonization temperature on EM shielding effectiveness at 2.45 GHz

3.7 Ohmic heating of activated carbon webs

Joule heating also known as ohmic heating or resistive heating is the process by which the passage of electric current through a conductor produces heat. Joule heating or ohmic heating of activated carbon webs prepared at 800, 1000 and 1200°C were checked at 1.5 voltage.

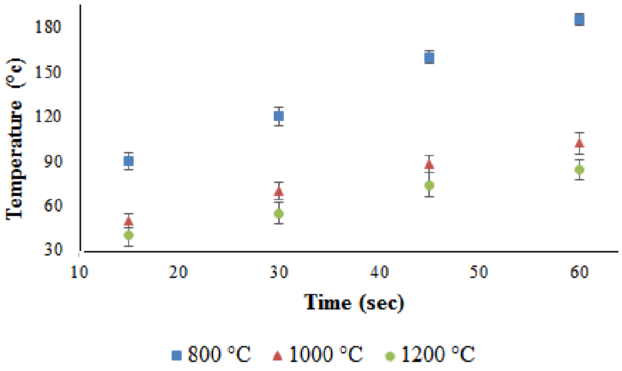

Figure 4 Rise in temperature as a function of time

After every 15 seconds of exposure to DC supply to the webs the generation of heat was observed with the help of thermal camera. From Figure 4 the rise in heat generation with increase in time can be seen. A sharp increase in temperature in all specimens was observed in the initial 30 seconds with the applied voltage than followed by a gradual increase in temperature as shown in Figure 4. It is clear from the figure that the web prepared at 800°C showed maximum increase in temperature due to less parallel orientation of chains hence more resistance offered for the flow of electrons as can be seen from Figure 5.

Since the rate of thermal energy generated within a resistive material is directly proportional to resistance. As the activated carbon web prepared at 800°C has more resistance as compared to AC web at 1000°C and 1200°C, because of more resistance offered by the flow of electrons it shows more rise of temperature. Hence when ohmic heating is measured it shows more rise of temperature in AC web prepared at low temperature after short interval of time at localized point (where electrodes were connected) shown by thermal camera. However, if both sides of AC are connected completely instead of electrode at one point it can be a good idea for measuring ohmic heating over long interval of time.

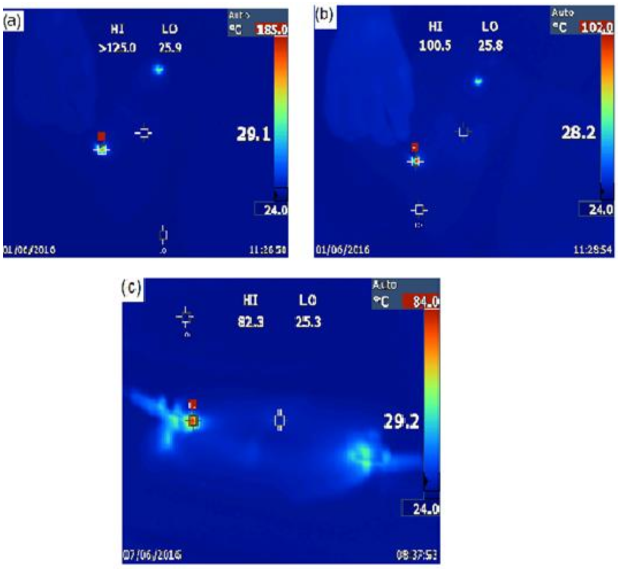

Figure 5 Ohmic heating of activated carbon webs

4 CONCLUSION

The present study aims at the development of a porous and electrically conductive activated carbon structure based electromagnetic shielding materials from acrylic wastes. This simple and new approach use here can introduce reflection and absorption properties of electromagnetic radiations into the shielding materials. This has been achieved by physical activation of needle punched nonwoven web of acrylic fibers. The carbonization is performed under the layer of charcoal at 800, 1000 and 1200°C with the heating rate of 300°C.h^{-1} and without any holding time. Further, the influence of carbonization temperature on physical and morphological properties of activated carbon has been investigated by using X-ray diffraction, EDX and SEM analysis. Finally the utility of these activated carbon webs is checked for electromagnetic shielding at high frequency region (i.e. at 2.45 GHz) and ohmic heating at 1.5 voltage. The electromagnetic shielding effectiveness of 28.29 dB, 26.06 dB and 3.34 dB is shown by activated carbon web produced at 1200, 1000C and 800°C, respectively. This behavior can be attributed due to stronger absorption and increased multiple internal reflections of electromagnetic radiations. However results of ohmic heating are otherwise due to more resistance offered by the activated carbon webs at low temperature carbonization. As the temperature for carbonization is keep on increasing more parallel orientation of carbon chains makes flow of electrons easily as a result decrease in the generation of heat.

ACKNOWLEDGEMENT: *This work was supported under the student grant scheme (SGS-21198, 2017) by Technical University of Liberec, Czech Republic and by the Ministry of Education, Youth and Sports of the Czech Republic and the European Union - European Structural and Investment Funds in the frames of Operational Programme Research, Development and Education - project Hybrid Materials for Hierarchical Structures (HyHi, Reg. No. CZ.02.1.01/0.0/0.0/16_019/0000843).*

5 REFERENCES

1. Negru D, Buda C.T., Avram D.: Electrical conductivity of woven fabrics coated with carbon black particles, Fibres and Textiles in Eastern Europe 90(1), 2012, pp. 53-56
2. Chen H.C., Lee K.C., Lin J.H., Koch M.: Comparison of electromagnetic shielding effectiveness properties of diverse conductive textiles via various measurement techniques, J. Mater. Process. Technol 192-193, 2007, pp. 549-554, doi: 10.1016/j.jmatprotec.2007.04.023
3. Safarova V., Tunak M., Militký J.: Prediction of hybrid woven fabric electromagnetic shielding effectiveness, Textile Research Journal 85(7), 2015, pp. 673-686, doi: 10.1177/0040517514555802
4. Safarova V., Militký J.: Electromagnetic shielding properties of woven fabrics made from high performance fibers, Textile Research Journal 84(12), 2014, pp. 1255-1267, doi: 10.1177/0040517514521118
5. Arjmand M., Sundararaj U.: Electromagnetic interference shielding of nitrogen-doped and undoped carbon nanotube/polyvinylidene fluoride nanocomposites: a comparative study, Compos Sci. Technol. 118, 2015, pp. 257-263, doi: 10.1016/j.compscitech.2015.09.012
6. Sano E., Akiba E.: Electromagnetic absorbing materials using nonwoven fabrics coated with multi-walled carbon nanotubes, Carbon 78, 2014, pp. 463-468, doi: 10.1016/j.carbon.2014.07.027
7. Rubeziene V., Baltusnikaite J., Varnaite-Zuravliova S., et al.: Development and investigation of electromagnetic shielding fabrics with different electrically conductive additives, Journal of Electrostatics 75, 2015, pp. 90-98, doi: 10.1016/j.elstat.2015.03.009

8. Farhan S., Wang R., Li K.: Electromagnetic interference shielding effectiveness of carbon foam containing in situ grown silicon carbide nanowires, Ceramics International 42(9), 2016, pp. 1133-1134, doi: 10.1016/j.ceramint.2016.04.054
9. Fletcher A., Gupta M., Dudley K L., Vedeler E.: Elastomer foam nanocomposites for electromagnetic dissipation and shielding applications, Composites Science and Technology 70(6), 2010, pp. 953-958, doi: 10.1016/j.compscitech.2010.02.011
10. Siqueira G., Abdillahi H., Bras J., et. al.: High reinforcing capability cellulose nanocrystals extracted from syngonanthus nitens, Cellulose 17(2), 2010, pp. 289-298, doi: 10.1007/s10570-009-9384-z
11. Safarova V, Tunak M, Truhlar M, et al.: A new method and apparatus for evaluating the electromagnetic shielding effectiveness of textiles, Textile Research Journal 86(1), 2016, pp. 44-56, doi: 10.1177/0040517515581587
12. Militky J., Safarova V.: Numerical and experimental study of the shielding effectiveness of hybrid fabrics, Vlakna a Textil (Fibres and Textiles) 19(1), 2012, pp. 21-27

XRD AND SEM ANALYSIS OF IRON OXIDE NANOPARTICLES FORMATION IN POLYAMIDE TEXTILE MATERIAL

Ya.V. Red’ko and N.P. Suprun

Kyiv National University of Technologies & Design, N.-Danchenko srt. 2, 01011 Kyiv, Ukraine
82yanet82@gmail.com, suprun.knutd@ukr.net

Abstract: *Functional textile materials with magnetic properties were prepared by synthesis of magnetite nanoparticles using ferric chloride, ferrous sulphate and sodium hydroxide. The morphology, crystal phase, magnetization properties and chemical structure of the textile materials were characterized by scanning electron microscopy (SEM), X-ray diffraction (XRD), vibrating sample magnetometry (VSM) and energy dispersive X-ray spectroscopy (EDX). It was found that Fe_3O_4 nanoparticles with average crystal sizes of about 12.5 nm. The uniform distribution of the iron oxide nanoparticles on the fiber surface was confirmed by SEM and EDX. The magnetite treated samples showed reasonable saturation magnetization values of about 7.5 emu.g^{-1}. Interestingly, the tensile properties of the treated samples were enhanced compared with the untreated polyamide textile materials.*

***Key words**: iron oxide nanoparticles, textile material, fiber, scanning electron microscopy, X-ray diffraction.*

1 INTRODUCTION

Over the past decade, there is increased interest in multi-functional textiles with potential technological application. Development of textile products that contain magnetic nanoparticles will provide the new properties for various applications [1-12]. The search for new approaches and methods for the creation of textile materials that contain nanoparticles of iron-oxide compounds is connected with the possible development of nanocomposite textile materials with a set of specified properties (magnetic and protective). Obtaining and investigation of properties of iron-oxide nanoparticles compounds are the subject of many studies, but to the questions of obtaining of the magnetic textile materials are devoted only a few works [13-15].

The purpose of the study: The investigation of morphological and structural characteristics the starting materials and of the magnetic nanocomposites based on them using XRD and SEM, determination of the chemical composition the surface of the textile material before and after the modification, determination of a particle size of the iron oxide inside and on the surface of the obtained composite materials.

2 EXPERIMENTAL

For studies was used polyamide comprehensive thread with a linear density of 15.6 tex and polyamide knitted fabric, which is obtained from this polyamide thread. There investigated of magnetite powder form synthesized without fiber under the same technology [13, 15].

Polyamide textile material containing particles of synthetic magnetite was obtained of using the mechanism *in situ*. As reagents were used chemical substances without further purification: iron chloride ($FeCl_3$), ferrous sulphate ($FeSO_4.7H_2O$) and ammonium hydroxide (NH_4OH).

Prior to the treatment polyamide fiber material washed with 1 g/l non-ionic detergent at 60°C for 20 minutes and then washed with distilled water to remove any impurities. Iron oxide particles were synthesized in the bath, in the presence of polyamide fiber material, that contains reagents $FeCl_3$, $FeSO_4$. $7H_2O$ in amounts previously calculated (Fe^{2+}/Fe^{3+} molar ratio = 2) and NH_4OH (pH = 11-12), total volume manufacturing bath is brought to 100 ml with distilled water. The process was carried out at 100°C for 1 h, resulting in the preparation of magnetite particles. Finally, the treated samples were washed with distilled water for 10 min and dried at room temperature.

X-ray diffraction analysis (XRD) was performed with a DRON-UM1 X-ray diffractometer using a Co Kα radiation source (*l* = 1.5418 A) operating at 40 kV to investigate the crystalline size and phases of the synthesized iron oxide nanoparticles in the polyamide fiber. The angular range was of 10-80°, in increments of 0.05°. Diffraction patterns are recorded digitally in a file format 2θ (°) − I (intensity, s^{-1}) and shown in Figure 1.

The surface morphology of the treated polyamide materials were characterized by scanning electron microscopy MIRA 3 LMU, Tescan, with a resolution of ±1 nm and energy-dispersive spectroscopy (EDX) with chemical analysis Oxford X – MAX 80 mm^2 with appliance uncertainty ±1%.

3 RESULTS AND DISCUSSION

Synthesis of iron oxide nanoparticles

In the preparation method, the iron oxide nanoparticles were formed after mixing the iron salts with NaOH solution. The end product is a black precipitate of Fe_3O_4 nanoparticles or red-brown hematite nanoparticles, depending on the applied temperature. The following reactions may proceed resulting in the nanoparticle compound:

$$Fe^{2+} + 2OH^- / Fe(OH)_2 \quad (1)$$

$$Fe^{3+} + 3OH^- / Fe(OH)_3 / FeOOH \quad (2)$$

FeOOH can be also formed by the partial oxidation of ferrous hydroxide by oxygen in dissolved air according to reaction (3).

$$3Fe(OH)_2 + 1/2O_2 / Fe(OH)_2 + 2FeOOH + H_2O \quad (3)$$

$$Fe(OH)_2 + 2FeOOH / Fe_3O_4 + 2H_2O \quad (4)$$

In this study, the Fe^{2+}/Fe^{3+} molar ratio was more than the stoichiometric ratio, guaranteeing a sufficient amount of Fe^{2+}, complete consumption of FeOOH and the formation of pure magnetite nanoparticles. According to the applied preparation procedure, the synthesis proceeded at high pH value, during which hydroxylation of Fe^{2+} and Fe^{3+} species occurred simultaneously (reactions (1) and (2)). Under the applied conditions as the reaction mixture contained an excess of OH^- ions and sufficient amount of iron ions, a large amount of particle seeds instantaneously formed. One hour duration of the process at boiling point allowed enough time for complete growth of the magnetite nucleus. Although the conventional pH for the preparation of magnetite nanoparticles is ~11, herein we adjusted the pH at 12 for simultaneous synthesis of particles in the polyamide fiber. It has been reported that the growth of Fe_3O_4 nuclei happens more easily when the solution pH is higher than 11. Therefore, the mean diameter of Fe_3O_4 nanoparticles increases with the increase of pH to higher than 11.

According to the heterogeneous nucleation process it can be postulated that the local concentration of hydrolyzing ions (Fe^{3+} and Fe^{2+}) at the solid/water interface is higher than that in the aqueous bulk phase, thus the iron oxide nanoparticles were more nucleated in the textile materials.

3.1 XRD investigation

Figure 1 shows the XRD spectra of the synthesized iron oxide nanoparticles (a) and the treated polyamide textile materials (b).

By comparison to the XRD pattern of the synthesized magnetite nanoparticles with diffraction peaks at 2θ angles 30°, 35° (major), 43° the successful synthesis of Fe_3O_4 nanoparticles in the treated polyamide sample can be confirmed by the characteristic peak at 2θ angle 35° in addition to the main peak of the original polyamide fiber at $2\theta=17°-25°$.

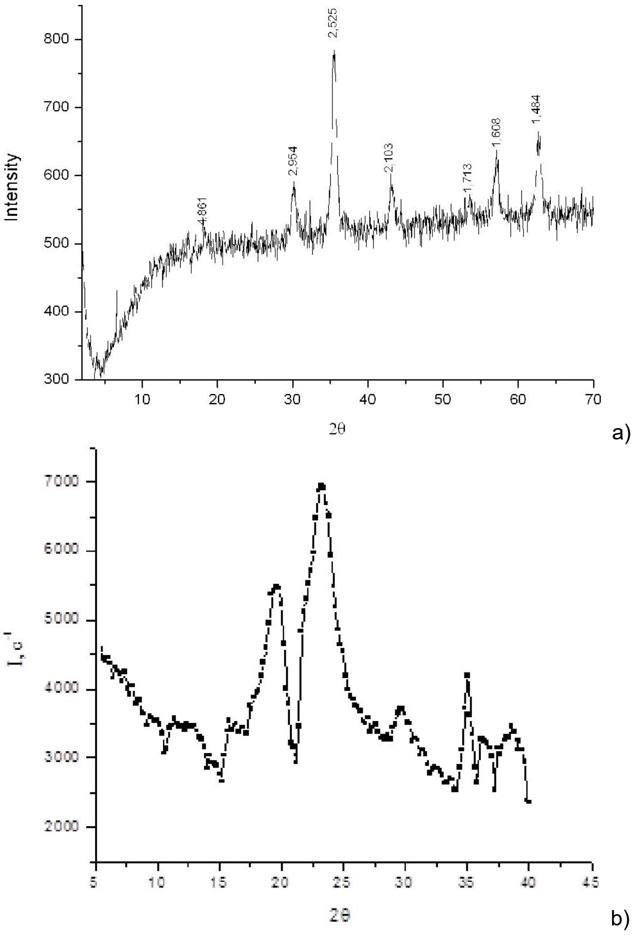

Figure 1 XRD spectra of the a) synthesized iron oxide nanoparticles and the b) treated polyamide textile materials

Using Scherer's equation and from the widths of the peaks at 30°, 35° and 43° the crystallite sizes of the Fe_3O_4 nanopowders and the synthesized nanoparticles in the treated textile materials were calculated to be 11.8 nm, 12.8 nm and 12.9 nm, respectively. The average size of nanoparticles is 12.5±0.47 nm.

For composite polyamide/nanomagnetite average size of the crystals of inorganic phase is 10.0±1.42 nm. For this composite systems also decrease the average size of magnetite crystals during their formation in the volume of polyamide matrix. It can be concluded that the synthesis of nanoparticles in the textile materials inhibited the further growth of the prepared iron oxide crystals resulting in smaller crystal sizes. The crystal structure of the textile materials in the processing did not change, indicating the placing nanomagnetite on the surface of microfibrils or amorphous areas of polyamide structure.

3.2 *SEM and EDX analyses*

The deposition of nanomagnetite particles in the volume of polyamide textile materials and particle size determination was studied by XRD. However, it is appropriate to consider and explore the surface of the textile materials after treatment with the use of SEM. The SEM images of the untreated polyamide textile materials and polyamide with nanoparticles of the Fe_3O_4 are shown in Figure 2. These micrographs show that there are areas with a continuous layer nanomagnetite and areas where nanomagnetite is in the form of individual particles Fe_3O_4/aggregates.

This composite system is characterized by coverage of the surface polyamide textile materials slightly higher than 60%, which is possibly due to the relative chemical inertness polyamide as substrate. During the deposition of the nanomagnetite on the surface of polyamide textile materials the layer the Fe_3O_4 nanoparticles with an average thickness of 360±56 nm is formed. In other parts of the surface covered with a layer of polyamide textile materials can be seen the individual particles of Fe_3O_4 of about 25 nm, the size of their aggregates 100-300 nm and micron size particles. Analysis of surface nanocomposite shows that the average size of individual particles of nanomagnetite is 54±30 nm.

With all things being equal can assume that the low reactivity of polyamide surface slightly affects the stability of the dispersion of magnetite nanoparticles and as a result the aggregation processes are expressed weakly. Formation of large-sized aggregates though it is, but is atypical for this composite system.

The structure of the surface layer of a large quantity identified small in size (about 20 nm) particles of nanomagnetite. Nanocomposites polyamide-nanomagnetite characterized by sufficient iron content in the surface layer, which reaches 22 wt.%.

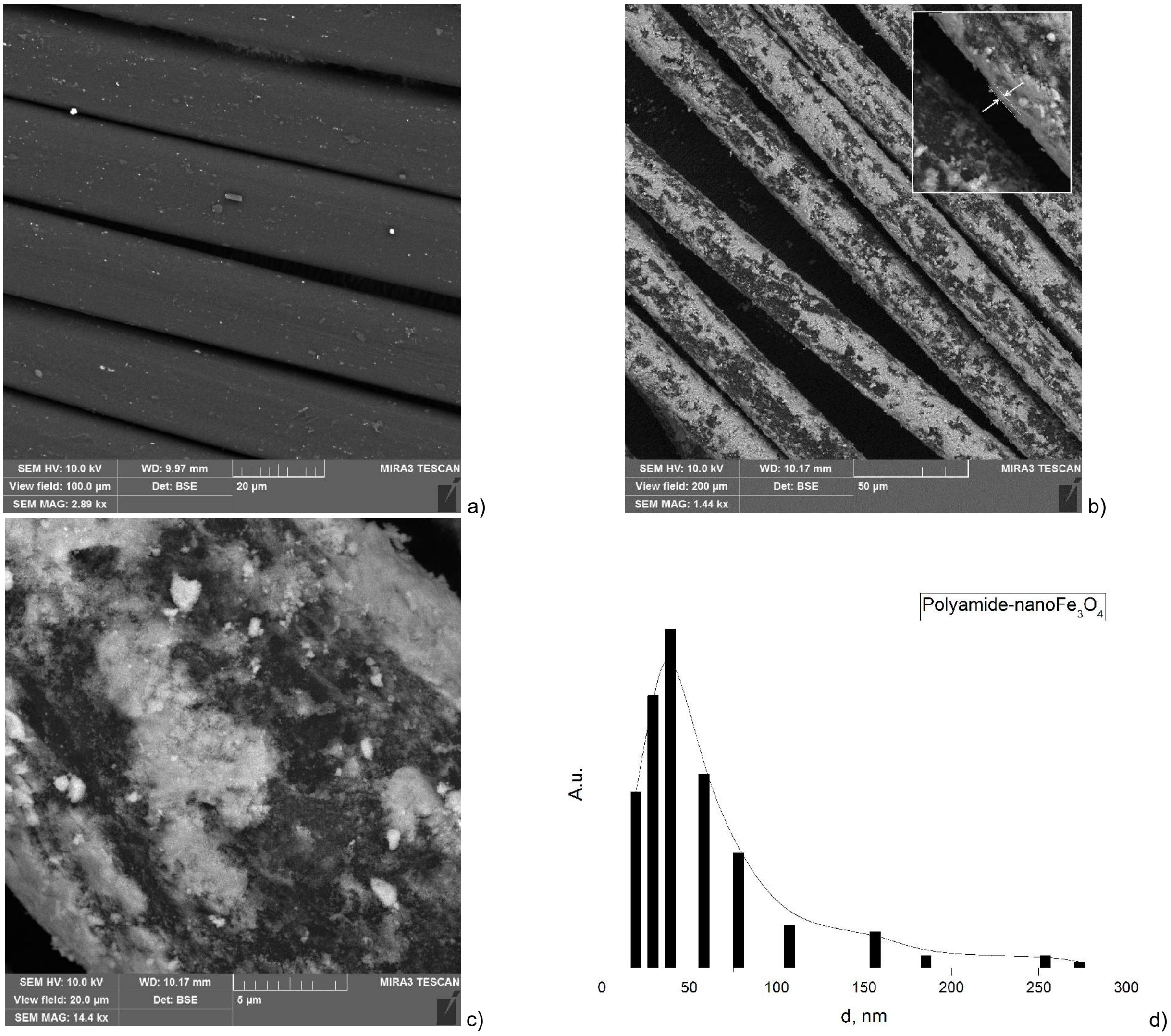

Figure 2 The SEM images of the a) untreated polyamide materials; b, c) polyamide with nanoparticles of the Fe_3O_4; and d) the histogram of distribution Fe_3O_4 in size

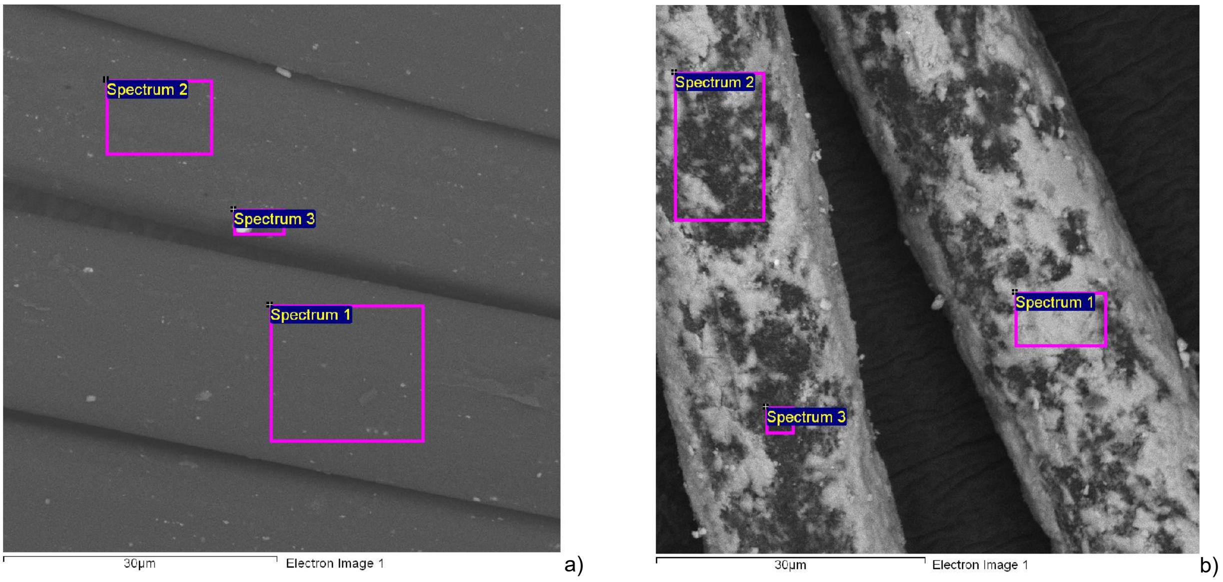

Figure 3 EDX spectra and mapping images of a) untreated and b) treated polyamide samples

The successful synthesis of the iron oxide nanoparticles on the treated samples was further confirmed by the chemical compositions analyzed by EDX. As shown in Figures 3a, 3b and in Table 1, iron and oxygen are two elements on the treated polyamide textile materials apart from the carbon that relates to the polyamide substrate.

Table 1 EDX results of untreated and modified polyamide textile material in selected areas

Elements / Areas of analysis	C	O	Fe
	Contents [%]		
Untreated sample 1	76.2	23.8	-
Untreated sample 2	77.5	22.5	-
Untreated sample 3	72.4	27.6	-
Treated sample, spectra 1	32.5	21.9	45.6
Treated sample, spectra 2	56.8	26.4	16.8
Treated sample, spectra 3	67.8	27.1	5.2

Moreover, the mapping images shown in Figure 3 further confirmed the presence of iron on the treated polyamide textile materials.

3.3 *Magnetic properties*

The magnetization curves of the synthesized magnetite nanoparticles and their corresponding treated polyamide textile materials were measured using a vibrating-sample magnetometer (VSM) at room temperature and the graphical representation of the relationship between the applied magnetic field (*H*) and the induced magnetization (*M*) is shown in Figure 4. A sharp increase in magnetization was observed by increasing the applied field from 0 to 8000 Oe, and the magnetization was saturated at about 7000, 3500, 5500 and 2500 Oe for synthesized magnetite nanoparticles, treated polyamide textile materials.

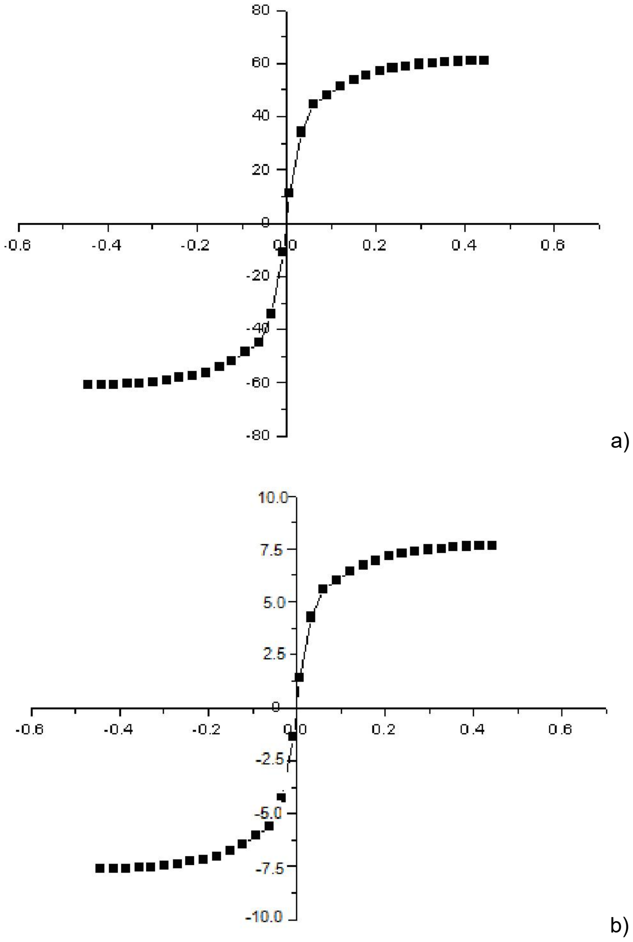

Figure 4 Magnetization curves of a) synthesized Fe_3O_4 nanoparticles, b) treated polyamide textile materials. *X* axis: magnetic field *H* [Oe], *Y* axis: magnetization *M* [emu.g^{-1}]

A decrease in saturation magnetization of the treated samples (treated sample: 7.5 emu.g^{-1}, Fe_3O_4 sample: 65 emu.g^{-1}) was obtained compared to the corresponding nanoparticles. Also, it is apparent that the magnetic hysteresis loop was narrow for the treated sample and extremely small coercivity and remanence values were obtained for the iron oxide nanoparticles synthesized on the polyamide indicating the almost superparamagnetic nature of these particles. This transition from ferromagnetic to superparamagnetic behavior could be due to the smaller crystal size of the prepared nanoparticles on the treated polyamide textile materials.

The magnetic sensitivity of the treated polyamide textile materials was also confirmed by attraction towards a magnet. The hydrothermal synthesis of magnetite nanoparticles on polyamide textile materials has been reported to create a magnetic fabric with the saturation magnetization of 3.8 emu.g^{-1}. Therefore, *in situ* synthesis of Fe_3O_4 nanoparticles in polyamide fiber in this study was more effective in producing a magnetic fiber with saturation magnetization of 7.5 emu.g^{-1}.

4 CONCLUSIONS

The possibility of determination of the size of structural elements in a variety of nanocrystalline materials using SEM and XRD methods was analyzed. It is shown that the size of the nanoparticles depends on the methods of synthesis (in powder or with the use fiber matrix by mechanism *in situ*). Functional composites based on the polyamide textile material with stable magnetic properties were obtained. The practical potential of the treated samples in shielding electromagnetic waves was predicted and is under investigation.

There were obtained functional composites based on polyamide textile material with stable magnetic properties. Practical potential of treated textile materials is the ability to shielding of electromagnetic radiation and in the presence of antimicrobial effect and is in the process of research.

5 REFERENCES

1. Gleiter H.: Nanostructured materials: Basic concepts and microstructure, Acta Materialia 48(1), 2000, pp. 1-29, https://doi.org/10.1016/S1359-6454(99)00285-2
2. Buschow K.H.J. (Ed.): Concise encyclopedia of magnetic and superconducting materials, Elsevier Science, 2nd Edition, 2005, 1360 p.
3. Taylor J.I., Hurst C.D., Davies M.J., Sachsinger N., Bruce I.J.: Application of magnetite and silica–magnetite composites to the isolation of genomic DNA, J. of Chromatography A 890(1), 2000, pp. 159-166, https://doi.org/10.1016/S0021-9673(00)00107-2
4. Perez J.M., Josephson L., O'Loughlin T., Hogemann D., Weissleder R.: Magnetic relaxation switches capable of sensing molecular interactions, Nat. Biotechnol. 20(8), 2002, pp. 816-820, DOI:10.1038/nbt720
5. Zhang Y., Kohler N., Zhang M.: Surface modification of superparamagnetic magnetite nanoparticles and their intracellular uptake, Biomaterials 23(7), 2002, pp. 1553-1561, https://doi.org/10.1016/S0142-9612(01)00267-8
6. Berry C., Curtis A.: Functionalisation of magnetic nanoparticles for applications in biomedicine, Journal of Physics D: Applied Physics 36(13), pp. R198-R206, https://doi.org/10.1088/0022-3727/36/13/203
7. Chiang C.L., Sung C.-., Wu T.F., Chen C.Y., Hsu C.Y.: Application of superparamagnetic nanoparticles in purification of plasmid DNA from bacterial cells, Journal of Chromatography B 822(1-2), 2005, pp. 54-60, DOI:10.1016/j.jchromb.2005.05.017
8. Xu C., Xu K., Gu H., Zheng R., Liu H., Zhang X., Guo Z., Xu B.: Dopamine as a robust anchor to immobilize functional molecules on the iron oxide shell of magnetic nanoparticles, Journal of the American Chemical Society 126(32), 2004, pp. 9938-9939, DOI:10.1021/ja0464802
9. Ito A, Shinkai M, Honda H, Kobayashi T..: Medical application of functionalized magnetic nanoparticles, Journal of Bioscience and Bioengineering 100(1), 2005, pp. 1-11, DOI:10.1263/jbb.100.1
10. Gu H., Xu K., Xu C., Xu B.: Biofunctional magnetic nanoparticles for protein separation and pathogen detection, Chemical Communications, 2006, pp. 941p949, doi: 10.1039/B514130C
11. Pan B., Cui D., Sheng Y., Ozkan C., Gao F., He R., Li Q., Xu P., Huang T.: Dendrimer-modified magnetic nanoparticles enhance efficiency of gene delivery system, Cancer Res. 67(17), 2007, pp. 8156-8163, DOI: 10.1158/0008-5472.CAN-06-4762
12. Chang S.Y., Zheng N.Y., Chen C.S., Chen C.D., Chen Y.Y., Wang C.R.: Analysis of peptides and proteins affinity-bound to iron oxide nanoparticles, Journal of the American Society for Mass Spectrometry 18(5), 2007, pp. 910-918, DOI: 10.1016/j.jasms.2007.01.011
13. Redko Ya.: Nanocomposite textile materials containing iron oxide compounds, in Proceedings of VI Ukrainian-Polish Scientific Dialogues: Conference, 21-24 October 2015, Khmelnytskyi, Ukraine, pp. 36-37
14. Rubacha M, Zięba J.: Magnetic textile elements, Fibres & Textiles in Eastern Europe 14(5), 2006, pp. 49-53
15. Red'ko Ya., Romankevich O.: Fiber decorated with magnetite using heterocoagulation, Fibre Chemistry 46(4), 2014, pp. 257-261, https://doi.org/10.1007/s10692-014-9601-x

ANTIBACTERIAL NANOADDITIVES PREPARED WITH NANO-SiO_2 CARRIER AND RESULTS OF THEIR APPLICATION IN POLYPROPYLENE FIBRES, POLYPROPYLENE AND POLYETHYLENE FOILS

Jozef Sestak and Katarina Scasnikova

VÚTCH-CHEMITEX, spol. s r.o., Žilina, Slovak Republic
jozef.sestak@vutch.sk

Abstract: *Research topic was to investigate preparation of antibacterial (AMB) nanoadditive using alternative nanotechnological procedures and three various types of nanocarriers based on SiO_2. Results of so-called standard method used to prepare AMB nanoadditive are compared with results of antimicrobial efficiency of a nanoadditive prepared by a method in which antibacterial nanosol containing Ag is used, or by direct incorporation of $AgNO_3$ into siloxane mixture and subsequent doping of nanoSiO_2 on the carrier surface. Results of Ag-content in different types of powder nanoadditives determined using atomic absorption spectrometry (AAS) and antimicrobial efficiency of the nanoadditive determined according to ASTM E 2149-13a method on Escherichia coli CCM 3954 bacterium are presented in table form. Besides, images of the nanoadditive surface obtained using SEM method and results obtained by analysis of Ag-content and form of the Ag ion using XPS method (X-ray analysis of atomic structure) are shown. Results from application of the AMB nanoadditive in polypropylene (PP) fibres, PP and polyethylene (PE) foils in the form of evaluation of antimicrobial efficiency using AATCC 100: 2015 method on Escherichia coli CCM 3954 bacterium are given in final part of the paper. Evaluation of the antimicrobial efficiency on the modified PP and PE foils was performed according to ASTM E 2149 method using Escherichia coli CCM 3954 bacterium. Results acquired on applying the AMB nanoadditive in PP fibres, PP and PE foils are focusing on fibre, textile and food industry.*

Keywords: *antibacterial nanoadditive, nanoSiO_2 carrier, antimicrobial efficiency*

1 INTRODUCTION

1.1 Methods for preparation of an antimicrobial (AMB) nanoadditive

It is possible to state on the base of our study and acquired knowledge that the issue of antimicrobial nanoadditives and their application in fibres, foils and fabrics is highly topical and significant from a viewpoint of human health protection [1, 2]. Numerous available information sources [1-5] confirm that it is an interesting theme for the scientists and researchers who explore it using various experimental procedures, different methods and source materials [3, 4-7]. Originality of our research solution, focusing on preparation of the AMB nanoadditive, consists in detailed examination of an innovative method to make AMB nanoadditive using AMB nanosol, prepared by coagulation and dispergation procedure or using siloxane nanosol to dope surface of SiO_2 nanocarrier with Ag particles in ionic form. Originality of preparation of solid dispersions of the AMB nanoadditive in polymeric matrix consists in detailed examination of compatibility of the system and investigation of influence of the nanoadditive on processing, rheological and colouristic properties of the developed solid dispersions as well as on morphological structure, mechanical and coloristic properties as well as performance characteristics (antimicrobial activity) of the nanocomposite PP fibres, PE and PP foils [8, 9].

Philosophy of our research focusing on preparation of the AMB nanoadditive is based on two options: so-called classical method and progressive one. The classical method arises from physico-mechanical compounding by means of a separate chemical reaction of the prepared Ag^+ ions in dispersion solution with subsequent surface doping of a silicate SiO_2 based nanocarrier [6, 7]. This method corresponds to a certain extent with knowledge about methods, currently used in the world, with subsequent preparation of concentrates in powder form and their application to the polymeric systems [4]. The progressive method assumes separate preparation of a silver-containing antimicrobial nanosol using specific procedures. Subsequent process involves compounding of the AMB nanosol with silicate nanocarrier in a solution, under specified conditions, from which powdered nanoadditive suitable for preparation of solid AMB nanodispersion in polymeric matrix is prepared. Another option is application of a sol-gel method using selected polysiloxane types in objectified ratio and subsequent incorporation of $AgNO_3$ into the nanosol solution. The prepared solution is subsequently compounded with the powdered SiO_2 nanocarrier. The above-mentioned methods to prepare the AMB nanoadditive (application of sol-gel method, compounding the nanosol with a nanocarrier, preparation of powdered nanoadditive from a solution) has not been described anywhere yet, what points to high topicality of the proposed research solution.

2 EXPERIMENTAL

2.1 Results from preparation of the AMB nanoadditives using SiO_2 based nanocarriers

Following three types of commercially available silicate nanocarriers were used in the experiments:

a) **S** - SiO_2 content 98 wt.%, particle size 18 nm, specific surface 190 m^2/g

b) **M** - SiO_2 content 44 wt.%, particle size 30 nm, specific surface 100 m^2/g

c) **U** - SiO_2 content 94 wt.%, particle size 25 nm, specific surface 15-30 m^2/g

The specific samples were marked according to method used for preparation of the AMB nanoadditive as follows:

I. **KM** – ***classical method***: physico-mechanical compounding of the nanoSiO_2 carrier + $AgNO_3$ + NaCl + distilled water, (samples marked KM/S - Table 1 and KM/M - Tables 1-2),

II. **PM –** ***progressive methods***:

PM/A – physico-mechanical compounding (when cold) of the AMB nanosol and nanoSiO_2 carrier with formation of dissociated silver citrate (using citric acid) in a form of a nanoadditive (samples marked PM/A/S, PM/A/U - Tables 1-4),

PM/B – direct formation of the AMB nanoadditive by hydrolysis of triethoxysilane + vinyltriethoxysilane mixture (sol formation) with subsequent reduction using $AgNO_3$ or silver citrate and gradual addition of the nanoSiO_2 carrier under determined conditions (samples marked PM/B/S, PM/B/U - Tables 1-4 and PM/B/M - Table 1). Selected samples of the prepared AMB nanoadditives including basic data on Ag-content and antimicrobial activity are given in Table 1.

Figures 1 and 3 show SEM images of surfaces of the prepared AMB nanoadditives using S and U carriers with identification of silver nanoparticles. Presence of biogenic nanoparticles in the form of Ag^+ ions was confirmed by X-ray photoelectron spectroscopy (XPS method) of the nanoadditive as is shown in the Figures 2 and 4.

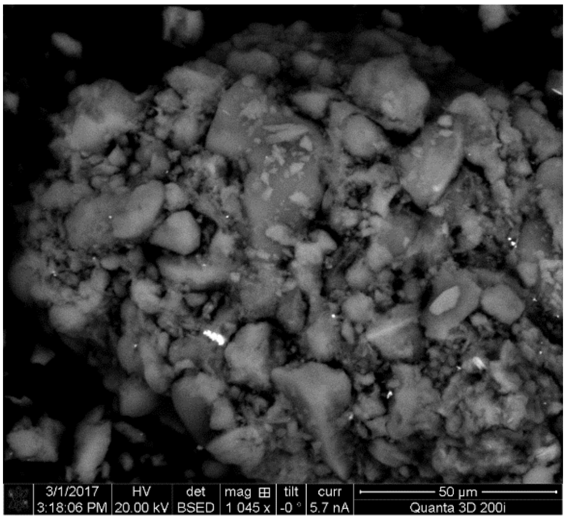

Figure 1 SEM image of AMB nanoadditive surface **with S** carrier (PM/B/S sample), magnification 1453x

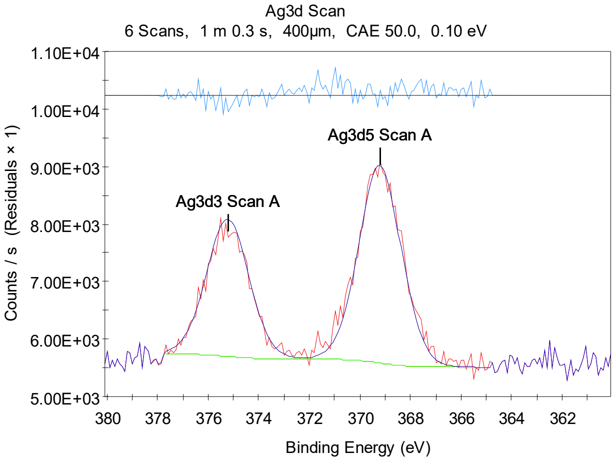

Figure 2 Graphical record of XPS analysis of PM/B/S sample with identification of Ag^+ ion at energetical wavenumber 369.3 eV

Table 1 Results of silver content and antimicrobial activity determined on powdered AMB nanoadditives prepared using nanoSiO_2 based nanocarriers

Sample	**Nanocarrier type**	**Determined Ag content - AAS method [wt.%]**	**Antimicrobial activity (AMA) – determined bacterial reduction [%]**
KM/S	S	1.19	R = 56.0
PM/A/S	S	0.025	R = 19.1
PM/B/S	S	0.32	R = 13.6
KM/M	M	0.90	R = 84.0
PM/A/U	U	0.06	R = 84.0
PM/B/M	M	0.28	R = 10.3
PM/B/U	U	0.52	R = 44.0

Notice: R - mean value of bacterial reduction, AAS - atomic absorption spectroscopy, AMA - antimicrobial efficiency of the nanoadditive determined according to ASTM E 2149-13a method on *Escherichia coli CCM 3954*

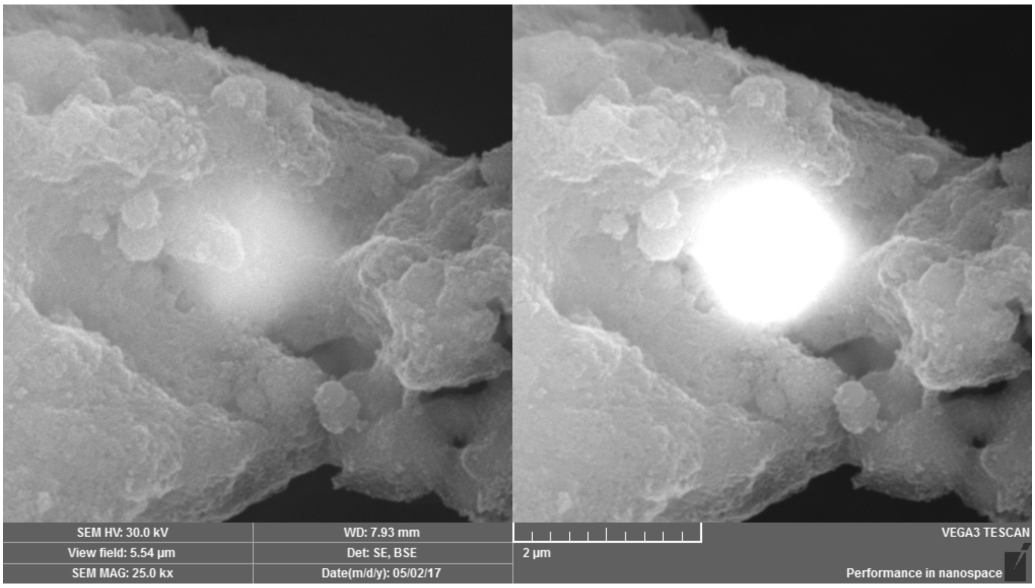

Figure 3 SEM image of AMB nanoadditive surface with **U** carrier (PM/B/U sample), magnification: 25000x, left: secondary ray, right: reflected ray

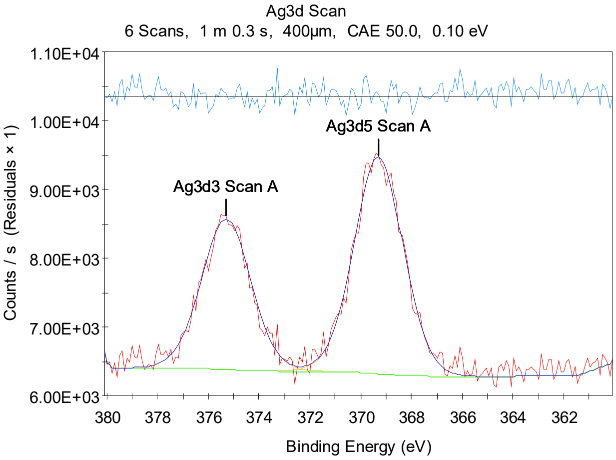

Figure 4 Graphical record of XPS analysis of the sample PM/B/U with identification of Ag^+ ion at energetical wavenumber 369.3 eV

Comparison of silver content in the AMB nanoadditives determined by different analytical methods shows that the samples are rather inhomogeneous and detected silver content depends also on sensitivity of the specific analytical method. It is possible to state that the XPS method, enabling also determination of ionic forms of Ag atom, has the best informative value. It can be concluded on the base of results, given in Table 2, that the progressive method using siloxane nanosol incorporating $AgNO_3$, in which biogenic silver form (Ag^+) arises, is most appropriate from a viewpoint of suitability of technology applied to prepare the AMB nanoadditive. This method used for preparation of the nanoadditive seems to be the best option to achieve considerable bacterial reduction in final products by means of biogenic silver nanoparticle.

Table 2 Results from evaluation of silver content (silver in various forms) using different analytical methods

Sample	**AAS method [wt.%]**	**EDAX method [wt.%]**	**XPS method [wt.%]**
Samples of the AMB nanoadditive prepared using different technologies with the same nanoSiO_2 carrier			
KM/S	1.190	9.76	1x0.3 (Ag^0)
PM/A/S	0.042	0.04	0,0
PM/A/M	0.023	0.87	5x0.1 (Ag^0)
PM/A/S	0.025	0.64	0.0
PM/B/S	0.390	2.13	4x0.2 (Ag^+)
PM/B/S	0.220	7.41	5x0.3 (Ag^+)
Samples of the AMB nanoadditive prepared with carrier U			
PM/A/U	0.060	undetermined	undetermined
PM/B/U	0.520	undetermined	0.3 (Ag^+)

Notice: For two samples PM/B/S and PM/A/S the different amount of carrier was used in the preparation of the nanoadditives,
EDAX method - X-ray fluorescence analysis method in combination with SEM analysis,
1x0.3 indicates determined one value with concentration of 0.3% by weight,
5x0.1 indicates determined five values with concentration of 0.1% by weight,
4x0.2 indicates determined four values with concentration of 0.2% by weight,
5x0.3 indicates determined four values with concentration of 0.3% by weight.

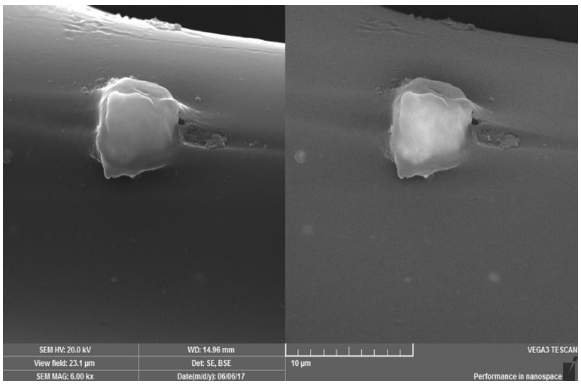

Figure 5 SEM image of PP fibre surface with a particle of AMB nanoadditive (sample PM/B/U – 10 wt.%, additive concentration 0.75 wt.%), magnification 6000x

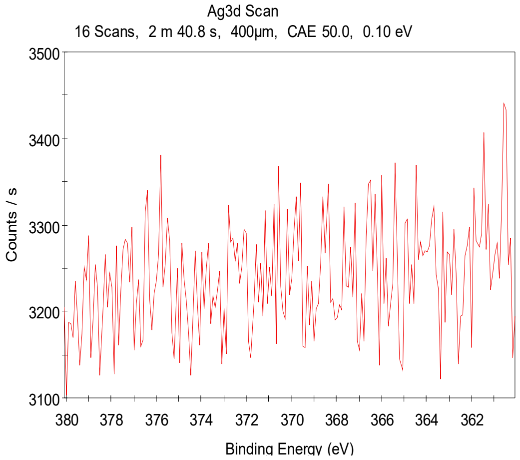

Figure 6 Graphical record of XPS analysis on a sample of PP fibre PM/B/U; where it was not possible to determine Ag ionic species using this method due to high scattering of Ag

2.2 Results from application of the prepared AMB nanoadditives using polymer dispersions of their concentrates in PP fibres, PP and PE foils

Samples of modified PP fibres (smooth fibre with fineness of 3 dtex) were prepared with 10 wt.% and 15 wt.% of the nanoadditive in the concentrate. Content of the AMB nanoadditive in the fibre was 0.75 wt.%. Results from the evaluation are shown in the Table 3.

It was not possible to identify exactly Ag ionic species on some samples of PP fibres using XPS analysis method due to its low content in the fibre or high scattering in the polymeric mass. Results of analysis of Ag content in various form (i.e. Ag^+ and/or Ag^0) have confirmed, that there is a direct relation between concentration of Ag ions and antimicrobial activity (AMA) of PP fibre, in a form of bacterial reduction of bacterium *Escherichia coli CCM 3954* determined according to ASTM 100:2015 method. The so-called progressive method, supporting existence of Ag^+ ions, enables to achieve relatively high bacterial reduction even without any need to increase content of dispersion of the concentrate with AMB nanoadditive in the polymeric system regardless which type of nanoSiO_2 carrier was used (see AMA results of PM/B/S and PM/B/U samples in Table 3). Besides, it was confirmed that the method of preparation according to PM/A alternative (see PM/A/S, PM/A/U in Tables 2 and 3) does not support formation of suitable Ag form (it generates colloidal form of Ag^0 only) and/or that it ensures low content of silver in the AMB nanoadditive, which is not sufficient for adequate antimicrobial activity.

Experimental research in the field of application of the AMB nanoadditives and solid dispersions, made from them, used in polymeric systems designed for preparation of extruded foils, allowed to ensure also sufficient level of AMA in selected types of PP and PE foils. The experiments have confirmed necessity to increase content of dispersion of the concentrate in the mass up to min. 15 wt.% and to ensure this way at least 2 wt.% content of the nanoadditive in the mass, so that AMA on PP and PE foils close to 50% bacterial reduction could be achieved.

However, in this case methods of PM/A as well as PM/B alternative have proved the most appropriate for preparation of suitable types of AMB nanoadditives. Results from evaluation of AMA on samples of PP and PE foils are shown in Table 4. Evaluation of the antimicrobial efficiency on the modified PP and PE foils was performed according to the ASTM E 2149-13a standard using bacterium *Escherichia coli CCM 3954.*

Table 3 Results from the analysis of antimicrobial activity (AMA) on selected types of modified PP fibres containing 10 and 15 wt.% of the nanoadditive in the concentrate

Bacterium	***Escherichia coli CCM 3954*** **CFU/sample**			
Sample of PP fibre (containing 10 wt.% of the additive in the concentrate), additive concentration in the fibre 0.75 wt.%	PM/A/S (carrier S)	PM/B/U (carrier U)	PM/A/U (carrier U)	PM/B/S (carrier S)
Bacterial reduction [%]	0	99.32	0	84.52
Sample of PP fibre (containing 15 wt.% of the additive in the concentrate), additive concentration in the fibre 0.75 wt.%	non-prepared fibre	PM/B/U (carrier U)	PM/A/U (carrier U)	PM/B/S (carrier S)
Bacterial reduction [%]	-	95.6	0	87.6

Notice: antimicrobial efficiency using AATCC 100: 2015 method on *Escherichia coli CCM 3954,*
CFU - the number of colonies of bacteria in the volume of the inoculum.

Table 4 Results of AMA analysis on selected types of modified PP and PE foils containing 15; 10 and 5 wt.% of the additive in the concentrate

Bacterium	***Escherichia coli CCM 3954*** **CFU/sample**			
Sample of PP foil (content 10% concentrate) additive portion 0.75 wt.%	PM/A/S (carrier S)	PM/B/U (carrier U)	PM/A/U (carrier U)	PM/B/S (carrier S)
Bacterial reduction (%)	8.4-19.5	17.2-20.5	11.6-12.1	0.0-14.4
Sample of PP foil (content 15% concentrate) additive portion 2.25 wt.%	Non-prepared sample	Non-prepared sample	PM/A/U (carrier U)	PM/B/S (carrier S)
Bacterial reduction (%)	-	-	46-53	38-45
Sample of PE foil (content 5% concentrate) additive portion 0.75 wt.%	PM/A/S (carrier S)	PM/B/U (carrier U)	PM/A/U (carrier U)	PM/B/S (carrier S)
Bacterial reduction [%]	0.0-10.9	0.0	0.0-5.5	4.2-7.9
Sample of PE foil (content 15% concentrate) additive portion 2.25 wt.%	Non-prepared sample	Non-prepared sample	PM/A/U (carrier U)	PM/B/S (carrier S)
Bacterial reduction [%]	-	-	36.7-48.5	35.6-43.5

AMA values confirm that after enhancement of the additive portion over 2 wt.% level bacteriostatic efficiency on PP and PE foils after application of AMB nanoadditives prepared using the alternative methods of PM/A and PM/B type is achieved.

3 CONCLUSION

Experiments with various nanoSiO$_2$ based carriers applied on preparation of the AMB nanoadditives were concluded by application of a new carrier U type, which has brought better results than carriers S and M type. Carrier U is characterized as spherical amorphous SiO$_2$, which is very suitable for dispergation in polymeric matrix. Surface area is set at 20 m^2/g, it contains small quantity of Fe$_2$O$_3$ and carbon (less than 0.20 wt.%). The carrier U assured good stability on preparation of the nanoadditive solution using the progressive method with application of AMB nanosol as well as AgNO$_3$. A positive result was achieved with variant PM/A, where high AMA was determined with relatively low Ag content, as well as with variant PM/B, where the progressive method enabled to suppress considerably negative influences in the method of nanoadditive preparation and where also Ag content increased up to the level of 0.5 wt.%. From a viewpoint of suitability of the specific nanoSiO$_2$ types for preparation of the AMB nanoadditive it is possible to determine sequence of their advisability as follows: carrier U – carrier S – carrier M. Besides, high antimicrobial activity of the prepared AMB nanoadditives with the carriers U and S after application in PP fibres (AMA at the level of min. 85% reduction – bactericidal efficiency), PP and PE foils (AMA at the level of min. 35-50% reduction, bacteriostatic or even bactericidal efficiency) was confirmed. The achieved level of antimicrobial efficiency in PP fibres surpasses highly practical requirements for application of PP fibres in the textiles (sufficient bacteriostatic level) and at the same time it is satisfactory in application in PP and PE foils for food packing (bacteriostatic level).

It is possible to expect also significant economical benefits whilst maintaining high antimicrobial efficiency in the final products - fibres and foils - regarding comparatively low Ag content in the polymeric mass of PP fibre, PP and PE foil after application of the AMB nanoadditive, prepared using the progressive methods (0.05-0.50 wt.%).

ACKNOWLEDGEMENT: *Results presented in the paper were achieved in the frame of elaboration of the research project APVV-15-0016 „Research on antimicrobial nanoadditive for fibres and foils“ supported from financial means of The Slovak Research and Development Agency with the seat in Bratislava, Slovak Republic.*

4 REFERENCES

1. Sang Y.Y., Hoon J.L., Sung H.: Preparation of nanocomposite fibers for permanent antibacterial effect, Journal of Materials Science 38(10), 2003, pp. 2143-2147, https://doi.org/10.1023/A:1023767828656
2. Jianguo C., Ruimin C.A.: Study of antimicrobial ability of the nano-zinc oxide polypropylene fiber, Advances in Material Chemistry 1, 2013, pp. 9-12
3. Malting B., Haufe H., Muschter K, Fischer A., Kim Y., Gutmann E., Reibold M., Meyer D. , Textor T., Kim C., Kang Y.: Silver nanoparticles in SiO$_2$ microspheres - Preparation by spray drying and use as antimicrobial agent, Acta Chimica Slovaca 57(2), 2010, pp. 451-457
4. Hou W., Wei L.I., Dai J., Jia H., Xu B.: Preparation and application of nano-silicon dioxide antibacterial agent carrying silver and zinc, China Synthetic Fiber Industry 3, 2004, Accessed from: http://en.cnki.com.cn/Article_en/CJFDTotal-HCXV200403003.htm
5. Mangesh D.T., Ravindra D.K.: Polyester nanocomposite fibers with antibacterial properties, Advances in Applied Science Research 2(4), 2011, pp. 491-502

6. Henry M.: Nanoscale silver - the next wave in smart textiles technologies, International Fiber Journal 26(6), 2012, pp. 16-19, USPS 004-973
7. An.: Hollow fiber with bacteriostatic properties, Chemical Fibers International 63(3), 2013, pp.132, ISSN 0340-3343
8. An.: Man-made fiber production 2020, Chemical Fibers Internatinal, 63(1), 2013, pp.20, ISSN 0340-3343
9. Purvis C.: Challenges in the global man-made fibers market, Proceedings of 49th Dornbirn Man-Made Fibers Congress, Austria, 15-17 September 2010, pp.48

YARN TENSION WHILE KNITTING TEXTILE FABRIC

Volodymyr Shcherban', Gennadiy Melnyk, Marijna Sholudko, Oksana Kolysko and Valerij Kalashnyk

Kyiv National University of Technologies and Design, Nemirovicha-Danchenko Str. 2, 01011 Kyiv, Ukraine
melnik2000@ukr.net

***Abstract:** Yarn tension in looms is a value defining intensity of formation process, structure of knitted fabric. Increased value of yarn tension before it enters knitting area causes a spiraling number of breaks and decreased value causes troubles for the process of lapping the yarn under the needle of the loom. Tension of yarns before they enter knitting area include its tension when going off the bobbin and additional tension arising by virtue of frictional forces between yarns and surfaces of guiding and working components of the loom having the torus form. It is very difficult to determine yarn tension in the loom within the area of textile fabric formation from experiments. It's appropriate to apply recursive approach and to determine tension within the threading areas in the loom from going off the bobbin to knitting area. Our work presents experimental research of interaction between different in their nature natural, synthetic and artificial yarns and spun yarn and surfaces in the form of torus, simulating surfaces of the yarn guides, yarn break detectors, needles and push downs of the looms with two types of tacking: an umbrella tacking, which is placed above knitting area; a tacking which is placed on the floor. As a result of the experiment the regression dependences were obtained between tension and guide curvature radius, contact angle and tension of yarn and spun yarn before the guide in the form of torus. Consistent application of regression dependences data allows determining tension of yarn and spun yarn within the knitting area for different types of natural yarns, for wide range of looms.*

***Keywords:** tension, warp yarns, weaving area, contact angle, curvature radius.*

1 INTRODUCTION

Simulation of the yarn processing using a (loom) knitting machines involves study of interaction between yarns and surfaces in the form of torus. These surfaces are dummies for surface of yarn guides, the yarn break detectors, needles and push downs of the looms with two types of tackings: an umbrella tacking, which is placed above knitting area; a tacking which is placed on the floor [1-3, 7]. When drafting the plan of the experiment, the direction connected to slip of rubbing surfaces [2, 10, 16, 17], yarn tension prior to guide [1, 2, 4, 6], yarn thickness and type of feedstock [5, 8, 9] should be considered. Flexural rigidity of the multifilaments and spun yarn with slight twist can be ignored while processing on the looms [1, 3, 13]. The above restrictions required development of all-new scheme of the experimental setup, which is different from previously developed [11, 12, 14, 15].

Figure 1 shows looms with tacking in different places.

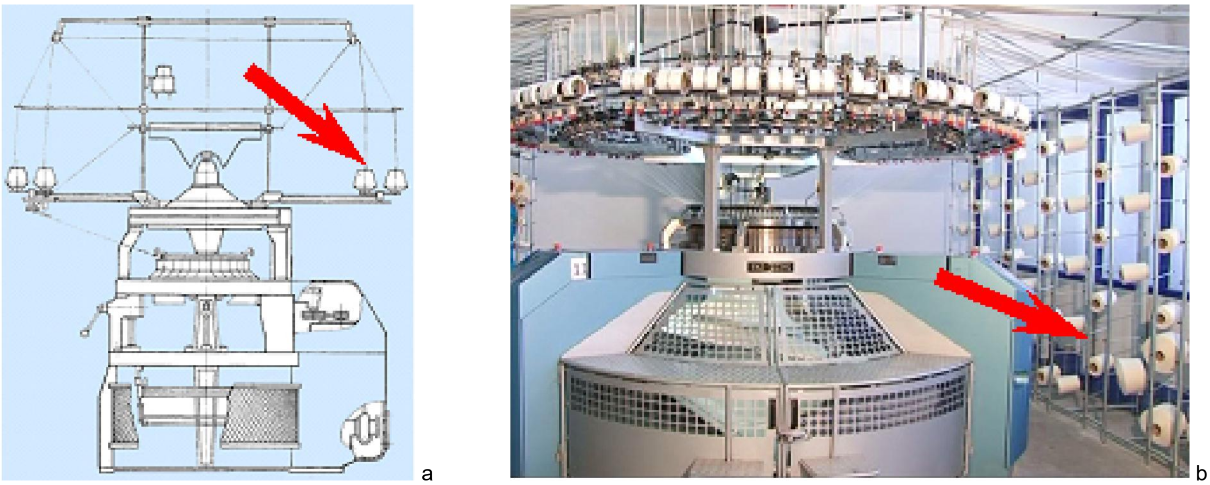
a
b

Figure 1 Looms: a - DL–4M; b - PaiLung

Figure 1a shows the loom DL–4M with umbrella tacking placed above the knitting area. The loom DL–4M is intended for knitting rib fabric to produce underwear and sportswear. Figure 1b shows the loom PaiLung with tacking placed on the floor. It is intended for knitting fabric with stockinette structure [7].

Figure 2 shows structural schemes of threading on the looms DL–4M and PaiLung. For the loom DL–4M (I – Figure 2) threading line may be divided into 11 sections (Figure 2 shows in red):

1r – from bobbin to guiding yarn; 2r – from guiding yarn to break detector; 3r – from break detector to guiding yarn; 4r – from guiding yarn to guiding yarn; 5r – from guiding yarn to cylindrical tensioner; 6r – from cylindrical tensioner to break detector; 7r – from break detector to vertical thread storage in the form of cylinder; 8r – from vertical thread storage in the form of cylinder to break detector; 9r – from break detector to inlet of yarn thread guide; 10 (Figure 2 shows in brown) – from inlet of yarn thread guide to knitting area; 11 (Figure 2 shows in yellow) – from knitting area to formed textile fabric.

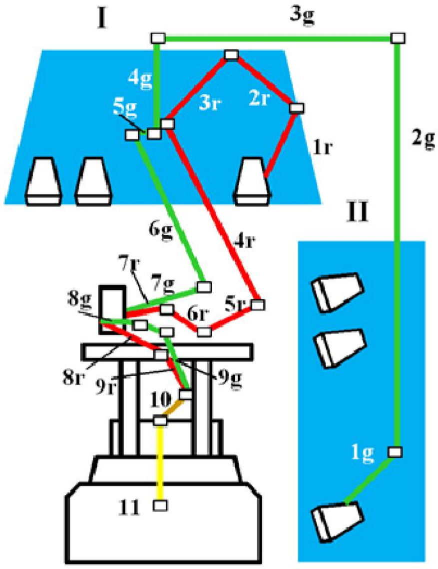

Figure 2 Structural scheme of threading on the looms DL–4M and PaiLung

For the loom PaiLung (II – Figure 2) threading line may be divided into 11 sections (Figure 2 shows in green):

1g – from bobbin to inlet of vertical cylindrical guide tube; 2g – from vertical cylindrical guide tube to rectangular connecting element; 3g – horizontal cylindrical guide tube between rectangular connecting elements; 4g – from rectangular connecting element to yarn tensioner in the form of two washers; 5g – from tensioner in the form of two washers to guiding yarn; 6g – from guiding yarn to vertical yarn storage in the form of cylinder; 7g – from vertical yarn storage in the form of cylinder to guiding yarn; 8g – from guiding yarn to break detector; 9g – from break detector to inlet of yarn thread guide; 10 (Figure 2 shows in brown) – from inlet of yarn thread guide to knitting area; 11 (Figure 2 shows in yellow) – from knitting area to formed textile fabric. Sections 10 and 11 for looms DL–4M and PaiLung are identical, that is why in Figure 2 they are shown in one colour. Yarn tension in the sections 1r and 1g will be equal to tension of the yarn when going off the bobbin.

Threading line has the form of spatial zigzag line. Table 1 shows elements of yarn supply system on the knitting machines DL–4M and PaiLung, which divide threading line into corresponding sections (Figure 2). Analysis of the structural scheme of the threading line shows its very complicated geometrical configuration both in plane and in space. In threading line inflection point the yarn or spun yarn are contacting with guide eyes in form of torus, tension devices, and control devices.

Figure 3 shows yarn thread guides and working components of the looms with which the yarn or the spun yarn interacts during its entry into the area of knitting the textile fabric.

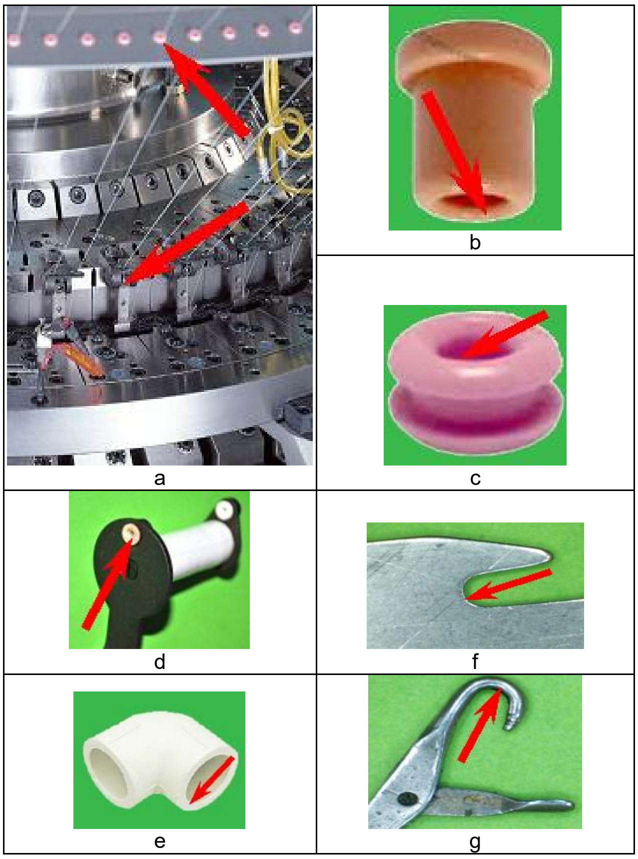

Figure 3 Structural elements in the form of torus of the threading system on the looms: a, c - yarn thread guides; b - components of break detectors; d - cylindrical yarn tensioner; e – rectangular connecting component; g – needles; f - push downs

Table 1 Elements of yarn supply system

No.	**Umbrella tacking (loom DL-4M)**		**A tacking on the floor (loom PaiLung)**	
	Area	***Guide***	***Area***	***Guide***
1	1r-2r		1g-2g	
2	2r-3r	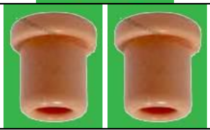	2g-3g	
3	3r-4r		3g-4g	
4	4r-5r		4g-5g	
5	5r-6r		5g-6g	
6	6r-7r	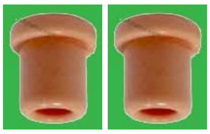	6g-7g	
7	7r-8r	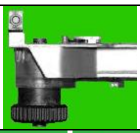	7g-8g	
8	8r-9r	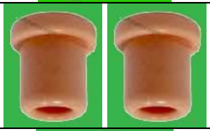	8g-9g	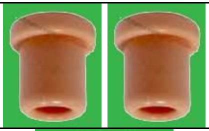
9	9r-10		9g-10	
10	10-11		10-11	

Curvature radius of these surfaces having the form of torus both significantly exceeds yarn cross-section radius and commensurable with it. Such type of interaction also occurs in implementation of similar technological processes [4, 6, 8, 9]. Figure 4 shows scheme of interaction between the yarn or spun yarn and cylindrical surface (Figure 4a) and surface in the form of torus (Figure 4b). Analysis shows that in the second case the forces of normal pressure in the section of the yarn, act not along a straight line, but along a curved surface in the form of a torus. In this case, frictional forces do not obey the friction laws known [1, 3].

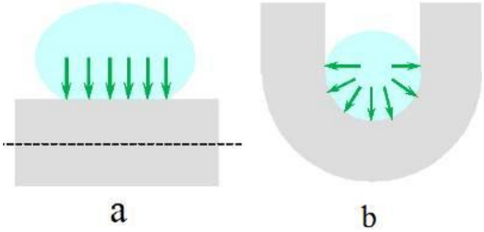

Figure 4 Scheme of interaction between the yarn and guiding surfaces: a – cylindrical; b - form of torus

2 EXPERIMENT

For the experiment, five types of yarns and spun yarns were chosen:

Series A: cotton yarn 29 Tex

Series B: wool 28 Tex

Series C: flax 30 Tex

Series D: viscose yarn 29 Tex

Series E: caprone multifilament 15.2x2 Tex.

The following yarn guides were chosen:

I – ceramic yarn guide (Figure 3c);

II – ceramic yarn guide at input and output in break detector (Figure 3b) and cylindrical yarn tensioner (Figure 3d);

III – rectangular connecting element (Figure 3e);

IV – needles and push downs of the loom (Figures 3f, 3g).

For each structural element I-IV (Figure 3) of the treading system on the loom, to determine joint influence of input tension of the yarn, radius of guide in the form of torus and calculated value of contact angle on output tension of yarn P.

In our work we planned and implemented orthogonal design of the second order for three factors. Standard form of regression equation shall be as follows [2]:

$$P = b_0 + b_1x_1 + b_2x_2 + b_3x_3 + b_{12}x_1x_2 + \\ + b_{13}x_1x_3 + b_{23}x_2x_3 + b_{11}x_1^2 + b_{22}x_2^2 + b_{33}x_3^2 \qquad (1)$$

The range of factors variability in equation (1) is determined by real conditions of yarns and spun yarn processing on looms.

<u>Factor x_1</u> - value of yarn or spun yarn tension up to structural element I-IV of the threading system of the loom:

- for guide of the yarn I changed within the range from P_{0I} = 3 cN to P_{0I} =33 cN;
- for ceramic guide of the yarn II at the entry and output in the break detector and cylindrical tensioner of the yarn changed from P_{0II} = 4 cN to P_{0II} = 16 cN;
- for rectangular connecting element III changed from P_{0III} = 4 cN to P_{0III} = 10 cN;
- for needles and push downs IV of the loom changed from P_{0IV} = 5 cN to P_{0IV} = 11 cN.

The range of tension change is determined by position of the structural element I-IV in threading line on the loom (Figure 2).

<u>Factor x_2</u> – curvature radius of the guide:

- for ceramic guide of the yarn I in the form of torus within the range from R_I = 2 mm to R_I = 4 mm;
- for ceramic guide of the yarn II in the form of torus at the entry and output in the break detector and cylindrical tensioner of the yarn within the range from R_{II} = 1 mm to R_{II} = 3 mm;
- for rectangular connecting element III of the yarn within the range from R_{III} = 1 mm to R_{III} = 3 mm;
- for needles and push downs IV of the loom within the range from R_{IV} = 2 mm to R_{IV} = 4mm.

The value of radii was determined using digital microscope (USB Digital microscope Sigeta).

<u>Factor x_3</u> – calculated value of the contact angle:

- for ceramic guide I of the yarn in the form of torus within the range from φ_I = 190 to φ_I = 920;
- for ceramic guide of the yarn II in the form of torus at the input and output in the break detector and cylindrical yarn tensioner within the range from φ_{II} = 170 to φ_{II} = 900;
- for rectangular connecting element III of the yarn calculated value of contact angle remained unchanged φ_{III} = 900;
- for needles and push downs IV of the loom within the range from φ_{IV} = 600 to φ_{IV} = 1800.

The value of the calculated contact angle is determined by the form of threading line and position of the structural element I-IV in the threading system.

At the first stage tension after the structural element I is determined. Table 2 shows matrix of orthogonal design of the second order for ceramic yarn guide I.

Table 2 Matrix of orthogonal design of the second order for ceramic yarn guide I

No.	Factors					
	Input tension		Curvature radius		Contact angle	
	χ_1	P_{0I} [cN]	χ_2	R_I [mm]	χ_3	φ_{IP} [°]
1	+1	30	+1	4	+1	85
2	-1	6	+1	4	+1	85
3	+1	30	-1	2	+1	85
4	-1	6	-1	2	+1	85
5	+1	30	+1	4	-1	25
6	-1	6	+1	4	-1	25
7	+1	30	-1	2	-1	25
8	-1	6	-1	2	-1	25
9	-1.215	3	0	3	0	55
10	+1.215	33	0	3	0	55
11	0	18	-1.215	1.8	0	55
12	0	18	+1.215	4.2	0	55
13	0	18	0	3	-1.215	19
14	0	18	0	3	+1.215	92
15	0	18	0	3	0	55

Connection between natural and encoded values for ceramic yarn guide I shall be as follows:

$$x1 = \frac{P_{0I} - 18}{12}, \quad x2 = \frac{R_I - 3}{1}, \quad x3 = \frac{\varphi_I - 55}{30}. \qquad (2)$$

At the second stage tension after the structural element II is determined. Table 3 shows matrix of orthogonal design of the second order for ceramic yarn guide II at the input and output: in the break detector and cylindrical tensioner.

Table 3 Matrix of orthogonal design of the second order for ceramic yarn guide II

No.	Factors					
	Input tension		Curvature radius		Contact angle	
	χ_1	P_{0II} [cN]	χ_2	R_{II} [mm]	χ_3	φ_{IIP} [°]
1	+1	15	+1	3	+1	83
2	-1	5	+1	3	+1	83
3	+1	15	-1	1	+1	83
4	-1	5	-1	1	+1	83
5	+1	15	+1	3	-1	23
6	-1	5	+1	3	-1	23
7	+1	15	-1	1	-1	23
8	-1	5	-1	1	-1	23
9	-1.215	4	0	2	0	53
10	+1.215	16	0	2	0	53
11	0	10	-1.215	0.8	0	53
12	0	10	+1.215	3.2	0	53
13	0	10	0	2	-1.215	17
14	0	10	0	2	+1.215	90
15	0	10	0	2	0	53

Connection between natural and encoded values for ceramic yarn guide II shall be as follows:

$$x1=\frac{P_{0II}-10}{5},\quad x2=\frac{R_{II}-2}{1},\quad x3=\frac{\varphi_{II}-53}{30} \tag{3}$$

At the third stage the tension after the structural element III is determined. Table 4 shows matrix of orthogonal design of the second order for rectangular connecting element III.

Table 4 Matrix of orthogonal design of the second order for rectangular connecting element III

No.	Input tension		Curvature radius	
	χ_1	P_{0III} [cN]	χ_2	R_{III} [mm]
1	+1	10	+1	20
2	-1	4	+1	20
3	+1	10	-1	10
4	-1	4	-1	10
5	-1	4	0	15
6	+1	10	0	15
7	0	7	-1	10
8	0	7	+1	20
9	0	7	0	15

Connection between natural and encoded values for rectangular connecting element III shall be as follows:

$$x1=\frac{P_{0III}-7}{3},\quad x2=\frac{R_{III}-15}{5} \tag{4}$$

At the fourth stage tension after the structural elements IV is determined. Table 5 shows matrix of orthogonal design of the second order for needles and push downs of the loom IV.

Connection between natural and encoded values for needles and push downs of the loom IV shall be as follows:

$$x1=\frac{P_{0IV}-8}{2},\quad x2=\frac{R_{IV}-0.7}{0.2},\quad x3=\frac{\varphi_{IV}-120}{50} \tag{5}$$

Figure 5 shows the scheme of experimental setup. Its assembly detailed in the work [2]. Distinctive feature is that unit 4 of the simulated conditions of interaction with surface in the form of torus included such structural elements as I – IV of the threading system of the loom (Figure 3)

Table 5 Matrix of orthogonal design of the second order for needles and push downs of the loom IV

No.	Factors					
	Input tension		Curvature radius		Contact angle	
	χ_1	P_{0I} [cN]	χ_2	R_I [mm]	χ_3	φ_{IP} [°]
1	+1	10	+1	0.9	+1	170
2	-1	6	+1	0.9	+1	170
3	+1	10	-1	0.5	+1	170
4	-1	6	-1	0.5	+1	170
5	+1	10	+1	0.9	-1	70
6	-1	6	+1	0.9	-1	70
7	+1	10	-1	0.5	-1	70
8	-1	6	-1	0.5	-1	70
9	-1.215	5.6	0	0.7	0	120
10	+1.215	10.4	0	0.7	0	120
11	0	8	-1.215	0.45	0	120
12	0	8	+1.215	0.94	0	120
13	0	8	0	0.7	-1.215	60
14	0	8	0	0.7	+1.215	180
15	0	8	0	0.7	0	120

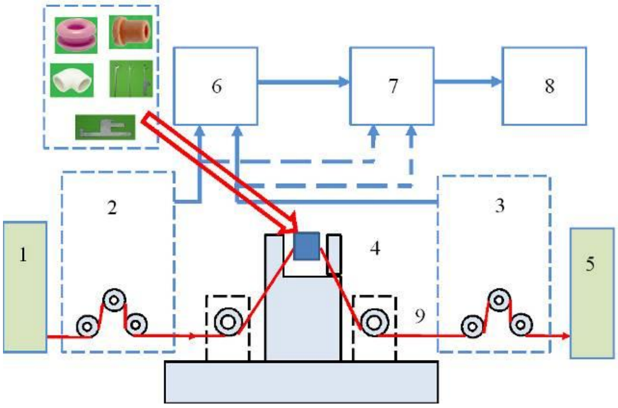

Figure 5 Scheme of the experimental setup:
1 – yarn threading unit; 2 – metering unit for yarn input tension; 3 – metering unit for yarn output tension; 4 – environment modelling unit for surface in the form of torus; 5 – yarn take up unit; 6 – amplifier; 7 – analogue to digital converter ADC; 8 – personal computer; 9 – yarn

The value of radii was determined using digital microscope (USB Digital microscope Sigeta) (Figure 6).

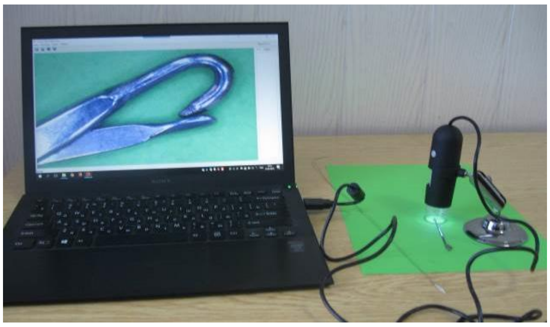

Figure 6 Setup for determining geometric dimensions of the structural elements I – IV of the threading system of the loom

3 RESULTS AND DISCUSSION

As a result of implementation of orthogonal design of the second order for three factors (Tables 2-5) for each of the series A, B, C, D, E (for five types of natural, synthetic and artificial spun yarn and yarns) for four types **I**, **II**, **III** and IV of yarns and spun yarn guides, 10 concurrent metering were conducted. Their average values represented in the Tables 6-10.

Table 6 Tension values – series A: cotton spun yarn 29 Tex

Experiment No.	Tension of natural spun yarn [cN]			
	Series A (Cotton spun yarn 29 Tex)			
	I	II	III	IV
1	44.82	22.31	14.78	33.05
2	8.79	7.31	5.93	18.28
3	48.79	27.36	14.79	51.98
4	9.07	8.13	5.93	25.67
5	34.62	17.22	5.93	18.77
6	6.79	5.15	14.78	10.53
7	37.18	20.51	10.36	27.48
8	6.99	6.21	10.36	14.01
9	3.87	5.22	10.36	14.18
10	44.47	21.75		30.05
11	25.22	16.23		30.83
12	23.38	12.93		18.92
13	20.38	11.41		15.32
14	27.96	15.69		30.74
15	23.82	13.35		21.72

Table 7 Tension values – series B: wool 28 Tex

Experiment No.	Tension of natural spun yarn [cN]			
	Series B (Wool 28 Tex)			
	I	II	III	IV
1	41.51	20.70	13.85	26.96
2	8.21	6.83	5.57	15.19
3	44.29	24.26	13.83	38.88
4	8.41	7.41	5.55	19.95
5	33.68	16.77	5.56	16.87
6	6.64	5.52	13.83	9.59
7	35.62	19.26	9.69	23.09
8	6.79	5.96	9.71	12.12
9	3.7	4.97	9.70	12.13
10	41.95	20.49		25.02
11	23.61	14.74		24.39
12	22.26	12.33		16.38
13	19.91	11.13		13.71
14	25.71	14.41		24.39
15	22.59	12.64		18.31

Table 8 Tension values – series C: flax spun yarn 30 Tex

Experiment No.	Tension of natural spun yarn [cN]			
	Series C (Flax spun yarn 30 Tex)			
	I	II	III	IV
1	43.23	21.53	14.32	29.77
2	8.51	7.08	5.75	16.65
3	46.48	25.64	14.33	44.25
4	8.74	7.75	5.74	22.38
5	34.13	16.98	5.74	17.68
6	6.71	5.58	14.32	10.01
7	36.29	19.73	10.04	24.71
8	6.89	6.06	10.04	12.85
9	3.79	5.09	10.03	13.04
10	43.20	21.09		27.17
11	24.37	15.36		26.93
12	22.84	12.63		17.55
13	20.12	11.25		14.35
14	26.87	15.05		27.24
15	23.21	12.99		19.79

Table 9 Tension values – series D: viscose yarn 29 Tex

Experiment No.	Tension of natural spun yarn [cN]			
	Series D (Viscose yarn 29 Tex)			
	I	II	III	IV
1	41.82	20.83	14.04	25.79
2	8.31	6.89	5.64	14.83
3	43.75	23.27	14.02	33.38
4	8.44	7.31	5.63	17.97
5	33.57	16.70	5.63	16.03
6	6.65	5.52	14.03	9.27
7	34.95	18.44	9.83	19.97
8	6.76	5.83	9.84	10.97
9	3.72	4.98	9.84	11.23
10	41.79	20.34		22.99
11	23.32	14.04		20.92
12	22.37	12.37		15.81
13	19.79	11.02		12.79
14	25.89	14.44		22.85
15	22.59	12.59		17.09

Table 10 Tension values – series B: caprone multifilament 15.2x2 Tex

Experiment No.	Tension of natural spun yarn [cN]			
	Series E (Caprone multifilament 15.2x2 Tex)			
	I	II	III	IV
1	47.18	23.45	15.37	38.67
2	9.17	7.63	6.15	20.95
3	52.45	30.17	15.42	66.83
4	9.54	8.71	6.16	31.67
5	35.31	17.55	6.15	20.53
6	6.89	5.73	15.38	11.35
7	38.53	21.71	10.79	32.36
8	7.14	6.43	10.76	15.97
9	3.98	5.39	10.77	16.05
10	46.38	22.73		35.05
11	26.51	17.63		38.03
12	24.14	13.34		21.15
13	20.75	11.63		16.88
14	29.57	16.63		36.93
15	24.71	13.88		24.99

Applying well-known methods to determine coefficient in the regression equation (1) for orthogonal design of the second order [1-2], considering dependences (2-10), the following regression dependences are obtained:

Series A (Cotton yarn 29 Tex):

for yarn guide **I**

$$P_{IA} = 1.22P_{0I} - 0.86R_I - 0.01\varphi_I + 0.33R_I^2 - \\ - 0.06P_{0I}R_I + 0.006P_{0I}\varphi_I - 0.98, \tag{6}$$

for yarn guide **II**

$$P_{IIA} = 1.42P_{0II} + 0.51R_{II} - 0.01\varphi_{II} - \\ - 0.17P_{0II}R_{II} + 0.01P_{0II}\varphi_{II} - 1.65 \tag{7}$$

for yarn guide **III**

$$P_{IIIA} = 0.31 + 1.44P_{0III}, \tag{8}$$

for yarn guide IV

$$P_{IVA} = 4.44P_{0IV} - 32.07R_{IV} + 0.07\varphi_{IV} + 50.99R_{IV}^2 - \\ - 5.24P_{0IV}R_{IV} + 0.02P_{0IV}\varphi_{IV} - 0.18R_{IV}\varphi_{IV} - 3.68 \tag{9}$$

Series B (wool 28 Tex):

for yarn guide I

$$P_{IB} = 0.59P_{0I} + 0.04R_I + 0.01\varphi_I - \\ - 0.05P_{0I}R_I + 0.002P_{0I}\varphi_I + 2.39 \tag{10}$$

for yarn guide II

$$P_{IIB} = 1.31P_{0II} + 0.36R_{II} - 0.004\varphi_{II} - \\ - 0.13P_{0II}R_{II} + 0.01P_{0II}\varphi_{II} - 0.81 \tag{11}$$

for yarn guide III

$$P_{IIIB} = 0.29 + 1.34P_{0III} \tag{12}$$

for yarn guide IV

$$P_{IVB} = 3.4P_{0IV} - 22.92R_{IV} + 0.04\varphi_{IV} + 33R_{IV}^2 - \\ - 3.4P_{0IV}R_{IV} + 0.02P_{0IV}\varphi_{IV} - 0.09R_{IV}\varphi_{IV} - 1.33 \tag{13}$$

Series C (Flax 30 Tex):

for yarn guide I

$$P_{IC} = 1.03P_{0I} - 0.69R_I - 0.01\varphi_I + \\ + 0.005P_{0I}\varphi_I + 1.66 \tag{14}$$

for yarn guide II

$$P_{IIC} = 1.34P_{0II} + 0.4R_{II} - 0.006\varphi_{II} - \\ - 0.14P_{0II}R_{II} + 0.01P_{0II}\varphi_{II} - 1.29 \tag{15}$$

for yarn guide III

$$P_{IIIC} = 0.28 + 1.39P_{0III} \tag{16}$$

for yarn guide IV

$$P_{IVC} = 3.73P_{0IV} - 25.72R_{IV} + 0.05\varphi_{IV} + 39.25R_{IV}^2 - \\ - 4.05P_{0IV}R_{IV} + 0.02P_{0IV}\varphi_{IV} - 0.13R_{IV}\varphi_{IV} - 2.38 \tag{17}$$

Series D (Viscose yarn 29 Tex):

for yarn guide I

$$P_{ID} = 1.01P_{0I} - 0.003\varphi_I + 0.005P_{0I}\varphi_I - 0.22 \tag{18}$$

for yarn guide II

$$P_{IID} = 1.03P_{0II} - 0.62R_{II} - 0.003\varphi_{II} + \\ + 0.005P_{0II}\varphi_{II} + 1.01 \tag{19}$$

for yarn guide III

$$P_{IIID} = 0.29 + 1.36P_{0III} \tag{20}$$

for yarn guide IV

$$P_{IVD} = 2.4P_{0IV} + 6.65R_{IV} - 0.02\varphi_{IV} - \\ - 2.1P_{0IV}R_{IV} + 0.01P_{0IV}\varphi_{IV} - 5.45 \tag{21}$$

Series E (Caprone multifilament 15.2x2 Tex):

for yarn guide I

$$P_{IE} = 1.28P_{0I} + 0.39R_I - 0.009\varphi_I - \\ - 0.08P_{0I}R_I + 0.01P_{0I}\varphi_I - 1.92 \tag{22}$$

for yarn guide II

$$P_{IIE} = 1.54P_{0II} + 0.67R_{II} - 0.01\varphi_{II} - \\ - 0.23P_{0II}R_{II} + 0.01P_{0II}\varphi_{II} - 2.23 \tag{23}$$

for yarn guide III

$$P_{IIIE} = 0.29 + 1.49P_{0III} \tag{24}$$

for yarn guide IV

$$P_{IVE} = 5.84P_{0IV} - 43.85R_{IV} + 0.11\varphi_{IV} + 75R_{IV}^2 - \\ - 7.7P_{0IV}R_{IV} + 0.03P_{0IV}\varphi_{IV} - 0.28R_{IV}\varphi_{IV} - 6.92 \tag{25}$$

Figures 7-11 show the response surfaces of the regression dependences (6-25). Tension dependences after the yarn guide from input tension and curvature radius of the surface guide in the form of torus were constructed at a fixed value of the calculated contact angle of the cylinder. This value corresponded to the centre of the experiment (Tables 1-4).

Adequacy of the obtained regression dependences was verified using SPSS software application for statistical processing of experimental findings [2]. Analysis of significance of the coefficient of the regression equations (6-25) allowed to discard insignificant ones [1, 7-8].

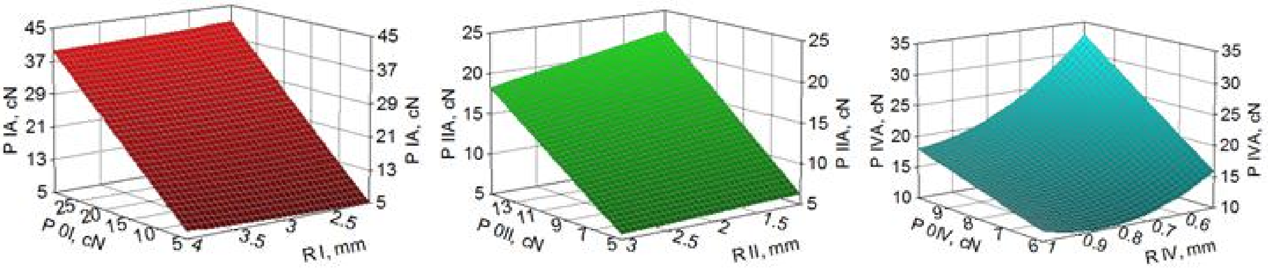

a b c

Figure 7 Response surfaces of the series A: a - for yarn guide I; b - for yarn guide II; c - for yarn guide IV

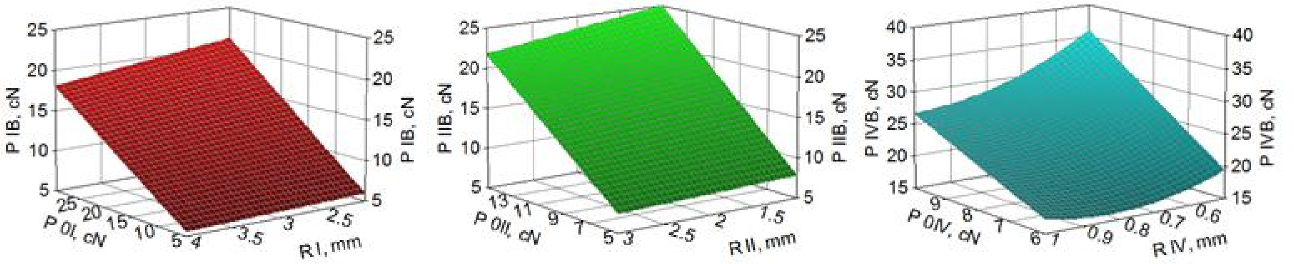

a b c

Figure 8 Response surfaces of the series B: a - for yarn guide I; b - for yarn guide II; c - for yarn guide IV

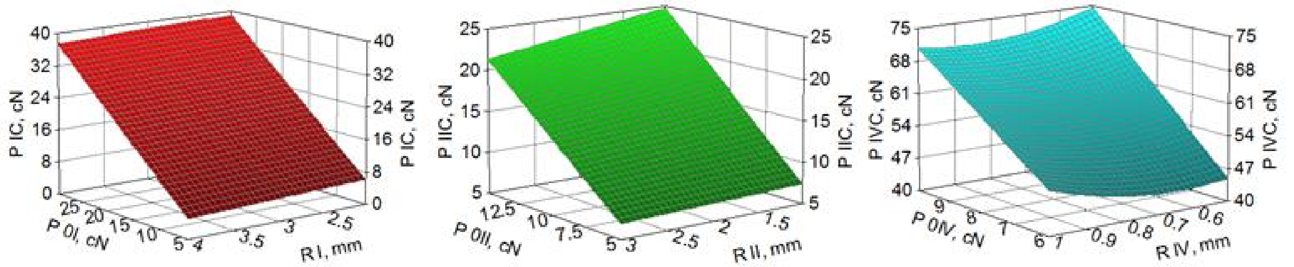

a b c

Figure 9 Response surfaces of the series C: a - for yarn guide I; b - for yarn guide II; c - for yarn guide IV

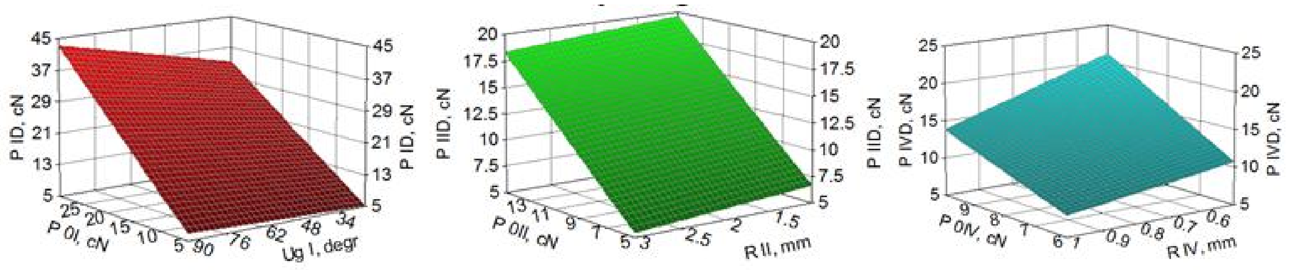

a b c

Figure 10 Response surfaces of the series D: a - for yarn guide I; b - for yarn guide II; c - for yarn guide IV

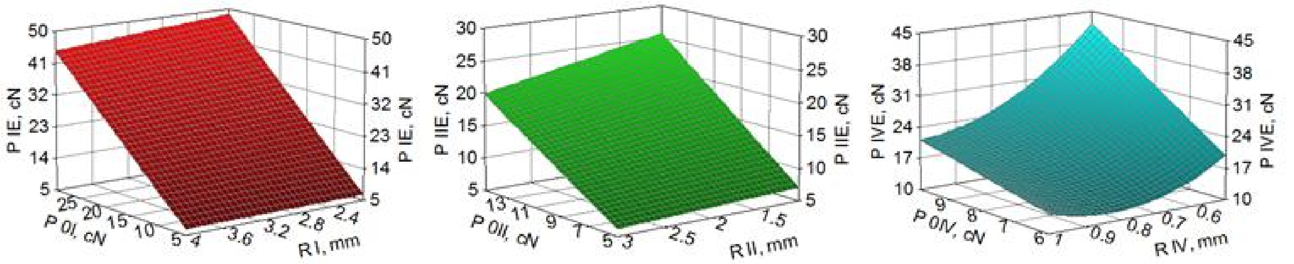

a b c

Figure 11 Response surfaces of the series E: a - for yarn guide I; b - for yarn guide II; c - for yarn guide IV

Using regression dependencies (6-25) the values of yarn and spun yarn tension were determined in the knitting area on the looms DL–4M and PaiLung. The value of the yarn and spun yarn tension when going off the bobbin was considered constant and such as not depending on its diameter.

Having been analysed, graphical dependences (Figure 12) allowed to determine that yarn tension is increasing from area to area an reaches its maximum before the mechanism of active yarn supply: area 6r-7r for loom DL–4M; area 5g-6g for loom PaiLung. After the mechanism of active supply the yarn will have the minimum tension. Its tension will gradually increase before knitting area at the expense of its interaction with structural elements I-IV. It should be noted that, loom PaiLung will have for different yarns and spun yarns (series A-E), the tension varied within 14-24 cN.

Received results may be used to optimize technological process of knitting of the textile fabric, when yet at the initial stage the intensity of the yarn and spun yarn processing on the looms may be determined.

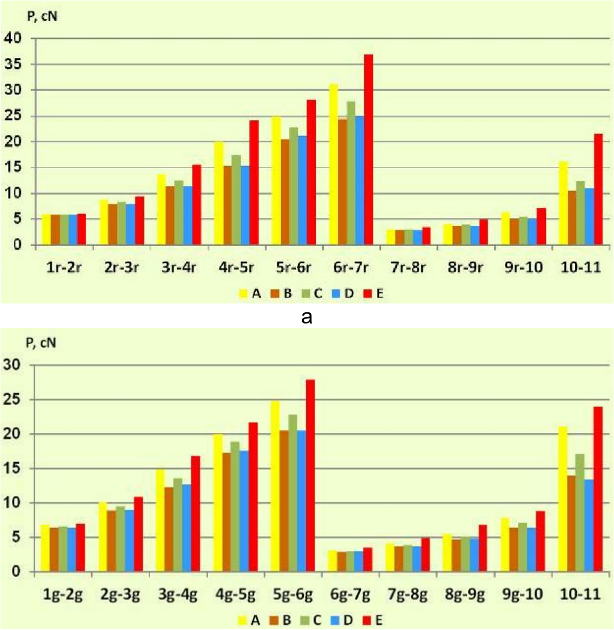

a

b

Figure 12 Yarns tension change histogram according to areas of yarn threading: a – loom DL–4M; b – loom PaiLung; 🟨 – Series A (cotton spun yarn 29 Tex); 🟥 – Series B (wool 28 Tex); 🟩 – Series C (flax 30 Tex); 🟦 – Series D (viscose spun yarn 29 Tex); 🟥 – Series E (caprone multifilament 15.2x2 Tex)

4 CONCLUSION

Resulting from conducted comprehensive experimental research of the process of interaction between yarns and surfaces in the form of torus, simulating surfaces of the yarn guides, elements of break detector devices, needles and push downs of looms, the regression dependencies were obtained. These dependencies allow to determine changes in yarn tension from the bobbin to the area of textile fabric knitting. Dependencies were obtained considering types of feedstock processed and constructions of the specific looms. Obtained results may be used to optimize technological process of knitting in terms of optimizing of geometrical form of yarn threading line on the loom, decreasing breaks, and increasing quality of the produced textile fabrics.

ACKNOWLEDGEMENT: *We are really grateful to the management of Danish Textiles for supporting our experiments with feedstock and providing us with possibility to test results of the investigation in a production environment. This study could not be completed without LGraph2 program for registering, visualising and processing of the analogue signals and technical support in processing of the experiments results provided by the L-Card Company.*

5 REFERENCES

1. Shcherban' V.Yu.: Thread mechanics, Ukrainian publishing house of forms, Kyiv, 2018
2. Shcherban’ V., Melnyk G. Sholudko M., Kalashnyk V.: Warp yarn tension during fabric formation, Vlákna a textil (Fibres and Textiles) 25(2), 2018, pp. 97-104
3. Vasilchenko V.N., Shcherban' V.Yu.: Influence of the twist of a capron complex filament on the value of its flexural rigidity, Izvestiya Vysshikh Uchebnykh Zavedenii, Technology of Textile Industry 4, 1986, pp.8-9
4. Vasilchenko V.N., Shcherban' V.Yu.: Equations of ground warp thread equilibrium in the area of multilayer technical fabric formation, Izvestiya Vysshikh Uchebnykh Zavedenii, Technology of Textile Industry 5, 1986, pp.44-47
5. Shcherban' V.Yu.: Determination of the geometrical characteristics of the axis form for thread moving along the deformable guiding surface, Izvestiya Vysshikh Uchebnykh Zavedenii, Technology of Textile Industry 6, 1990, pp.52-55
6. Koo Y., Kim H.: Friction of cotton yarn in relation to fluff formation on circular knitting machines, Textile Research Journal 72, 2002, pp.17-20, https://doi.org/10.1177/004051750207200103
7. Vasconcelos F.B., Marcicano J.P.P., Sanches R.A.: Influence of yarn tension variations before the positive feed on the characteristics of knitted fabrics, Textile Research Journal 85, 2015, pp.1864-1871, https://doi.org/10.1177/0040517515576327
8. Shcherban' V.Yu.: Determination of the technological efforts during the beating process when forming multilayer technical fabric, Izvestiya Vysshikh Uchebnykh Zavedenii, Technology of Textile Industry 3, 1990, pp.44-47
9. Shcherban' V.Yu.: Determining the technological forces during beating-up in the production of multilayer industrial fabrics, Izvestiya Vysshikh Uchebnykh Zavedenii, Technology of Textile Industry 4, 1990, pp.41-44
10. Kovar R.: Impact of directions on frictional properties of a knitted fabric, Vlákna a textil (Fibres and Textiles) 14(2), 2007, pp.15-20
11. Sodomka L., Chrpová E.: Method of determination of euler friction coefficients of textiles, Vlákna a textil (Fibres and Textiles) 15(2-3), 2008, pp.28-33
12. Donmez S., Marmarali A.: A Model for predicting a yarn’s knittability, Textile Research Journal 74, 2004, pp. 1049-1054, https://doi.org/10.1177/004051750407401204

13. Weber M.O., Ehrmann A.: Necessary modification of the Euler-Eytelwein formula for knitting machines, The Journal of The Textile Institute 103, 2012, pp. 687-690, https://doi.org/10.1080/00405000.2011.598665
14. Liu X., Chen N., Feng X.: Effect of yarn parametrs on the knittability of glass ply yam, Fibres & Textiles in Eastern Europe 16, 2008, pp.90-93
15. Hammersley M.J.: 7-A Simple yarn-friction tester for use with knitting yarns, The Journal of the Textile Institute 64, 1973, pp.108-111, https://doi.org/10.1080/00405007308630420
16. Yakubitskaya I.A., Chugin V.V., Shcherban' V.Yu.: Dynamic analysis of layout conditions on the end sections of the groove of the winding drum, Izvestiya Vysshikh Uchebnykh Zavedenii, Technology of Textile Industry 5, 1997, pp.33-37
17. Yakubitskaya I.A., Chugin V.V., Shcherban' V.Yu.: Differential equations of the relative motion of the filament element on the end sections of the coil of the winding drum, Izvestiya Vysshikh Uchebnykh Zavedenii, Technology of Textile Industry 6, 1997, pp.50-54

ECONOMIC EFFECT OF HYDRO-JET FORMING WOMENS HEADWEAR DETAILS OF HOSPITALITY ESTABLISHMENST

Olena Yakymchuk[1], Dmytro Yakymchuk[2], Natalia Kovalska[2], Irina Shvets[3] and Yuriy Shvets[3]

[1]Kherson National Technical University, Berislav highway 24, Kherson, Ukraine
[2]Kherson State University, 40 rokiv Zhovtnya St. 27, Kherson, Ukraine
[3]Financial University, Leningradskij prospekt 49, Moscow, Russia
olenayakymchuk03@gmail.com; starcon84@gmail.com; kovalsknatasha@ukr.net; i.y.shvets@gmail.com;
goldenfish3000@gmail.com

Abstract: *The process of forming heads hats from fabrics of new developed hydro-jet technology is described in the article. A number of experiments were conducted to optimize the hydro-jet forming and its optimal technological parameters that were determined. Formed headwears from coat fabrics and costume assortment. Completed comparison of developed technology with existing and installed economic effect from its application.*

Keywords: *hydro-jet forming, headwear details, LAWE, hospitality establishments, fabric, fibers.*

1 INTRODUCTION

Headwear, as a component of a women's suit, is an integral part of the completeness of any image. As a rule, hats are picked up under a suit using a similar material. Modern fashion trends intensively offer headdresses costume supplement of various shapes and materials. But for today headwear quality assurance requires the improvement of structures and technologies. It is also necessary to reduce the cost of materials and improving their consumer properties.

For better fitting of clothes on a person's figure, it is necessary to give it a volumetric form in certain areas. This is realized in accordance with the artist's plan and the anatomical features of the body structure. There are many technologies and ways to solve this problem for today.

Parts quality of volume form headdresses conditioned by structural performance fabrics. Also – the way of formation, an important factor of which is the power field. For a rational selection of formation modes, is expedient to forecast the process due to the analysis of applied actions to the detail of the loads headdresses. Also perspective is development of recommendations regarding the application of different loads schemes taking into account the features of the contour parts.

Increasing consumer demands for product quality makes use of new methods, techniques and research equipment for the development of production technologies.

Providing details of headdresses difficult spatial form from fabrics without constructive intervention is an extremely hard task. To do this is necessary plastify the fabric and attach it some effort. This scheme is implemented in forming volumetric details of headwear by hydrojet method due to use liquid-active working environment (LAWE) [1]. It plastify the fabric and transfers the molding effort by flooded hydrojet stream [2].

Conducting experiments on the specified equipment using LAWE will allow to optimize the formation process parts of hats of different fabrics. This will improve the quality of the products.

Thus, the actual task is to conduct research the process of hydrojet forming of women's headwear of hospitality establishments to determine the optimal technological parameters of the specified equipment. Also, it is necessary to determine the economic effect of the application proposed technology. As known, fibers have certain deformation properties, which then transmitted to threads and then – fabrics.

Considering in the complex the composition and structure of the fiber, we can make a definite conclusion. It is established that the most flexible are cotton fibers and the hardest – linen. Forming fabrics of wool fibers is happening at the expense of scales located on their surface. This significantly increases the coefficient of friction with the joining of fibers [3].

Adding chemical fibers to natural improves the shape resistance of the fabric. In particular, the use of wool with fibers, which have high plastic deformation, will increase the quality of the formed detail [4].

With decreasing fabric density, but with the same thickness of fibers and interlacing and with a decrease in the number of fibers by 10 cm the fabric becomes more mobile [5]. With a decrease in fabric bonding, the fibers are easier to move one to another and stiffness of fabric decreases [6]. The most bonded and stiff is canvas weave [7]. With an increase in the size of the main and overlap weft the connectivity and stiffness of the fabric decreases [8] which is typical for atlases, satins, and serge [9]. Such characteristic features of the fabrics with different weaving determine the complexity and difficult of their research with a wide range of desired parameters [10].

Known hydrodynamic formation method of headwear details [11] which has one common feature with hydrostatic formation. This is the use of a fluid-active working environment (LAWE) as a working environment. But with this the vector of the applied effort is always directed along the normal to each point of detail surface. This limits the ability to form difficult spatial forms.

There is a variety of equipment [12], the main element of which is the use of hydrojet technology. Typically, such equipment used in many industries.

Known study [13], which describes the process of jet penetration into a multilayer package of materials. However, it does not allow the use of hydrojet technology for non-metallic materials. Also, it is known to use a hydrojet for ground soils with the use of special technology [14]. The description of the concept of physical principles for ground soiling with the corresponding characteristics of strength is described. However, conducted studies have narrow direction. Hydrojet technology has been used in the design of underground structures [15]. At the same time to ensure the passage of relevant processes special calculations are carried out [16]. They allow to predict the impact of the jet on different materials. Formulated problems for perspective future research [17]. It should be noted, that in fact there are no studies of the process of hydrojet formation headwear details of hospitality establishments.

Therefore, there is a need investigated the process of hydrojet formation of women's headwear in designing clothing for hospitality facilities. For this need to take into account the various factors that directly affect the process and also establish the economic effect of hydrojet forming.

2 EXPERIMENTAL

The process of hydro-jet forming of hats from fabrics of a suit-coat assortment was modeled. For this reviewed the process of hydro-jet forming hat heads from appropriate fabrics taking into account the following process parameters: H_{sr} – fabric filling coefficient; C – fabric bonding coefficient; S_{nas} – area of outgoing hole nozzle; l – the distance between the tip of nozzle and detail; d – corrected sampled variance of normalized deviations ordinate of the contour formed part of headwear from the ordinates of forming element contour; R – headwear form detail relaxation ; α – angle of attack; n – headwear detail speed rotation; t – forming time; P – LAWE pressure in the system.

In conducting researches it was established that the shape resistance of the head depends on the following factors: characteristics of fabrics and yarn (fiber composition, spinning system, bonding coefficients C and filling of N_{sr} fabric); geometric parameters of nozzles and hydro-jets (shape and area of nozzle outlet hole, distance between end of nozzle and detail); mode of formation (LAWE pressure in system P, time of formation t, rotation speed of the headwear part n, angle of attack for each technological part of the headwear α).

On the basis of conducted research, a new method of hydro-jet forming was developed. It consists of the following stages:

1. The choice of a jet nozzle according to the shape and size of the outlet.
2. The semi-finished product is prepared for formation:
   - from the fabric cut out flat sample with a diameter of 170 mm;
   - sample of fabric is fixed by clamping ring on forming element, the contour of which conditionally divided for five technological parts.
3. In the working window of the developed program introduced initial data:
   - made choice of the desired contour of headgear surface parts;
   - distance from the jet nozzle end to the detail surface;
   - the magnitude of the angle of attack for each from five technological areas;
   - the number of cycles that corresponds to a certain time of formation.
4. Shaping element with fabric installed into the work camera of the equipment.
5. The camera is full by LAWE.
6. The engine is turned on which transfers the rotation on the shaft with the forming element.
7. The "Start" button is pressed in the application window, which leads to action specialized equipment. At the same time, the nozzle begins to move along a predetermined contour of the headwear surface at a certain distance from it and changing the angle of attack on the relevant technological parts.
8. Upon completion of the formation, the LAWE is pumped into the reservoir.
9. Forming element with detail is removed from the working camera and to the inverted side of the head applying a glutinous solution (carbamol CEC - 22 g/l, PVA - 75 g/l, magnesium chloride - 3 g/l) [18].

10. Detail is dried with form stabilization when applying infrared radiation and with the simultaneous removal of moisture with a vacuum pressure of 0.0008-0.0012 MPa for 15 min taking into account the recommendations [19].
11. Performing quality assessment of molded parts by graph-analytical method.

Thus, the developed method will allow to explore the process of hydro-jet forming and determine the optimal parameters of formation for fabrics of a suit-coat assortment (Figure 1).

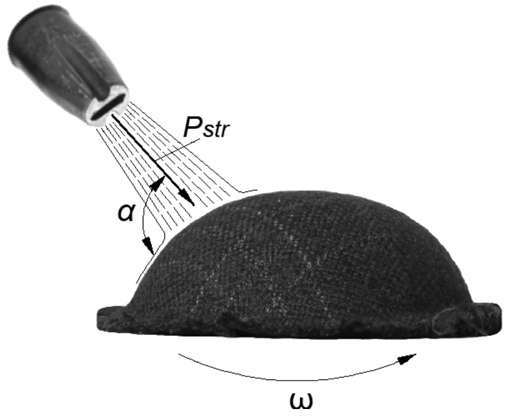

Figure 1 Theme of technological process of hydro-jet forming

A number of experiments were conducted. Input factors for which are chosen specified above factors. Fixed factors were: elliptical area of output section of conoidal jet forming nozzle S_{nas} = 7.2 mm^2; distance from the end of the nozzle to detail surface l = 5 mm; angle of attack on the five sections of the detail α_I = 90°, $\alpha_{II\text{-}IV}$ = 45°.

In the experiment two optimization options were used. First – corrected sample variance normalized deviations of real values ordinate points of the contour molded part from the values of ordinates contour points of forming element *d*. Second – relaxation value of headwear detail form after 48 hours rest *R* [%].

Obtained correlation indicate to interconnection of the parameters form stability *d* and *R* with different factors. These include the LAWE pressure in the system *P*, formation time *t* and detail speed rotation *n*. On both optimization parameters were listed factors affected in different ways. On decrease of corrected sample dispersion of normalized deviations significant impact exerts LAWE pressure in the system and its growth. The smaller – the speed of rotation, but insignificant factor, was time of formation. The greatest impact on the reduction value of detail form relaxation makes double interaction of LAWE pressure in the system and forming time. Less influence the time forming increase and also the LAWE pressure in the system. At the same time insignificant factor was detail rotational speed of headwear.

Results analysis allows to assert about the greatest impact of the LAWE pressure on the system on process of hydro-jet formation for different fabrics such as costume and coat fabrics. This explained the power aspect of the latter.

After conducted research determined optimal values of hydro-jet forming modes of experimental samples of headwear heads for the coat and costume fabrics group (Table 1).

Table 1 Technological parameters of hydro-jet forming experimental samples of headwear heads

Technological parameter	Marking	Coat fabrics group	Costume fabrics group
Hydro-jet pressure	P_{str}	0.07 MPa	0.06-0.09 MPa
Forming time	t	115-159 s	115-157 s
Rotation frequency	n	180 rpm	116-157 rpm
Inclination angles of nozzle axis relative to the head surface	α_{II}	15-25°	15-20°
	α_{III}	35-40°	35-40°
	$\alpha_{IV\text{-}V}$	45°	45°

Based on the results of research were made two models of headwear with molded heads in real size by hydro-jet method (Figure 2). For headwear manufacture applied following modes of head formation (Table 2).

Figure 2 Formed headwear by hydro-jet method

Table 2 Technological parameters of hydro-jet forming headwears heads in natural size

Technological parameter	Marking	Coat fabric	Costume fabric
Hydro-jet pressure	P_{str}	0.07 MPa	0.06 MPa
Forming time	t	203 s	203 s
Rotation frequency	n	157 rpm	145 rpm
Inclination angles of nozzle axis relative to the head surface	α_{II}	25°	20°
	α_{III}	35°	40°

So, after conducted research by using proposed process of hydro-jet forming produced hats from coat and costume fabrics.

3 RESULTS AND DISCUSSION

To determine economic effect of developed technology it must be compared with the existing - hydrodynamic forming and felt headwears heads forming. In the application of the hydrodynamic method [20] created pressure at expense of external effort on the LAWE by pulsating compressed air. This method based on the environment properties evenly distributes forming effort. At the same time details forming passes when created in the camera pressure variations, resulting in vibrational oscillations of the LAWE.

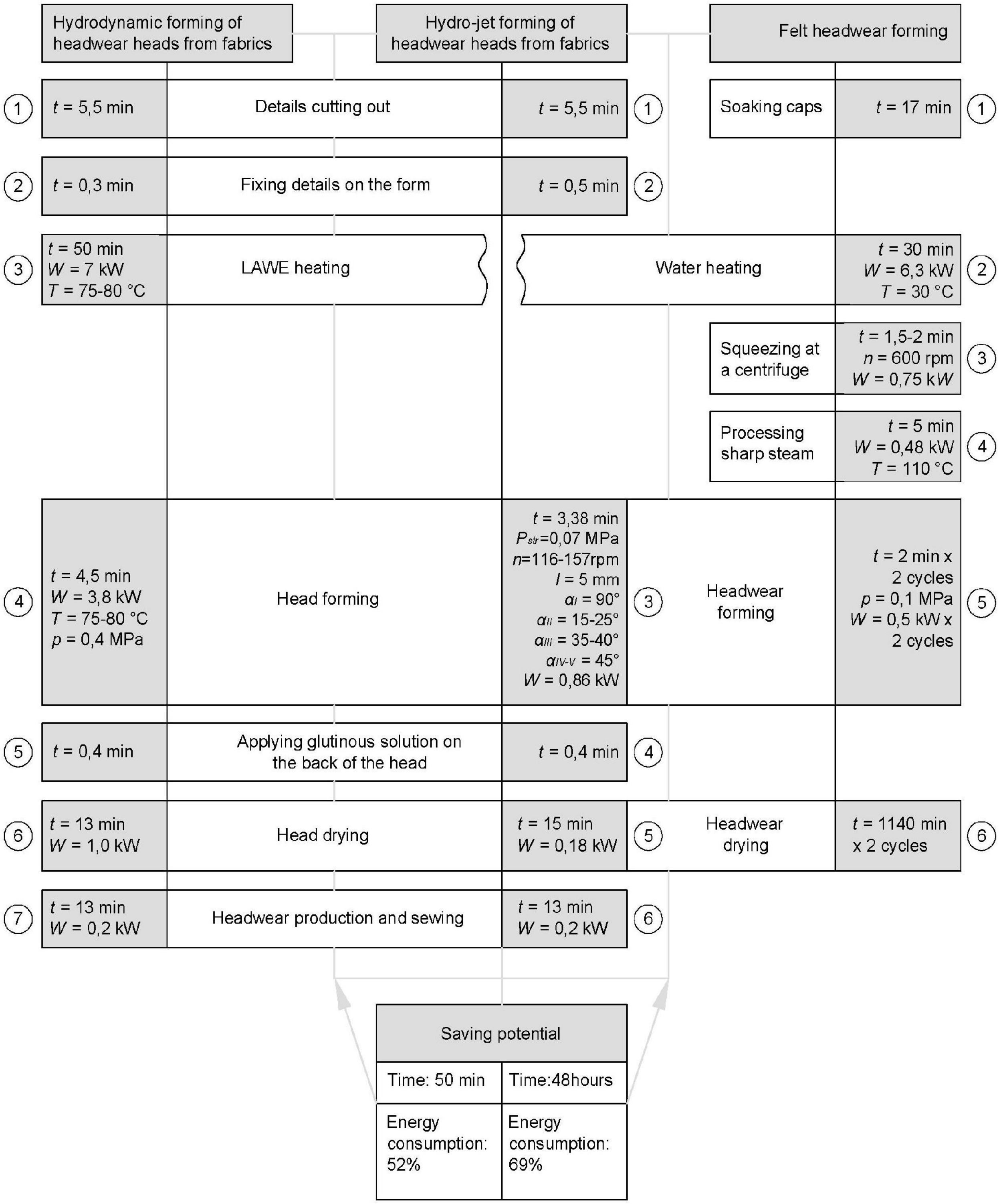

Figure 3 Saving potential developed hydro-jet technology in comparison with hydrodynamic forming and felt forming

After this LAWE derived from the camera.

In the manufacture of molded headwear are using caps of three forms: cone-shaped, caps with an enlarged head, chapels – caps with curved fields. All made from felt.

For the manufacture of felt caps used machines for wool weaving in the approximate form of headgear. They consist of a roller system, brushes and belts with a needle headset, which transfer the wool on a rotating perforated metal cone cartridge (or the same piece of netting). At the same time the fibers in the cap are chaotic, not oriented. After that the finished cap is removed from the cone. To provide the caps shape stability they are glued applying shellac – glue from natural resin released by some plants. Thus, the technology of manufacturing felt hats consists of number operations, which require additional time expenditures. As a result, the cost of finished products increases.

4 CONCLUSION

A new technology of hydro-jet forming of women's hats details is developed.

The optimization parameters for the hydro-jet head forming of headwear from the fabrics of the costume (P_{str} = 0.06 MPa, t = 203 s, n = 145 rpm, α_{II} = 20°, α_{III} = 40°) and coat assortment (P_{str} = 0.07 MPa, t = 203 s, n = 157 rpm, α_{II} = 25°, α_{III} = 35°) are determined.

It was completed comparison of developed technology with existing and installed economic effect from its application. It was determined that the economic potential of time is 50 min in comparison with hydrodynamic forming and 48 hours in comparison with the forming of felt. The economic potential of energy consumption is 52%, compared with hydrodynamic forming and 69% - forming of felt.

5 REFERENCES

1. Popovych O.V, Kushchevskyi M.O.: Hydro-jet method of forming parts sewing products of volumetric-spatial form, Pat. 46731 UA, DO6F 73/00, 200902654, 2010, 1, 2 (in Ukranian)
2. Prybeha D.V., Kushchevskyi M.O., Zlotnikov V.O., Popovych O.V.: Hydro-jet method of forming parts sewing products of volumetric-spatial form, Pat. 46811 UA, A42C 1/00, 200906453, 2010, 1, 2 (in Ukranian)
3. Buzov B.A., Modestova T.A., Alymenkova N.D.: Materials science of sewing production, Lehprombytizdat, 1986, 424, (in Russian)
4. Kukin H.N., Solovev A.N., Kobliakov A.I.: Textile materials science, Lehprombytizdat, 1989, 352 (in Russian)
5. Maltseva I.P.: Materials science of sewing production, Lehkaia i Pishchevaia Promyshlennost, 1983, 232 (in Russian)
6. Damianov H.B., Bachaev T.Z., Surnina N.P.: The structure of the fabric and modern methods of its design, Lehkaia i Pishchevaia Promyshlennost, 1984, 240 (in Russian)
7. Yudenich H.V.: Interlacing and fabrics analysis, Lehkaia industriia, 1986, 164 (in Russian)
8. Urazov N.K.: Structure and design of fabrics, Ukituvchi, 1971, 264 (in Russian)
9. Hordeev V.A.: Weaving interlacing and fabrics analysis, Lehkaia industriia, 1979, 120 (in Russian)
10. Bukaev P.T., Onnikov E.A., Malkov L.A.: Cotton-weaving, Lehprombytizdat, 1987, 576 (in Russian)
11. Kushchevskyi M.O., Bukhantsova L.V.: Hydromechanical method of textile materials forming, Visnyk Khmelnytskoho Natsionalnoho Universytetu, 2007, 6, pp. 33-36 (in Ukranian)
12. Hulti E, Abouali S., Ben Hucine M., Mansour M., Nedeljković M.S., Ilić V.: Influence of hydrodynamic conditions and nozzle geometry on appearance of high submerged cavitating jets. Thermal Science 17(4), 2013, pp. 1139-1149, DOI: 10.2298/TSCI120925045H
13. Kang Y.L., Jiang J.W., Men S.Y.: Numerical study of charge jet formation end penetration into multi-layer with different liner material, Advanced Material Research 148-149, 2010, pp. 744-748, https://doi.org/10.4028/www.scientific.net/AMR.148-149.744
14. Ibragimov M.N.: Characteristics of soil grouting by hydro-jet technology, Soil Mechanics & Foundation Engineering 50(5), 2013, pp. 200-205, https://doi.org/10.1007/s11204-013-9234-8
15. Zege S.O., Broid I.I.: Procedural characteristics of the design of underground structures installed with use of jet technology, Soil Mechanics and Foundation Engineering 46(2), 2009, pp. 53-58
16. Zege S.O., Broid I.I.: Design features of soil-concrete structures built by means of jet geotechnology, Soil Mechanics and Foundation Engineering 44(4), 2007, pp. 143-145, https://doi.org/10.1007/s11204-009-9046-z
17. Shimizu S.: Structure and erosive characteristics of water jet issuing from fan jet nozzle, 18th International Conference on Water Jetting, Poland, 2006, pp. 337-345
18. Koshevko Y.V., Kulakov O.I., Kushchevskyi M.O.: Development of tools for fixing the wear resistant forms, Visnyk Khmelnytskoho Natsionalnoho Universytetu 5, 2009, pp. 122-125 (in Ukranian)
19. Yakymchuk O.V.: Study of the hydro-jet forming of head hats depending on the angle of attack change, Visnyk Khmelnytskoho Natsionalnoho Universytetu 5, 2010, pp. 88-91 (in Ukranian)
20. Bukhantsova L.V., Kushchevskyi M.O.: Study of the influence of fabrics structure on the quality of headwear formation, Visnyk Khmelnytskoho Natsionalnoho Universytetu 6(2), 2007, pp. 26-31 (in Ukranian)

INSTRUCTIONS FOR AUTHORS

The journal ,,**Vlákna a textil**" (**Fibres and Textiles**) is the scientific and professional journal with a view to technology of fibres and textiles, with emphasis to chemical and natural fibres, processes of fibre spinning, finishing and dyeing, to fibrous and textile engineering and oriented polymer films. The original contributions and works of background researches, new physical-analytical methods and papers concerning the development of fibres, textiles and the marketing of these materials as well as review papers are published in the journal.

Manuscript

The original research papers are required to be written in English language with summary. The advertisements will be published in a language according to the mutual agreement.

The first page of the manuscript has to contain:

The title of the article (16 pt bold, capital letters, centred)

The full *first name* (s) and also *surnames* of all authors (11 pt, bold, centred).

The complete address of the working place of the authors, e-mail of authors (9 pt, italic, centred)

Abstract (9 pt, italic)

Key words (9 pt, italic)

The manuscript has to be written in A4 standard form, in **Arial, 10 pt**.

The text should be in ***double-column format*** *(width 8.1 cm)* ***in single line spacing***.

Page margins: up and down 2.5 cm; left and right 2.0 cm.

Do not number the pages and do not use footnotes. Do not use business letterhead.

Figures, tables, schemes and photos (centered) should be numbered by Arabic numerals and titled over the table and under the figure or picture.

Photos and schemes have to be sufficiently contrastive and insert in text as pictures.

Figures, tables, schemes and photos, please, send in separate file.

Mathematical formulae should be centred on line and numbered consecutively on the right margin.

Physical and technical properties have to be quantified in SI units, names and abbreviations of the chemical materials have to be stated according to the IUPAC standards.

References in the text have to be in square brackets and literature cited at the end of the text. References (9 pt), have to contain names of all authors.

[1] Surname N., Surname N.: Name of paper or Chapter, In Name of Book, Publisher, Place of Publication, YYYY, pp. xxx-yyy

[2] Surname N., Surname N.: Name of paper, Name of Journal Vol. (No.), YYYY, pp. xxx-yyy

[3] Surname N., Surname, N.: Title of conference paper, Proceedings of xxx xxx, conference location, Month and Year, Publisher, City, Surname N. (Ed.), YYYY, pp. xxx-yyy

[4] Surname N., Surname N.: Name of Paper, Available from http://www.exact-address-of-site, Accessed: YYYY-MM-DD

The final template of manuscript is available on **http://www.vat.ft.tul.cz**

Authors are kindly requested to deliver the paper (in Word form) to be published together with information about at least 3 recommended reviewers from institutions others than the parent (name, e-mail, institution, department) by e-mail: marcela.hricova@stuba.sk

After successful review procedure there is charged fee (article processing charge) of EUR 100. All articles after review process are freely available online and this fee helps to cover the costs of taking a manuscript and turning it into a finished article.

Address of the Editor Office:

Marcela Hricová

Faculty of Chemical and Food Technology,

Slovak University of Technology in Bratislava

Radlinskeho 9

812 37 Bratislava,

Slovakia